INPUT-OUTPUT ANALYSIS: GRAPHICAL AND ALGORITHMIC METHODS

THOMAS CHAFFEY

WOLFSON COLLEGE,
UNIVERSITY OF CAMBRIDGE

This thesis is submitted for the degree of Doctor of Philosophy.

MARCH 2022

To my parents, my first teachers.

I believe that the only excuse we have for being musicians and for making music in any fashion, is to make it differently, to perform it differently, to establish the music's difference, vis-a-vis our own difference.

— GLENN GOULD

DECLARATION

This thesis is the result of my own work and includes nothing which is the outcome of work done in collaboration except as declared in the preface and specified in the text. I further state that no substantial part of my thesis has already been submitted, or is being concurrently submitted for any such degree, diploma or other qualification at the University of Cambridge or any other University or similar institution except as declared in the preface and specified in the text. It does not exceed the prescribed word limit for the relevant Degree Committee.

Thomas Chaffey, March 2022

ABSTRACT

Input/output analysis: graphical and algorithmic methods
Thomas Chaffey

This thesis describes new methods in input/output systems theory.

The first part of this thesis develops a novel graphical method for the stability analysis of feedback systems. The Scaled Relative Graph (SRG), a recent concept from monotone operator theory, is shown to generalize the classical Nyquist diagram of an LTI transfer function, and may be plotted for arbitrary nonlinear operators. Applying the SRG to the analysis of feedback interconnections leads to a graphical incremental stability theorem, which unifies and generalizes the Nyquist criterion, circle criterion, incremental passivity theorem, incremental small gain theorem and incremental secant condition. A novel special case of this theorem concerns systems which only violate the assumptions of the incremental passivity theorem when their incremental gains are small. This captures systems whose incremental passivity is destroyed by common effects such as delay and saturation.

The second part of this thesis develops algorithmic methods for solving nonlinear circuits composed of monotone elements. Monotonicity is a generalization of the linear property of passivity, and is a fundamental property in the theory of large-scale convex optimization. Modern splitting methods, which invert sums of operators, are shown to correspond to the series or parallel interconnection of circuit elements which are monotone, and may be used to solve the steady-state behavior of such circuits. Consideration of circuits with arbitrary series/parallel interconnections leads to a new splitting algorithm, the *nested forward-backward algorithm*, which inverts operators composed of sums and inverses.

Finally, these methods are extended to circuits composed of the difference of monotone elements. The steady-state behavior of such circuits can be solved via an adaptation of Difference of Convex (DC) Programming. Such circuits include the classical van der Pol oscillator and the FitzHugh-Nagumo model of an excitable neuron, which both consist of an LTI transfer function in parallel with monotone and anti-monotone nonlinear resistors. A new algorithm, the *difference-of-monotone Douglas-Rachford algorithm*, is proposed, which matches the mixed-feedback structure of these circuits.

ACKNOWLEDGEMENTS

Thanks, above all, to my supervisor Rodolphe Sepulchre. For your support, incredible optimism and enthusiasm, I am deeply grateful. And your creativity; your balance of interests in the fundamental and the practical, the questions of the day and the history of questions and solutions; and your amazing ability to see the grand ideas through the technical details; have truly shaped the way I think.

Thanks to Fulvio Forni, for your support, optimism and enthusiasm, and for teaching me to slow down and think carefully and precisely (or try, at least!).

Thanks to my collaborator Amritam Das, and to all my colleagues and friends in the control group at Cambridge. I count myself very lucky to have spent these years with a group of such humble, open, creative and motivated people.

Thanks to Madi, for all your sacrifices.

COLLABORATIONS

Chapter 2: Fulvio Forni, Rodolphe Sepulchre

Chapter 3: Fulvio Forni, Rodolphe Sepulchre

Chapter 4: Amritam Das, Fulvio Forni, Rodolphe Sepulchre

CONTENTS

1 INTRODUCTION

Nonlinear effects are ubiquitous in electrical circuits, and nonlinear behaviors such as switches and oscillations are often fundamental to their operation. Many such nonlinear effects can be understood in terms of a mixture of positive and negative feedback channels – positive feedback creates a switch; negative feedback regulates to equilibrium. Control theory is the study of feedback, yet control theory has had a modest impact on nonlinear circuit theory.

The gap between nonlinear control theory and nonlinear circuit theory is the motivation for this thesis, which describes new methods in input/output systems theory. These new methods arise from revisiting classical input/output systems theory with methods from the modern theory of mathematical optimization – in particular, the theory of monotone operators. Both input/output systems theory and monotone operator theory originated in the study of analog electrical circuits, although such applications have been largely forgotten. The study of analog electrical circuits is, however, timely – advances in memristive semiconductor devices has seen a surge of interest in analog artificial neural networks [1]–[3], and the past several years has seen a boom in interest in neuromorphic circuits [4]–[8].

Input/output analysis is the study of systems which map an input signal to an output signal. Feedback systems have a natural input/output structure, and the earliest results in the theory of systems and control, such as the Nyquist criterion [9], Bode's integral relations [10] and root locus [11] pertain to a class of linear, time invariant input/output operators called *transfer functions*. These tools were developed for the study of feedback amplifiers in telecommunication systems. While the high dimensional differential equations were difficult to analyse with current tools, the Nyquist and Bode diagrams allowed the behavior of such systems to be neatly summarized [12]. Transfer functions also arise in the early theory of electrical networks; for example, in the study of passive network synthesis by Cauer, Brune, Bott and Duffin [13]–[15]. Input/output theory is naturally suited to the study of linear, time invariant electrical circuits, synthesised by series/parallel interconnection of inductors, capacitors and resistors. Indeed, the celebrated passive synthesis result of Bott and Duffin [15] gives a correspondence between manipulations to a transfer function and circuit interconnections.

Nonlinear input/output systems theory was inspired by Norbert Wiener [16], who first suggested functional analysis as a tool for studying feedback systems. Wiener inspired a line of research on functional analysis throughout the 1950s [17]–[21]. The first major progress, however, was the thesis of George Zames [22], which introduced the method of functional iteration to systems theory. Other important early work includes that of Sandberg [23] and Willems [24]. The motivation for nonlinear input/output

systems theory was the study of nonlinear electrical circuits; it was desired to extend the elegant theory of linear time invariant (LTI) filters to nonlinear filters. Zames' archetypical nonlinear input/output system is an amplifier.

While nonlinear input/output systems theory originally aimed at extending the power of transfer function methods to nonlinear circuits, it has never had a great impact in circuit theory, and after early momentum in the 1960s and 1970s, the theory has declined in popularity. One reason for this is certainly historical – the 1960s and 1970s mark the rise of state space theory, and in the subsequent decades, systems and control focussed on the study of mechanical systems, for which the state space paradigm is natural. Other reasons pertain to the theory itself: while LTI state space theory comes equipped with closed-form solutions to optimal control problems [25] and computationally tractable methods from the theory of linear matrix inequalities [26], and LTI input/output theory comes with the powerful graphical tools of the Nyquist and Bode diagrams [9], nonlinear input/output theory lacks general algorithmic or graphical methods, and furthermore is riddled with technical difficulties to do with causality and invertibility. Speaking of the latter, Jan Willems writes [27]:

> With arrow-ridden signal flow diagrams, one does not get off the ground for modelling even simple electrical circuits, the paradigmatic example of interconnected systems.

This motivated Willems' development of behavioral theory [28], which models systems as bundles of trajectories, without imposing conditions such as causality or an input/output structure.

This thesis contributes new methods to nonlinear input/output systems theory which aim to address some of its short-comings: the lack of general graphical tools, and the lack of algorithmic tractability. The spirit of Willems' behavioral theory is retained: systems are modelled as *relations*, or catalogues of input/output pairs, which are readily invertible, by simply exchanging the "input" and "output" labels.

Zames' interest was in studying systems through bulk properties rather than detailed models [29]. The two central properties are gain (signal amplification) and passivity (energy dissipation). A choice must be made between studying the worst-case, or *incremental*, gain and passivity, measured between any two pairs of input/output trajectories, or to measure gain and passivity with respect to a nominal trajectory. Only in the linear case are the two equivalent, and the zero trajectory can always serve as the nominal trajectory. In nonlinear system analysis, the choice of a nominal trajectory is often arbitrary. If a system has finite gain (measured from zero), it is *bounded* – the output never explodes. If a system has finite incremental gain, it is *continuous* – small changes in the input give small changes in the output. In his thesis, Zames emphasised the latter property, continuity:

> It is now desired to compute or bound the norm of the output of a system when that of the input is known. In order to do this, it is necessary to know the

> amplification of the system, which will differ, in general, for every input. We are especially interested in the largest incremental amplification that a system is capable of. The maximum incremental gain of an operator is therefore defined as the largest possible ratio of the norm of the difference between any two output to that between the inputs.

Several years later, Zames writes [30]:

> In order to behave properly an input/output system must usually have two properties:
>
> 1. Bounded intputs must produce bounded outputs – i.e., the system must be nonexplosive.
> 2. Outputs must not be critically sensitive to small changes in inputs – changes such as those caused by noise.

Despite this early emphasis on continuity, input/output theory has subsequently focussed almost exclusively on properties measured from zero – perhaps due to the focus on regulating systems to a desired equilibrium behavior. If, however, the solution of interest is not an equilibrium, or one is interested in questions of sensitivity, it becomes essential to study incremental properties. One salient example is the sensitivity of neural network classifiers to so-called adversarial examples – a minor change in the input, for example, the addition of some noise, results in a misclassification with high confidence [31]. This phenomenon motivates methods for training neural networks with Lipschitz constants, or, in the language of systems theory, finite incremental gain [32], [33].

One area where incremental analysis has thrived is in the theory of optimization. It is natural in optimization to study properties defined between arbitrary pairs of trajectories, as one cannot know the special trajectory of interest (the solution) until the optimization problem is solved. One of the central properties in the theory of optimization, and also in many of the developments of this thesis, is *monotonicity*, a generalization of "energy dissipation". Duffin, in 1946, studied circuits with *quasi-linear* resistors – resistors with non-decreasing $i - v$ characteristic. These resistors were a prototypical monotone element. Other related properties appear in the work of Golomb [34], Zarantonello [35] and Dolph [36], but it was Minty [37]–[39] who refined the concept of quasi-linearity to found the theory of monotonicity, again in the context of nonlinear circuits. Further work on monotonicity in nonlinear circuits was done by Desoer and Wu [40], before the influential paper of Rockafellar [41] established monotonicity as a fundamental property in the theory of optimization. Monotonicity has since become a pillar of the theory of convex optimization [42]–[47], forming the basis of a large body of work on tractable first order methods for large-scale and nonsmooth optimization problems, which have seen a surge of interest in the last decade. However, the physical significance of maximal monotonicity

in nonlinear circuit theory has been somewhat forgotten. This thesis revisits nonlinear circuit theory with modern developments in monotone operator theory.

This thesis is divided in two parts: graphical methods and algorithmic methods. Chapter 2 describes graphical methods for studying the incremental properties of input/output systems connected in feedback. The Scaled Relative Graph (SRG) [48], a new tool in the theory of monotone operators, is shown to be a generalization of the classical Nyquist diagram [9] which may be plotted for nonlinear operators. This opens a new avenue for the graphical analysis of the properties of nonlinear operators. We apply the SRG to incremental stability analysis, and give a simple graphical stability test for stable nonlinear operators in feedback which encompasses results such as the Nyquist criterion, incremental circle criterion, incremental small gain theorem, incremental passivity theorem and incremental secant condition.

Chapter 3 describes algorithmic methods for solving nonlinear circuits formed from the series and parallel interconnection of devices which are monotone. This represents a generalization of the linear theory of passivity which retains a connection between physics and computation – in this case, the connection arises from the equivalence between the splitting methods of modern optimization theory and series/parallel port interconnections of circuit theory. A new splitting algorithm is presented which matches an arbitrary series/parallel structure, and may be used to efficiently solve large scale circuits with arbitrary series/parallel structure.

Chapter 4 extends these methods to circuits formed by the *difference* of monotone circuits. This encompasses circuits such as the van der Pol oscillator and FitzHugh Nagumo model, which exhibit steady state oscillatory behavior. A generalization of the Douglas-Rachford splitting algorithm is developed which suits the *mixed feedback* structure of these two circuits: a passive, LTI network in feedback with the difference of two monotone operators.

In the remainder of this chapter, we give a brief overview of the mathematical preliminaries in input/output systems theory and monotone operator theory which will be used throughout the thesis.

1.1 MATHEMATICAL BACKGROUND

1.1.1 *Signal spaces, operators and relations*

A Hilbert space $\mathcal{H}$ is a vector space equipped with an inner product, $\langle \cdot | \cdot \rangle : \mathcal{H} \times \mathcal{H} \to \mathbb{C}$, and an induced norm $\|x\| \coloneqq \sqrt{\langle x|x \rangle}$.

We will pay particular attention to Lebesgue spaces of square-integrable functions. Given a time axis $\mathbb{T}$, which is one of $(-\infty, \infty)$, $[0, \infty)$ or $[0, T]$, and a field $\mathbb{F} \in \{\mathbb{R}, \mathbb{C}\}$, we

define the space $L^n_{2,\mathbb{T}}(\mathbb{F})$ by the set of signals $u : \mathbb{R}_{\geq 0} \to \mathbb{F}^n$ such that

$$\|u\| \coloneqq \left(\int_{\mathbb{T}} \bar{u}(t) u(t) \, \mathrm{d}t \right)^{\frac{1}{2}} < \infty,$$

where $\bar{u}(t)$ denotes the conjugate transpose of $u(t)$. The inner product of $u, y \in L^n_{2,\mathbb{T}}(\mathbb{F})$ is defined by

$$\langle u | y \rangle \coloneqq \int_{\mathbb{T}} \bar{u}(t) y(t) \, \mathrm{d}t \, .$$

The Fourier transform of $u \in L^n_{2,\mathbb{T}}(\mathbb{F})$ is defined as

$$\hat{u}(j\omega) \coloneqq \int_{\mathbb{T}} e^{-j\omega t} u(t) \, \mathrm{d}t \, .$$

We omit the dimension, field and time axis when they are immaterial or clear from context.

The discrete-time counterpart of $L_{2,\mathbb{T}}$ is denoted by $l_{2,\mathbb{T}}$, the space of square-summable sequences:

$$\Sigma_{\mathbb{T}} u^\top(t) u(t) < \infty,$$

where $\mathbb{T} \subseteq \mathbb{Z}$. Again, this is a Hilbert space with inner product

$$\langle u | y \rangle \coloneqq \Sigma_{\mathbb{T}} u^\top(t) y(t)$$

and induced norm $\|u\| \coloneqq \sqrt{\langle u | u \rangle}$.

For some $T \in \mathbb{R}_{\geq 0}$, define the truncation operator P_T by

$$(P_T u)(t) \coloneqq \begin{cases} u(t) & t \leq T, \\ 0 & t > T, \end{cases}$$

where $t \in \mathbb{R}_{\geq 0}$ and u is an arbitrary signal. Define the *extension of* $L^n_{2,[0,\infty)}(\mathbb{F})$ [30], [49, p. 22], [50, p. 172] to be the space

$$L^n_{2,e}(\mathbb{F}) \coloneqq \{ u : \mathbb{R}_{\geq 0} \to \mathbb{F}^n \mid \|P_T u\| < \infty \text{ for all } T \in \mathbb{R}_{\geq 0} \} \, .$$

An *operator*, or *system*, on a space $\mathcal{X}$, is a possibly multi-valued map $R : \mathcal{X} \to \mathcal{X}$. The identity operator, which maps $u \in \mathcal{X}$ to itself, is denoted by I. We denote the domain of an operator R by $\operatorname{dom} R$. The *graph*, or *relation*, of an operator, is the set $\{u, y \mid u \in \operatorname{dom} R, y \in R(u)\} \subseteq \mathcal{X} \times \mathcal{X}$. We use the notions of an operator and its relation interchangeably, and denote them in the same way. The relation of an operator may be thought of as an input/output partition of a behavior [51, Def. 3.3.1].

The usual operations on functions can be extended to relations:

$$\begin{aligned} S^{-1} &= \{(y, u) \mid y \in S(u)\} \\ S + R &= \{(x, y + z) \mid (x, y) \in S, (x, z) \in R\} \\ SR &= \{(x, z) \mid \exists \, y \text{ s.t. } (x, y) \in R, (y, z) \in S\}. \end{aligned}$$

Note that S^{-1} always exists, but is not an inverse in the usual sense. In particular, it is in general not the case that $S^{-1}S = I$.

An operator R on L_2 or $L_{2,e}$ is said to be *causal* if $P_T(R(u)) = P_T(R(P_T u))$ for all u.

1.1.2 *Incremental input/output systems theory*

Incremental properties feature heavily in Desoer and Vidyasagar's classic text [50]. The general pattern is that requiring a property to be verified for every possible input, rather than just a single distinguished input ($u = 0$, for example), leads to much stronger results, often comparable to the results that may be proved for linear systems. This is perhaps unsurprising, as any property of a linear system is automatically incremental.

In this section, we define the input/output properties of systems considered throughout the thesis. We begin with a definition of incremental stability.

Definition 1.1. Let $R : L_{2,e} \to L_{2,e}$. The *incremental L_2 gain* of R is

$$\mu \coloneqq \lim_{T\to\infty} \sup_{u_1,u_2\in\operatorname{dom} R} \frac{\|P_T y_1 - P_T y_2\|}{\|P_T u_1 - P_T u_2\|},$$

where $y_1 \in R(P_T u_1)$, $y_2 \in R(P_T u_2)$. If $\mu < \infty$, R is said to have *finite incremental L_2 gain*, or be *incrementally L_2 stable*. ⌟

The second class of properties relate to passivity.

Definition 1.2. Let $R : L_{2,e} \to L_{2,e}$. Let $\langle u|y\rangle_T \coloneqq \int_0^T u^\top(t)y(t)\mathrm{d}t$. Then:

1. R is said to be *incrementally passive* if

   $$\langle u_1 - u_2|y_1 - y_2\rangle_T \geq 0$$

   for all $T \geq 0$, all $u_1, u_2 \in \operatorname{dom} R$ and $y_1 \in R(u_1), y_2 \in R(u_2)$.

2. R is said to be *λ-input-strict incrementally passive* if

   $$\langle u_1 - u_2|y_1 - y_2\rangle_T \geq \lambda\|P_T u_1 - P_T u_2\|^2$$

   for all $T \geq 0$, all $u_1, u_2 \in \operatorname{dom} R$ and $y_1 \in R(u_1), y_2 \in R(u_2)$.

3. R is said to be *γ-output-strict incrementally passive* if

   $$\langle u_1 - u_2|y_1 - y_2\rangle_T \geq \gamma\|P_T y_1 - P_T y_2\|^2$$

   for all $T \geq 0$, all $u_1, u_2 \in \operatorname{dom} R$ and $y_1 \in R(u_1), y_2 \in R(u_2)$. ⌟

1.1.3 *Monotone operator theory*

Monotonicity on a Hilbert space $\mathcal{H}$ is defined as follows.

Definition 1.3. A relation $S \subseteq \mathcal{H} \times \mathcal{H}$ is called *monotone* if

$$\langle u_1 - u_2|y_1 - y_2\rangle \geq 0$$

for any $(u_1, y_1), (u_2, y_2) \in S$. A monotone relation is called *maximal* if it is not properly contained in any other monotone relation. ⌟

By way of example, a relation $S \subseteq \mathbb{R} \times \mathbb{R}$ is monotone if its graph is non-decreasing, and maximal if its graph has no endpoints. Note that this definition refers to monotonicity in the operator theoretic sense, and this is distinct from the notion of monotonicity in the sense of partial order preservation by a state-space system (see, for example, [52]).

Definition 1.4. A relation S has a *Lipschitz constant of* $\lambda > 0$, or is λ-*Lipschitz* if, for all $(u_1, y_1), (u_2, y_2) \in S$,

$$\|y_1 - y_2\| \leq \lambda \|u_1 - u_2\|.$$

If $\lambda < 1$, S is called a *contraction*. If $\lambda = 1$, S is called *nonexpansive*. ⌟

Note that if S is λ-Lipschitz, it is also $\bar{\lambda}$-Lipschitz for all $\bar{\lambda} > \lambda$.

Definition 1.5. Given $\vartheta \in (0, 1)$, a relation S is said to be ϑ-*averaged* if $S = (1 - \vartheta)I + \vartheta G$, where I is the identity relation and G is some nonexpansive relation. ⌟

Definition 1.6. Given $\mu > 0$, a relation S is μ-*coercive* or μ-*strongly monotone* if, for all $(u_1, y_1), (u_2, y_2) \in S$,

$$\langle u_1 - u_2 | y_1 - y_2 \rangle \geq \mu \|u_1 - u_2\|^2.$$

S is called μ-*hypomonotone* in the case that $\mu < 0$. If the sign of μ is unknown, we simply say S is μ-*monotone*. ⌟

Definition 1.7. Given $\gamma > 0$, a relation S is γ-*cocoercive* if, for all $(u_1, y_1), (u_2, y_2) \in S$,

$$\langle u_1 - u_2 | y_1 - y_2 \rangle \geq \gamma \|y_1 - y_2\|^2.$$

S is called γ-*cohypomonotone* in the case that $\gamma < 0$. ⌟

It is seen immediately that F is μ-coercive if and only if F^{-1} is μ-cocoercive. It also follows from the Cauchy-Schwarz inequality that F has a Lipschitz constant of $1/\gamma$ if F is γ-cocoercive. Finally, if A is μ-coercive (resp. γ-cocoercive) and B is monotone, $A + B$ is is μ-coercive (resp. γ-cocoercive). For more details on these properties, we refer the reader to [44, §2.2] and [53].

Monotone operator theory is closely related to the classical input/output theory of nonlinear systems. All of the properties studied in the theory of monotone operators correspond to a property in input/output system theory, the difference being that the former are defined for an arbitrary Hilbert space, while the latter are defined on L_2 or $L_{2,e}$.

Table 1.1 shows these equivalences. In the remainder of this thesis, we adopt "positivity" for operators on L_2 or l_2, "monotonicity" for operators on other Hilbert spaces, and "passivity" for operators on $L_{2,e}$ or $l_{2,e}$, and when referring to the theorems classically referred to as *passivity theorems* [50, Chapter 6]. These different names have historically been applied in different fields, and all refer to essentially the same property - the monotonicity of an operator (or family of operators) on a Hilbert space. Passivity is a stronger property than positivity, the two coinciding only when the operator is causal [50,

Lemma 2, p. 200]. The methods of this thesis apply equally well to causal and non-causal operators, and no assumptions, nor guarantees, of causality are made. This allows the results to apply verbatim to applications where causality is irrelevant, such as spatial dynamics. If causality is important, however, it must be verified by additional analysis.

property	$L_{2,[0,\infty)}$	$L_{2,e}$	Hilbert
$\|y_1 - y_2\| \leq \mu \|u_1 - u_2\|$	finite incremental gain	finite incremental gain	Lipschitz
$\langle u_1 - u_2 \| y_1 - y_2 \rangle \geq 0$	incremental positivity	incremental passivity	monotonicity
$\langle u_1 - u_2 \| y_1 - y_2 \rangle \geq \lambda \|u_1 - u_2\|^2$	incremental input-strict positivity	incremental input-strict passivity	strong monotonicity or coercivity
$\langle u_1 - u_2 \| y_1 - y_2 \rangle \geq \gamma \|y_1 - y_2\|^2$	incremental output-strict positivity	incremental output-strict passivity	cocoercivity

Table 1.1: A partial bilingual dictionary from input/output system theory to monotone operator theory. The first column gives properties between pairs of inputs u_1, u_2 and the corresponding outputs y_1, y_2. Greek letters denote positive scalars. The second and third columns give the system theory names of properties of operators on either $L_{2,[0,\infty)}$ or $L_{2,e}$, as defined by [50]. The fourth column gives the names of these properties in monotone operator theory, for operators on an arbitrary Hilbert space – see, for example, [48].

1.2 PUBLICATIONS

Preprints

- T. Chaffey, F. Forni & R. Sepulchre (2021), *Graphical Nonlinear System Analysis*, `arXiv:2107.11272` (submitted to IEEE Transactions on Automatic Control)
- T. Chaffey & R. Sepulchre (2021), *Monotone one-port circuits*, `arXiv:2111.15407` (submitted to IEEE Transactions on Automatic Control)
- T. Chaffey & A. Padoan, *Circuit Model Reduction with Scaled Relative Graphs*, `arxiv:2204.01434` (submitted to CDC 2022)

Journal papers

- T. Chaffey (2022), *A rolled-off passivity theorem*, Systems and Control Letters (162)

- A. Das, T. Chaffey & R. Sepulchre (2022), *Oscillation in Mixed-Feedback Systems*, Systems and Control Letters (166)

Conference papers

- T. Chaffey, F. Forni & R. Sepulchre, *Scaled relative graphs for system analysis*, 2021 IEEE Conference on Decision and Control (Outstanding Student Paper Award)
- T. Chaffey & R. Sepulchre, *Monotone RLC Circuits*, 2021 European Control Conference (Best Student Paper Award)

Conference tutorial sessions

- T. Chaffey & R. Sepulchre, *Scaled relative graphs for system analysis*, 2022 European Control Conference (forthcoming)

2 SYSTEM ANALYSIS WITH SCALED RELATIVE GRAPHS

ABSTRACT

We use the recently introduced concept of a Scaled Relative Graph (SRG) to develop a graphical analysis of input-output properties of feedback systems. The SRG of a nonlinear operator generalizes the Nyquist diagram of an LTI system. In the spirit of classical control theory, important robustness indicators of nonlinear feedback systems are measured as distances between SRGs.

2.1 INTRODUCTION

The graphical analysis of a feedback system via the Nyquist diagram of its return ratio is a foundation of classical control theory. It underlies the analysis concept of stability margins and the design concept of loop shaping, which themselves provide the grounds for the gap metric [54], [55] and H_∞ control [56].

The Nyquist diagram also has a fundamental place in the theory of nonlinear systems of the Lur'e form (that is, systems composed of an LTI forward path in feedback with a static nonlinearity). The circle and Popov criteria allow the stability of a Lur'e system to be proved by verifying a geometric condition on the Nyquist diagram of the LTI component [50]. The geometric condition is determined by the properties of the static nonlinearity. Notably, only the Nyquist diagram of the LTI component is defined, owing to a lack of a suitable definition of phase for nonlinear systems. At best, the frequency response of a nonlinear system may be computed approximately. The describing function [57]–[59] gives rise to a family of Nyquist curves for a nonlinearity, parameterized by the amplitude of the input. Other efforts to generalize frequency response to nonlinear systems include the work of Pavlov, van de Wouw, and Nijmeijer [60] on Bode diagrams for convergent systems, and two recently introduced notions of nonlinear phase by Chen *et al.* [61], [62].

In this chapter, we show that the Scaled Relative Graph of Ryu, Hannah, and Yin [48] generalizes the Nyquist diagram of an LTI transfer function, and may be plotted for nonlinear input/output operators. The SRG has been introduced in the theory of optimization to visualize incremental properties of nonlinear operators, that is, properties that are measured between pairs of input/output trajectories, such as Lipschitz continuity and maximal monotonicity. Such properties may be verified by checking geometric conditions on the SRG of an operator. Algebraic manipulations to the operator correspond to geometric manipulations to the SRG. The SRG gives rise to simple, intuitive and rigorous proofs of the convergence of many algorithms in convex optimization. Furthermore, the

tool is particularly suited to proving tightness of convergence bounds, and has been used to prove novel tightness results [48], [63].

The SRG allows the classical techniques of the Nyquist diagram to be applied to nonlinear input/output feedback systems, giving graphical methods to determine incremental properties, such as finite incremental gain and incremental passivity. In Section 2.3.1, we prove a version of the Nyquist criterion for stable nonlinear operators, recovering the familiar "leave the point -1 on the left" rule of thumb for stable LTI transfer functions. The distance from the SRG to the point -1 is a nonlinear stability margin; like the classical stability margin, it is the inverse of the incremental gain of the sensitivity operator. In Section 2.3.2, we show that placing a second system in the return path of the feedback interconnection corresponds to inflating the -1 point to the negative of the SRG of the second system. This allows a nonlinear robustness margin to be defined as the distance between two SRGs - the margin is the inverse of the incremental gain of the feedback interconnection. This result encompasses the incremental circle, small gain and passivity theorems [30], [50], [64], and furthermore allows an incremental gain bound to be calculated.

The idea of proving stability by showing that two graphs are separated is not new, and indeed is the basis of the line of research on the gap and related metrics [54], [55], [65], [66]. Georgiou and Smith [67] define robustness margins for nonlinear systems by calculating the distance between the graphs of two input/output operators. Analysis using Integral Quadratic Constraints [68] also relies on showing the separation of two graphs [69], and unifies earlier results on using multipliers to allow the passivity theorem to be applied to feedback interconnections of non-passive systems [70]–[72]. The primary advantage of SRG techniques is the ability to visualize margins graphically. Furthermore, SRGs pertain to incremental input-output properties, whereas classical graph-based methodologies have focussed on non-incremental properties. For instance, L_2 stability only guarantees boundedness of the input-output operator, whereas incremental L_2 stability ensures continuity of the operator. Efforts to prove continuity using IQCs and multipliers have been hindered by the limitations of large classes of dynamic multipliers for incremental analysis [73].

Sections 2.4 and 2.5 give explicit characterizations of the SRGs of several important classes of systems. In Section 2.4, we show that the SRG of an LTI transfer function is the convex hull of its Nyquist diagram under a particular change of coordinates. In Section 2.5, we derive a bound on the SRG of a static nonlinearity which is incrementally in a sector. This bound is closely related to the circles of the incremental circle criterion. We then show that if the characteristic curve of the nonlinearity contains a point where the slope switches from one extreme to the other, the SRG of the nonlinearity fills this bounding region. This gives a precise characterization of the SRGs of the saturation nonlinearity and the rectified linear unit (ReLU), and the limiting cases of the ideal relay and diode.

In Section 2.7, we study cyclic feedback systems, and give an SRG for the cascade of

n output-strict incrementally passive operators. Consideration of the gain margin gives rise to the incremental version of the secant condition [74]–[76], and gives a geometric interpretation to the original result. In Sections 2.6 and 2.8, we show that SRG techniques can be used to study feedback systems with pure delay. Finally, in Section 2.9, we define a property that describes systems which only violate incremental positivity when their incremental gain is small, and prove a relaxation of the incremental passivity theorem for such systems. We begin in Section 2.2 by formally introducing the SRG.

2.2 SCALED RELATIVE GRAPHS

We define SRGs in the same way as Ryu, Hannah, and Yin [48], with the minor modification of allowing complex valued inner products.

Let $\mathcal{L}$ be a Hilbert space. The angle between $u, y \in \mathcal{L}$ is defined as

$$\angle(u, y) \coloneqq \operatorname{acos} \frac{\operatorname{Re}\langle u|y\rangle}{\|u\|\|y\|}.$$

Let $R : \mathcal{L} \to \mathcal{L}$ be an operator. Given $u_1, u_2 \in \mathcal{U} \subseteq \mathcal{L}$, $u_1 \neq u_2$, define the set of complex numbers $z_R(u_1, u_2)$ by

$$z_R(u_1, u_2) \coloneqq \left\{ \frac{\|y_1 - y_2\|}{\|u_1 - u_2\|} e^{\pm j \angle(u_1 - u_2, y_1 - y_2)} \;\middle|\; y_1 \in R(u_1), y_2 \in R(u_2) \right\}.$$

If $u_1 = u_2$ and there are corresponding outputs $y_1 \neq y_2$, then $z_R(u_1, u_2)$ is defined to be $\{\infty\}$. If R is single valued at u_1, $z_R(u_1, u_1)$ is the empty set.

The *Scaled Relative Graph* (SRG) of R over $\mathcal{U} \subseteq \mathcal{L}$ is then given by

$$\operatorname{SRG}_{\mathcal{U}}(R) \coloneqq \bigcup_{u_1, u_2 \in \mathcal{U}} z_R(u_1, u_2).$$

If $\mathcal{U} = \mathcal{L}$, we write $\operatorname{SRG}(R) \coloneqq \operatorname{SRG}_{\mathcal{L}}(R)$.

If R is linear and $\operatorname{dom} R$ is a linear subspace of $\mathcal{L}$, $Ru_1 - Ru_2 = R(u_1 - u_2) = Rv$ for some $v \in \operatorname{dom} R$, and we can define

$$z_R(v) \coloneqq \frac{\|Rv\|}{\|v\|} e^{\pm j \angle(v, Rv)}$$

and

$$\operatorname{SRG}_{\operatorname{dom} R}(R) \coloneqq \{z_R(v) | v \in \operatorname{dom} R, v \neq 0\}.$$

In the special case that R is linear and time invariant with transfer function $R(s)$, and $v(t) = e^{j\omega t}$, $\lim_{T\to\infty} \|R(P_T v)\|/\|P_T v\| = |R(j\omega)|$ and $\lim_{T\to\infty} \angle(P_T v, R(P_T v)) = |\arg R(j\omega)|$. Thus the gain and phase of the SRG generalize the classical notions of the gain and phase of an LTI transfer function.

2.2.1 *System properties from SRGs*

If $\mathcal{A}$ is a class of operators, we define the SRG of $\mathcal{A}$ by

$$\mathrm{SRG}(\mathcal{A}) \coloneqq \bigcup_{R \in \mathcal{A}} \mathrm{SRG}(R).$$

Note that a class of operators can be a single operator.

A class $\mathcal{A}$, or its SRG, is called *SRG-full* if

$$R \in \mathcal{A} \quad \Longleftrightarrow \quad \mathrm{SRG}(R) \subseteq \mathrm{SRG}(\mathcal{A}).$$

By construction, the implication $R \in \mathcal{A} \implies \mathrm{SRG}(R) \subseteq \mathrm{SRG}(\mathcal{A})$ is true. The value of SRG-fullness is in the reverse implication: $\mathrm{SRG}(R) \subseteq \mathrm{SRG}(\mathcal{A}) \implies R \in \mathcal{A}$. This allows class membership to be tested graphically. If $\mathcal{A}$ is the class of systems with a particular system property, SRG-fullness of $\mathcal{A}$ allows this property to be verified for a particular operator R by plotting its SRG. If $\mathrm{SRG}(R) \subseteq \mathrm{SRG}(\mathcal{A})$, R has the property.

The following proposition gives the SRGs of the classical system properties introduced in Section 1.1.2.

Proposition 2.1. *The SRGs of incrementally positive systems (top left), input-strict incrementally positive systems (top right), output-strict incrementally positive systems (bottom right) and incrementally L_2 bounded systems (bottom left) are shown below.*

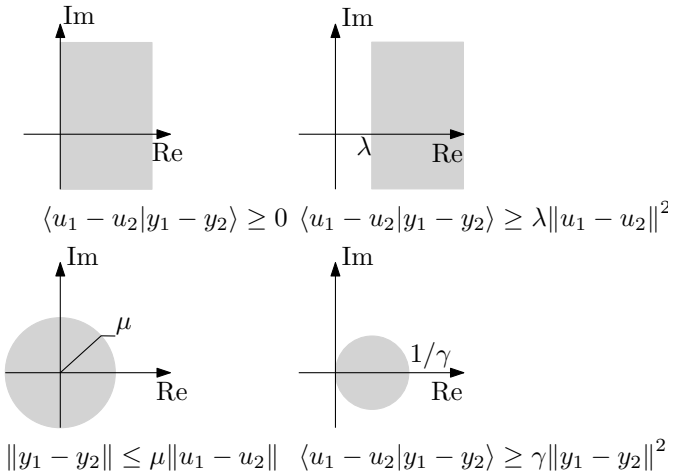

All of these classes are SRG-full.

Proof. These SRGs are proved in [48], and all of the shapes follow from quick calculations. SRG-fullness follows from [48, Thm. 3.5]. □

SRG-fullness of the classes of Proposition 2.1 means, for example, that if the SRG of a system lies in the right half plane, the system is incrementally positive, and if the SRG of a system is bounded, the system has finite incremental L_2 gain. These are reminiscent of the facts that an LTI system is passive if its Nyquist diagram lies in the right half plane,

and has finite H_∞ norm if its Nyquist diagram is bounded. We will show in Section 2.4 that Proposition 2.1 is indeed a generalization of these classical properties.

The properties of finite incremental L_2 gain and incremental positivity are particular examples of incremental Integral Quadratic Constraints (IQCs) [68]. A striking corollary of Ryu, Hannah, and Yin [48, Thm. 3.5] is that any SRG defined by a soft incremental IQC is SRG-full.

Proposition 2.2. *Let $u_i(t)$ denote the input to an arbitrary operator on L_2, and $y_i(t)$ denote a corresponding output. Let $\Delta u = u_1 - u_2$ and $\Delta y = y_1 - y_2$, and $\hat{x}(\omega)$ denote the Fourier transform of signal $x(t)$. Then the classes of operators which obey either of the constraints*

$$\int_{-\infty}^{\infty} \begin{pmatrix} \Delta\hat{u}(\omega) \\ \Delta\hat{y}(\omega) \end{pmatrix}^* \begin{pmatrix} a & b \\ c & d \end{pmatrix} \begin{pmatrix} \Delta\hat{u}(\omega) \\ \Delta\hat{y}(\omega) \end{pmatrix} \mathrm{d}\omega \geq 0, \tag{2.1}$$

$$\int_{0}^{\infty} \begin{pmatrix} \Delta u(t) \\ \Delta y(t) \end{pmatrix}^* \begin{pmatrix} a & b \\ c & d \end{pmatrix} \begin{pmatrix} \Delta u(t) \\ \Delta y(t) \end{pmatrix} \mathrm{d}t \geq 0, \tag{2.2}$$

where $a, b, c, d \in \mathbb{R}$, are SRG-full.

Proof. Equation (2.1) gives

$$a\|\Delta\hat{u}\|^2 + (b+c)\langle\Delta\hat{u}|\Delta\hat{y}\rangle + d\|\Delta\hat{y}\|^2 \geq 0.$$

By Parseval's theorem, this is equivalent to

$$a\|\Delta u\|^2 + (b+c)\langle\Delta u|\Delta y\rangle + d\|\Delta y\|^2 \geq 0,$$

which is also implied by (2.2). The result then follows from [48, Thm. 3.5]. □

A class of operators defined by a geometric region is SRG-full.

Proposition 2.3. *Let $\mathcal{C} \subseteq \mathbb{C}$. The class of operators $\mathcal{A}$ defined by*

$$\mathcal{A} \coloneqq \{R \text{ an operator} \,|\, \mathrm{SRG}(R) \subseteq \mathcal{C}\}$$

is SRG-full.

Proof. The definition of $\mathcal{A}$ can be written as

$$R \in \mathcal{A} \iff \mathrm{SRG}(R) \subseteq \mathcal{C},$$

which is the definition of SRG-fullness. □

This fact is particularly useful for system analysis, as it allows the SRG of an operator to be over-approximated by a geometric region if, for example, the precise SRG is unknown, or the SRG does not obey the properties necessary to apply a theorem. Over-approximating an SRG simply amounts to making the analysis more conservative.

2.2.2 *Interconnections*

Under mild conditions on the SRG, system interconnections correspond to geometric manipulations of their SRGs. These interconnection results are proved by Ryu, Hannah, and Yin [48] in Theorems 4.1-4.5. We recall the statements of these theorems in the following five propositions.

Proposition 2.4. *If $\mathcal{A}$ and $\mathcal{B}$ are SRG-full, then $\mathcal{A} \cap \mathcal{B}$ is SRG-full, and*

$$\mathrm{SRG}\,(\mathcal{A} \cap \mathcal{B}) = \mathrm{SRG}\,(\mathcal{A}) \cap \mathrm{SRG}\,(\mathcal{B}).$$

Proposition 2.5. *Let $\alpha \in \mathbb{R}, \alpha \neq 0$. If $\mathcal{A}$ is a class of operators,*

$$\mathrm{SRG}\,(\alpha\mathcal{A}) = \mathrm{SRG}\,(\mathcal{A}\alpha) = \alpha\,\mathrm{SRG}\,(\mathcal{A}),$$
$$\mathrm{SRG}\,(I + \mathcal{A}) = 1 + \mathrm{SRG}\,(\mathcal{A}).$$

Furthermore, if $\mathcal{A}$ is SRG-full, then $\alpha\mathcal{A}$, $\mathcal{A}\alpha$ and $I + \mathcal{A}$ are SRG-full.

We define inversion in the complex plane by the Möbius transformation $re^{j\omega} \mapsto (1/r)e^{j\omega}$. This is "inversion in the unit circle": points outside the unit circle map to the inside, and vice versa. The points 0 and ∞ are exchanged under inversion.

Proposition 2.6. *If $\mathcal{A}$ is a class of operators, then*

$$\mathrm{SRG}\,(\mathcal{A}^{-1}) = (\mathrm{SRG}\,(\mathcal{A}))^{-1}.$$

Furthermore, if $\mathcal{A}$ is SRG-full, then $\mathcal{A}^{-1}$ is SRG-full.

Define the line segment between $z_1, z_2 \in \mathbb{C}$ as $[z_1, z_2] \coloneqq \{\alpha z_1 + (1-\alpha)z_2 \,|\, \alpha \in [0,1]\}$. A class of operators $\mathcal{A}$ is said to satisfy the *chord property* if $z \in \mathrm{SRG}\,(\mathcal{A}) \setminus \{\infty\}$ implies $[z, \bar{z}] \subseteq \mathrm{SRG}\,(\mathcal{A})$.

Proposition 2.7. *Let $\mathcal{A}$ and $\mathcal{B}$ be classes of operators, such that $\infty \notin \mathrm{SRG}\,(\mathcal{A})$ and $\infty \notin \mathrm{SRG}\,(\mathcal{B})$. Then:*

1. *if $\mathcal{A}$ and $\mathcal{B}$ are SRG-full, then* $\mathrm{SRG}\,(\mathcal{A} + \mathcal{B}) \supseteq \mathrm{SRG}\,(\mathcal{A}) + \mathrm{SRG}\,(\mathcal{B})$.
2. *if either $\mathcal{A}$ or $\mathcal{B}$ satisfies the chord property, then* $\mathrm{SRG}\,(\mathcal{A} + \mathcal{B}) \subseteq \mathrm{SRG}\,(\mathcal{A}) + \mathrm{SRG}\,(\mathcal{B})$.

Under additional assumptions, ∞ can be allowed - see the discussion following [48, Thm. 4.4].

Define the *right-hand arc*, $\mathrm{Arc}^+\,(z, \bar{z})$, between z and $\bar{z}$ to be the arc between z and $\bar{z}$ with centre on the origin and real part greater than or equal to $\mathrm{Re}(z)$. The *left-hand arc*, $\mathrm{Arc}^-\,(z, \bar{z})$, is defined the same way, but with real part less than or equal to $\mathrm{Re}(z)$. Formally,

$$\begin{aligned}\mathrm{Arc}^+\,(z, \bar{z}) \coloneqq \{&re^{j(1-2\vartheta)\phi} \mid z = re^{j\phi},\\ &\phi \in (-\pi, \pi],\, \vartheta \in [0,1],\, r \geq 0\},\\ \mathrm{Arc}^-\,(z, \bar{z}) \coloneqq &-\mathrm{Arc}^+\,(-z, -\bar{z}).\end{aligned}$$

A class of operators $\mathcal{A}$ is said to satisfy the *right hand (resp. left hand) arc property* if, for all $z \in \mathrm{SRG}(\mathcal{A})$, $\mathrm{Arc}^+(z, \bar{z}) \in \mathrm{SRG}(\mathcal{A})$ (resp. $\mathrm{Arc}^-(z, \bar{z}) \in \mathrm{SRG}(\mathcal{A})$).

Proposition 2.8. *Let $\mathcal{A}$ and $\mathcal{B}$ be classes of operators, such that $\infty \notin \mathrm{SRG}(\mathcal{A})$, $\mathcal{A} \neq \varnothing$, $\infty \notin \mathrm{SRG}(\mathcal{B})$ and $\mathcal{B} \neq \varnothing$. Then:*

1. *if $\mathcal{A}$ and $\mathcal{B}$ are SRG-full, then $\mathrm{SRG}(\mathcal{AB}) \supseteq \mathrm{SRG}(\mathcal{A})\,\mathrm{SRG}(\mathcal{B})$.*
2. *if either $\mathcal{A}$ or $\mathcal{B}$ satisfies an arc property, then $\mathrm{SRG}(\mathcal{AB}) \subseteq \mathrm{SRG}(\mathcal{A})\,\mathrm{SRG}(\mathcal{B})$.*

Under additional assumptions, ∞ and $\varnothing$ can be allowed - see the discussion following [48, Thm. 4.5].

2.2.3 *Scaled graphs about particular solutions*

Scaled relative graphs capture the behavior of an operator with respect to any possible operating point. However, the behavior about one or several specific inputs (for example, stable equilibria) may be of particular interest. The methods of this paper apply equally to the analysis of properties with respect to particular inputs, via the *scaled graph* (SG). For notational convenience, we only define the SG over the full space, but the SG can be restricted to a subset of the input space in the same way as the SRG.

Definition 2.1. Let $R : \mathcal{L} \to \mathcal{L}$. The *scaled graph* of R over $\mathcal{L}$ with respect to the input $u^\star$ is

$$\mathrm{SG}_{u^\star}(R) \coloneqq \bigcup_{u \in \mathcal{H}} z_R(u, u^\star). \qquad \lrcorner$$

Note that the SG of an LTI operator with respect to any input is equal to its SRG.

In the remainder of this section, we highlight the difference between incremental and input-specific properties, using the example of positivity.

Definition 2.2. An operator $H : L_2 \to L_2$ is said to be *positive about $u^\star \in L_2$* if, for all $u \in L_2$, $y \in H(u)$ and $y^\star \in H(u^\star)$, $\langle u - u^\star | y - y^\star \rangle > 0$. $\lrcorner$

From this definition, it follows immediately that an operator is positive about $u^\star$ if and only if its SG about $u^\star$ belongs to the closed right half plane. However, this does not mean its SG about any other input necessarily lies in the right half plane - Figure 2.1 gives such an example.

Taking the union of SGs over multiple trajectories allows properties that lie between trajectory-dependent and incremental to be verified. For example, Hines, Arcak, and Packard [77] define *equilibrium-independent passivity* to be passivity with respect to every constant input to the system (under assumptions on the system that ensure that there is a constant output for every constant input). This can be verified by checking that the union of SGs over constant inputs lies in the right half plane.

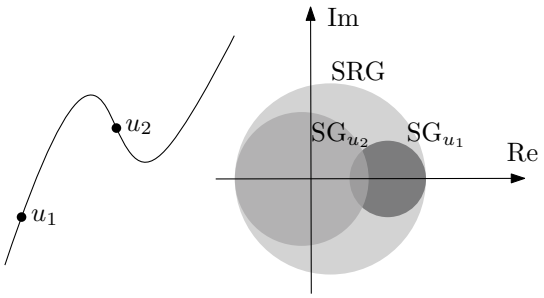

Figure 2.1: On the left is the $i - v$ characteristic of a resistor with a region of negative resistance. The resistor is passive about some operating points (including u_1), but not about others (such as u_2). On the right are the SGs computed at u_1 and u_2, as well as the SRG.

2.3 FEEDBACK ANALYSIS WITH SCALED RELATIVE GRAPHS

In this section, we demonstrate the use of scaled relative graphs for the stability analysis of feedback interconnections. We begin by using the SRG to generalize the Nyquist criterion to a stable nonlinear operator in unity gain negative feedback, and introduce a nonlinear stability margin. We then formulate a general stability theorem by inflating the point -1 to the negative of the SRG of an operator in the feedback path, and show that this theorem encompasses both the incremental small gain and incremental passivity theorems.

The SRG analysis holds provided the feedback system is a well-defined operator, which may not be known *a priori*. We deal with this issue using a homotopy argument similar to Megretski and Rantzer [68]. We place a gain $\tau \in [0,1]$ in the feedback loop, and assume stability for $\tau = 0$ (no feedback). We then use SRGs to show stability for every $\tau \in (0,1]$, which implies that there is no loss of stability as the feedback is introduced. This guarantees that the feedback interconnection defines an operator on L_2.

2.3.1 *A Nyquist stability criterion for stable nonlinear operators*

The Nyquist criterion characterizes the stability of a transfer function L in unity gain negative feedback (Figure 2.2) in terms of the distance between the Nyquist diagram of L and the point -1. This distance is called the *stability margin*, and is the inverse of the H_∞ norm of the sensitivity transfer function [78, p. 50]. In this section, we show that the Nyquist criterion and stability margin can be generalized to stable nonlinear operators by replacing the Nyquist diagram with an SRG. For such stable nonlinear operators, the closed loop system is stable if the SRG of the loop operator leaves -1 on the left.

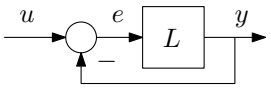

Figure 2.2: Unity gain negative feedback around the relation L.

Theorem 2.1. *Let $L : L_2 \to L_2$ be an operator with finite incremental L_2 gain. The closed loop operator shown in Figure 2.2 maps L_2 to L_2 and has finite incremental L_2 gain from u to y if*

$$0 \notin 1 + \tau\,\mathrm{SRG}\,(L) \quad \textit{for all } \tau \in (0, 1]. \tag{2.3}$$

The closed loop gain from u to e in Figure 2.2 is less than $1/s_m$, where s_m is the shortest distance between $\mathrm{SRG}\,(L)$ *and* -1.

Proof. We show that the mapping from τ to the incremental gain from u to y is continuous if (2.3) holds. Let the distance between $\mathrm{SRG}\,(L^{-1})$ and $-1/\tau$ be $r_\tau > 0$. Then $\mathrm{SRG}\,(L^{-1} + \tau I)$ is at least a distance of r_τ from the origin, so its inverse is at most r_τ from the origin, giving a bound of $1/r_\tau$ on the incremental gain from u to y, as illustrated below.

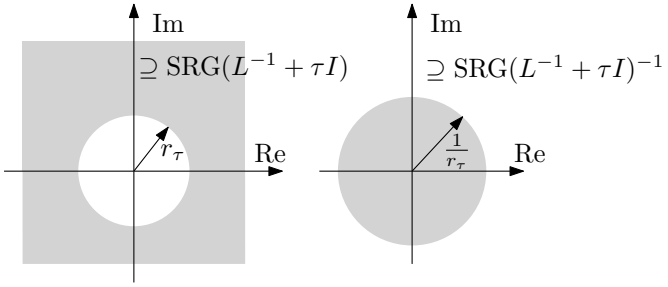

Let $\varepsilon > 0$ be smaller than r_τ. Then there exists a δ (positive or negative) such that, if τ is changed to $\tau + \delta$, the distance r_τ decreases by ε. Furthermore, as $\varepsilon \to 0$, $\delta \to 0$. This is a statement of the fact that the distance between a set and a point varies continuously with the position of the point. The closed incremental gain bound then increases to $1/(r_\tau - \varepsilon)$. This is bounded provided $\varepsilon < r_\tau$ (in which case δ small enough that $-(\tau + \delta)$ doesn't intersect $\mathrm{SRG}\,(L^{-1})$) and approaches r_τ as $\delta \to 0$. This shows continuity from τ to the closed loop incremental gain from u to y, and shows that finite incremental gain is preserved provided $\mathrm{SRG}\,(L^{-1})$ never intersects $-1/\tau$. In particular, all inputs in L_2 continue to map to outputs in L_2. We conclude finite incremental gain from u to y by setting $\tau = 1$.

To prove the second part of the theorem, note that the relation from u to e is given by

$$e = (I + L)^{-1} u.$$

If $\mathrm{SRG}\,(I + L)$ is bounded away from 0 by a distance s_m, then $(I + L)^{-1}$ has an L_2 gain bound of $1/s_m$. □

2.3.2 *A general feedback stability theorem*

The Nyquist stability criterion presented in the previous section can be generalized to allow a second nonlinear operator in the feedback path, by inflating the point -1 into the SRG of the feedback operator. The following theorem encompasses the classical small gain and passivity theorems as special cases.

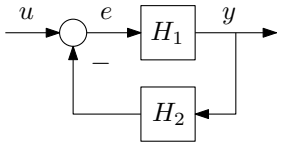

Figure 2.3: Negative feedback interconnection of H_1 and H_2.

Let $\mathcal{H}$ be a class of operators. By $\bar{\mathcal{H}}$, we will denote a class of operators such that $\mathcal{H} \subseteq \bar{\mathcal{H}}$ and $\mathrm{SRG}(\bar{\mathcal{H}})$ satisfies the chord property.

Theorem 2.2. *Consider the feedback interconnection shown in Figure 2.3 between any pair of operators $H_1 \in \mathcal{H}_1$ and $H_2 \in \mathcal{H}_2$, where $\mathcal{H}_1$ is a class of operators on L_2 with finite incremental gain, and $\mathcal{H}_2$ is a class of operators on L_2. If, for all $\tau \in (0,1]$,*

$$\mathrm{SRG}(\mathcal{H}_1)^{-1} \cap -\tau\,\mathrm{SRG}(\bar{\mathcal{H}}_2) = \varnothing,$$

then the feedback interconnection maps L_2 to L_2, and its incremental L_2 gain from u to y is bounded by $1/r_m$, where r_m is the shortest distance between $\mathrm{SRG}(\mathcal{H}_1^{-1})$ and $-\mathrm{SRG}(\bar{\mathcal{H}}_2)$.

The choice of which SRG to over-approximate is arbitrary. In the theorem, we have chosen $\mathrm{SRG}(\mathcal{H}_2)$, but it could just as well be $\mathrm{SRG}(\mathcal{H}_1^{-1})$.

Proof of Theorem 2.2. For a gain of τ in the feedback path, the class of operators from u to y is given by

$$(\mathcal{H}_1^{-1} + \tau\mathcal{H}_2)^{-1}.$$

Suppose there exists a positive number r_τ such that $|z - w| \geq r_\tau$ for all $z \in \mathrm{SRG}(\mathcal{H}_1^{-1})$, $w \in \mathrm{SRG}(-\tau\bar{\mathcal{H}}_2)$.

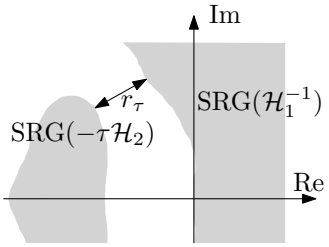

Since $\mathrm{SRG}(\mathcal{H}^{-1} + \tau H_2) \subseteq \mathrm{SRG}(\mathcal{H}^{-1}) + \tau\,\mathrm{SRG}(\bar{\mathcal{H}}_2)$, where $H_2 \in \bar{\mathcal{H}}_2$, it follows that $\mathrm{SRG}(\mathcal{H}_1^{-1} + \tau H_2)$ is bounded away from zero by a distance of r_τ for all $H_2 \in \bar{\mathcal{H}}_2$. In particular, this holds for every operator $H_2 \in \mathcal{H}_2$.

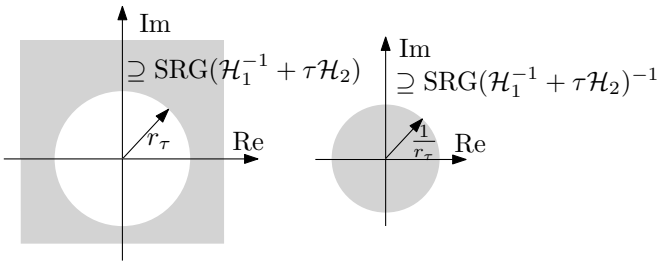

Applying the inverse transformation gives an incremental L_2 gain bound of $1/r_\tau$.

Ensuring this holds for all $\tau \in (0, 1]$ means the finite incremental gain of $\mathcal{H}_1$ is never lost, so the feedback interconnection remains defined on L_2. r_m corresponds to r_1. □

One case where the criteria of Theorem 2.2 are automatically satisfied is the classical small gain setting.

Corollary 2.1. *Consider the feedback interconnection shown in Figure 2.3 between any pair of operators $H_1 \in \mathcal{H}_1$ and $H_2 \in \mathcal{H}_2$, where $\mathcal{H}_1$ and $\mathcal{H}_2$ are the classes of operators on L_2 with finite incremental L_2 gain bounds of γ and λ, respectively. If $\gamma\lambda < 1$, then the feedback interconnection maps L_2 to L_2, and its incremental L_2 gain from u to y is bounded by $\gamma/(1-\gamma\lambda)$.*

Proof. The result follows directly from Theorem 2.2. The conditions of the theorem are shown to be satisfied by the geometry below.

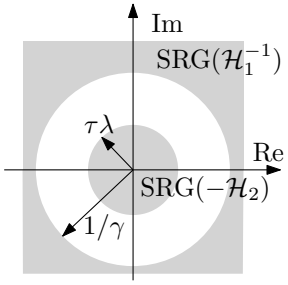

□

The second case where the conditions of Theorem 2.2 are automatically satisfied is in the feedback interconnection of incrementally passive systems. The classical incremental passivity theorem [30] is proved in the following corollary.

Corollary 2.2. *Consider the feedback interconnection shown in Figure 2.3 between any pair of operators $H_1 \in \mathcal{H}_1$ and $H_2 \in \mathcal{H}_2$, where $\mathcal{H}_1$ is the class of λ-input-strict incrementally positive operators which have an incremental L_2 gain bound of μ, and $\mathcal{H}_2$ is the class of incrementally positive operators. Assume $\lambda > 0$. Then the feedback interconnection maps L_2 to L_2, and its incremental L_2 gain from u to y is bounded by μ^2/λ.*

Proof. The SRGs of H_1 and H_2 are contained in the SRGs shown below. Note that these both satisfy the chord property.

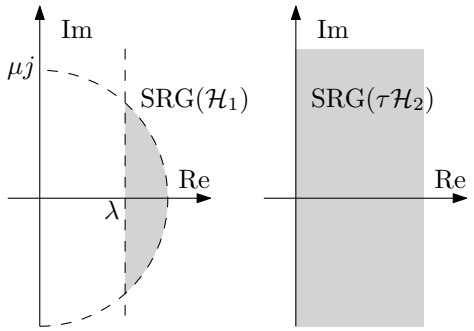

The SRG of the class of λ-input-strict incrementally positive operators is the circle with centre $1/(2\lambda)$ and radius $1/(2\lambda)$ (Proposition 2.1). This circle is parameterized as $\{(1/\lambda)\cos(\vartheta)\exp(j\vartheta), \mid 0 \leq \vartheta \leq 2\pi\}$. The semicircle with centre at the origin, positive real part and radius μ, which is the SRG of the class of incrementally positive operators with an incremental L_2 gain bound of μ, is parameterized as $\{\mu\exp(j\phi), \mid -\pi/2 \leq \phi \leq \pi/2\}$. The result then follows from Theorem 2.2 and the geometry below.

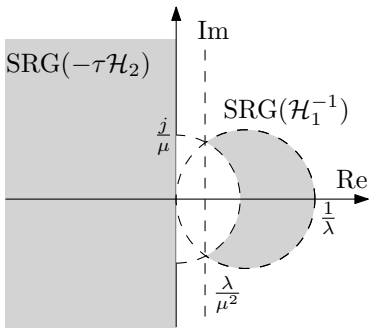

□

Corollary 2.2 characterizes the incremental gain of the closed loop. We can also characterize the incremental positivity of the closed loop, with another form of the classical passivity theorem. The following theorem generalizes [79, Prop. 8].

Theorem 2.3. *Consider the feedback interconnection shown in Figure 2.3 between any pair of operators $H_1 \in \mathcal{H}_1$ and $H_2 \in \mathcal{H}_2$, where $\mathcal{H}_1$ is the class of operators which are γ-output-strict incrementally positive, and $\mathcal{H}_2$ is the class of operators which are λ-input-strict incrementally positive (that is, have a shortage of input-strict incremental positive). If*

$$\lambda + \gamma \geq 0,$$

then the operator from u to y is $(\gamma + \lambda)$-output-strict incrementally positive.

Proof. Assume, without loss of generality, that $\lambda < 0$. We first prove the case where $\lambda + \gamma > 0$. This follows from the geometry shown below.

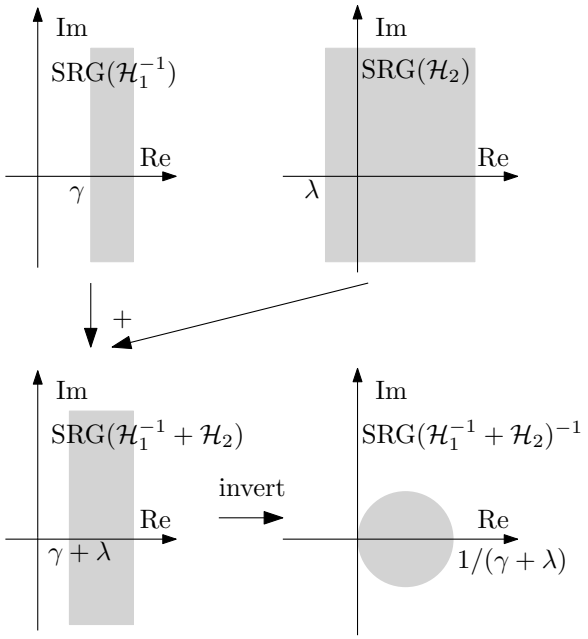

The case where $\lambda + \gamma = 0$ then follows by taking the limit $\lambda \to -\gamma$, and allowing the radius of the circle in the final panel above to tend to ∞. □

The definition of a stability margin for nonlinear operators leads us naturally to pose an "H_∞ design problem", in the same vein as Zames [56], to do with the maximization of the stability margin over a set of admissible controllers. A generalization of the H_∞ design question to nonlinear operators is as follows: given a plant G (modelled by an operator on L_2) in feedback with an uncertain block Δ known to be bounded by a particular SRG, design a controller C to maximize the distance between $\mathrm{SRG}\,(CG)^{-1}$ and $-\mathrm{SRG}\,(\Delta)$.

2.4 THE SCALED RELATIVE GRAPH OF AN LTI TRANSFER FUNCTION

In this section, we show that the SRG of a stable LTI transfer function is the convex hull of its Nyquist diagram, under the Beltrami-Klein mapping. We first presented this result in [79], and it was noted by Pates [80] that this is a special case of a more general phenomenon involving the numerical range of a linear operator. This allows computational methods for the numerical range to be applied directly to computation of the boundary of an SRG.

We begin by introducing some preliminaries from hyperbolic geometry in Section 2.4.1, before giving the main result in Section 2.4.2.

2.4.1 *Hyperbolic geometry*

We recall some necessary details from hyperbolic geometry. The notation is consistent with Huang, Ryu, and Yin [63].

Definition 2.3. Let $z_1, z_2 \in \mathbb{C}_{\mathrm{Im}\geq 0} \coloneqq \{z \in \mathbb{C} \mid \mathrm{Im}(z) \geq 0\}$, the upper half complex plane. We define the following sets:

1. $\mathrm{Circ}\,(z_1, z_2)$ is the circle through z_1 and z_2 with centre on the real axis. If $\mathrm{Re}(z_1) = \mathrm{Re}(z_2)$, this is defined as the infinite line passing through z_1 and z_2.

2. $\mathrm{Arc}_{\min}\,(z_1, z_2)$ is the arc of $\mathrm{Circ}\,(z_1, z_2)$ in $\mathbb{C}_{\mathrm{Im}\geq 0}$. If $\mathrm{Re}(z_1) = \mathrm{Re}(z_2)$, then $\mathrm{Arc}_{\min}\,(z_1, z_2)$ is $[z_1, z_2]$.

3. Given $z_1, \ldots, z_m \in \mathbb{C}_{\mathrm{Im}\geq 0}$, the *arc-edge polygon* is defined by: $\mathrm{Poly}\,(z_1) \coloneqq \{z_1\}$ and $\mathrm{Poly}\,(z_1, \ldots, z_m)$ is the smallest simply connected set containing S, where

$$S = \bigcup_{i,j=1\ldots m} \mathrm{Arc}_{\min}\,(z_i, z_j).$$

⌟

Note that, as $\mathrm{Poly}\,(z_1, \ldots, z_{m-1}) \subseteq \mathrm{Poly}\,(z_1, \ldots, z_{m-1}, z_m) \subseteq \mathbb{C}_{\mathrm{Im}\geq 0}$, the set $\mathrm{Poly}\,(Z)$, where Z is a countably infinite sequence of points in $\mathbb{C}_{\mathrm{Im}\geq 0}$, is well defined as the limit $\lim_{m\to\infty} \mathrm{Poly}\,(Z_m)$, where Z_m is the length m truncation of Z (see [81, p. 111]).

Definition 2.3 forms the basis of the Poincaré half plane model of hyperbolic geometry. Under the Beltrami-Klein mapping, $f \circ g$, where

$$f(z) = \frac{2z}{1 + |z|^2},$$
$$g(z) = \frac{z - i}{z + i},$$

$\mathbb{C}_{\mathrm{Im}\geq 0}$ is mapped onto the unit disc, and $\mathrm{Arc}_{\min}\,(z_1, z_2)$ is mapped to a straight line segment. We make the following definitions of convexity and the convex hull in the Poincaré half plane model.

Definition 2.4. A set $S \subseteq \mathbb{C}_{\mathrm{Im}\geq 0}$ is called *hyperbolic-convex* or *h-convex* if

$$z_1, z_2 \in S \implies \mathrm{Arc}_{\min}\,(z_1, z_2) \in S.$$

Given a set of points $P \in \mathbb{C}_{\mathrm{Im}\geq 0}$, the *h-convex hull of* P is the smallest h-convex set containing P. ⌟

Note that h-convexity is equivalent to Euclidean convexity under the Beltrami-Klein mapping. $\mathrm{Arc}_{\min}\,(z_1, z_2)$ is the minimal geodesic between z_1 and z_2 under the Poincaré metric, so h-convexity may be thought of as geodesic convexity with respect to this metric. We recall the following useful lemma of Huang, Ryu, and Yin [63].

Lemma 2.1. *(Lemma 2.1 [63]): Given a sequence of points $Z \in \mathbb{C}_{\mathrm{Im}\geq 0}$, Poly (Z) is h-convex.*

In our terminology, given a sequence of points $Z \in \mathbb{C}_{\mathrm{Im}\geq 0}$, $\mathrm{Poly}\,(Z)$ is the h-convex hull of Z.

2.4.2 *SRGs of LTI transfer functions*

Let $g : L_2 \to L_2$ be linear and time invariant, and denote its transfer function by $G(s)$. g maps a complex sinusoid $u(t) = ae^{j\omega t}$ to the complex sinusoid $y(t) = a|G(j\omega)|e^{j\angle G(j\omega)+j\omega t}$. These signals do not belong to L_2, but are treated as limits of sequences in L_2. Precisely, we define the points on the SRG corresponding to sinusoidal signals by taking the gain and phase to be

$$\lim_{T\to\infty} \frac{\|P_T y\|}{\|P_T u\|}$$
$$\lim_{T\to\infty} \angle(P_T u, P_T y).$$

Both these limits exist when u and y are sinusoidal. The Nyquist diagram $\mathrm{Nyquist}(G)$ of an operator $g : L_2(\mathbb{C}) \to L_2(\mathbb{C})$ is the locus of points $\{G(j\omega) \mid \omega \in \mathbb{R}\}$.

Theorem 2.4. *Let $g : L_2(\mathbb{C}) \to L_2(\mathbb{C})$ be linear and time invariant, with transfer function $G(s)$. Then $\mathrm{SRG}(g) \cap \mathbb{C}_{\mathrm{Im}\geq 0}$ is the h-convex hull of $\mathrm{Nyquist}(G) \cap \mathbb{C}_{\mathrm{Im}\geq 0}$.*

The proof of Theorem 2.4 is closely related to the proof of Huang, Ryu, and Yin [63, Thm. 3.1], and is deferred to Section 2.11. A consequence of Theorem 2.4 is that the SRG of an LTI operator is bounded by its Nyquist diagram. For example, the SRG of the transfer function $1/(s^3+5s^2+2s+1)$ is illustrated in 2.4. Further examples are given in [79].

Given Theorem 2.4, we recover two familiar properties of the Nyquist diagram as special cases of Proposition 2.1, namely that passivity is equivalent to the Nyquist diagram lying in the right half plane, and the H_∞ gain is the maximum magnitude of the Nyquist diagram.

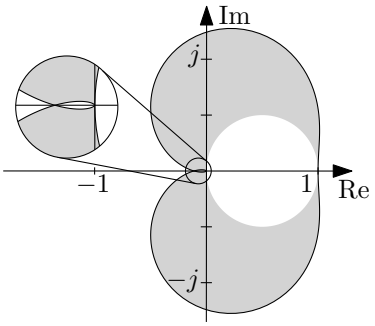

Figure 2.4: SRG of the transfer function $1/(s^3+5s^2+2s+1)$. The black curve is its Nyquist diagram, the grey region is the SRG.

2.5 SCALED RELATIVE GRAPHS OF STATIC NONLINEARITIES

LTI systems map complex sinusoids to complex sinusoids, and the behavior of an LTI system on L_2 can be fully characterized by its behavior on complex sinusoids. Similarly,

static nonlinearities map square waves to square waves. Here, we show that the behavior of these functions on L_2, insofar as it is captured by the scaled relative graph, is fully characterized by their behavior on a two-dimensional subspace of L_2 spanned by two Haar wavelets (truncations of a square wave to a single period). In particular, we show that the SRGs of the saturation and ReLU are identical, and closely related to the SRG of a first order lag. The use of square waves allows us to test the effect of different input amplitudes on the output, which is analogous to the use of sinusoids to test the effect of different input frequencies on the output of an LTI system.

Proposition 2.9. *Suppose $S : L_2 \to L_2$ is the operator given by a SISO static nonlinearity $s : \mathbb{R} \to \mathbb{R}$, such that for all $u_1, u_2 \in \mathbb{R}$, $y_i \in s(u_i)$,*

$$\mu(u_1 - u_2)^2 \leq (y_1 - y_2)(u_1 - u_2) \leq \lambda(u_1 - u_2)^2. \tag{2.4}$$

Then the SRG of S is contained within the disc centred at $(\lambda + \mu)/2$ with radius $(\lambda - \mu)/2$.

Proof. Define an operator $\bar{S}$ by $u \mapsto \bar{y} \coloneqq S(u) - \mu u$. Let $\Delta u(t) = u_1(t) - u_2(t)$ and $\Delta\bar{y}(t) = \bar{y}_1(t) - \bar{y}_2(t)$. We drop the t dependence in the remainder of this proof. By assumption on s, for all Δu and corresponding incremental output $\Delta\bar{y}$, we have

$$0 \leq \Delta u(\Delta y - \mu \Delta u) \leq \lambda \Delta u^2, \tag{2.5}$$

$$0 \leq \Delta u \Delta\bar{y} \leq \lambda \Delta u^2. \tag{2.6}$$

It then follows that $\Delta u \Delta\bar{y} \geq 0$ and $\Delta u \Delta\bar{y} - (\lambda - \mu)\Delta u^2 \leq 0$, from which the following series of equivalent statements follow:

$$\begin{aligned} \Delta u \Delta\bar{y}(\Delta u \Delta\bar{y} - (\lambda - \mu)\Delta u^2) &\leq 0 \\ \Delta\bar{y}(\Delta\bar{y} - (\lambda - \mu)\Delta u \Delta\bar{y}) &\leq 0 \\ \Delta u \Delta\bar{y} &\geq \frac{1}{\lambda - \mu}\Delta\bar{y}^2. \end{aligned}$$

This shows that $\bar{S}$ is output-strict incrementally positive with constant $1/(\lambda - \mu)$, so its SRG is the disc with centre $(\lambda - \mu)/2$ and radius $(\lambda - \mu)/2$. The result then follows by noting that S is the parallel interconnection of $\bar{S}$ with μI, so its SRG is the SRG of $\bar{S}$ shifted to the right by μ. □

The same bounding region can be obtained for the SG with respect to an input $u^\star$, by restricting the second input in the proof of Proposition 2.9 to be $u^\star$. This is stated formally below.

Proposition 2.10. *Suppose $S : L_2 \to L_2$ is the operator given by a SISO static nonlinearity $s : \mathbb{R} \to \mathbb{R}$, such that, for all $u_1 \in \mathbb{R}$, $y_1 \in s(u_1)$, $y^\star \in s(u^\star)$,*

$$\mu(u_1 - u^\star)^2 \leq (y_1 - y^\star)(u_1 - u^\star) \leq \lambda(u_1 - u^\star)^2. \tag{2.7}$$

Then the SG of S with respect to $u^\star$ is contained within the disc centred at $(\lambda + \mu)/2$ with radius $(\lambda - \mu)/2$.

The discs obtained in the previous two propositions are closely related to the discs of the classical incremental circle criterion [70] - indeed, taking the negative and inverting transforms one to the other.

We now show that, for a large class of systems, the disc bound on the SRG cannot be improved. If the characteristic curve of s contains a "maximal elbow", that is, a point where the slope switches from maximum to minimum, then small signals centred around the elbow can be used to generate the perimeter of the bound of Proposition 2.9. Furthermore, if the region of minimum slope extends to infinity, then large signals can be used to generate the interior of the bound of Proposition 2.9. This is formalized in the following two propositions. We treat only an elbow from slope 1 to slope 0, as a loop transformation can be used to convert any other elbow to this form.

Proposition 2.11. *Suppose $S : L_2 \to L_2$ is a memoryless nonlinearity defined by a map $s : \mathbb{R} \to \mathbb{R}$ which satisfies* (2.4) *with $\mu = 0$ and $\lambda = 1$. Furthermore, suppose there are real numbers $u^\star$ and $\delta > 0$, such that,*

$$s(u^\star + \varepsilon_u) - s(u^\star) = 0 \text{ for all } \varepsilon_u \in [0, \delta] \tag{2.8}$$

$$s(u^\star) - s(u^\star - \varepsilon_l) = \varepsilon_l \text{ for all } \varepsilon_l \in [0, \delta]. \tag{2.9}$$

Then the SRG of S contains the circle centred at $1/2$ with radius $1/2$.

Proof. We consider two input signals, supported on $[0, 1]$:

$$u_1(t) = u^\star, \quad u_2(t) = \begin{cases} u^\star + \varepsilon & 0 \le t < \tau \\ u^\star - \varepsilon & \tau \le t \le 1, \end{cases}$$

where $\tau \in [0, 1]$. The corresponding output signals are given by

$$y_1(t) = s(u^\star), \quad y_2(t) = \begin{cases} s(u^\star + \varepsilon) & 0 \le t < \tau \\ s(u^\star - \varepsilon) & \tau \le t \le 1, \end{cases}$$

giving the incremental signals

$$\Delta u(t) = \begin{cases} -\varepsilon & 0 \le t < \tau \\ \varepsilon & \tau \le t \le 1, \end{cases} \qquad \Delta y(t) = \begin{cases} 0 & 0 \le t < \tau \\ \varepsilon & \tau \le t \le 1. \end{cases}$$

Δy can be written as $k(t)\Delta u(t)$, where

$$k(t) = \begin{cases} 0 & 0 \le t < \tau \\ 1 & \tau \le t \le 1. \end{cases}$$

Calculating gain then gives

$$\|\Delta y\| = \left(\int_0^1 k^2(t) \Delta u^2(t) \, \mathrm{d}t \right)^{\frac{1}{2}} = \left(\int_\tau^1 \Delta u^2(t) \, \mathrm{d}t \right)^{\frac{1}{2}} = \gamma \|\Delta u\|,$$

for some γ which varies between 0 and 1 as τ varies between 1 and 0. It follows that

$$\frac{\|\Delta y\|}{\|\Delta u\|} = \gamma.$$

Calculating the phase gives

$$\begin{aligned}\operatorname{acos} \frac{\langle \Delta u | \Delta y \rangle}{\|\Delta u\| \|\Delta y\|} &= \operatorname{acos} \frac{\int_0^1 k(t) \Delta u^2(t) \, \mathrm{d}t}{\gamma \|\Delta u\|^2} \\ &= \operatorname{acos} \frac{\int_\tau^1 \Delta u^2(t) \, \mathrm{d}t}{\gamma \|\Delta u\|^2} \\ &= \operatorname{acos}(\gamma).\end{aligned}$$

Since $\gamma \in [0,1]$, we can define ϑ by $\cos(\vartheta) = \gamma$. We then have the locus of points on the SRG given by

$$\cos(\vartheta) \exp(\pm j\vartheta), \quad 0 \le \vartheta \le \pi/2,$$

which is the circle with centre $1/2$ and radius $1/2$. □

Proposition 2.12. *Suppose $S : L_2 \to L_2$ is a memoryless nonlinearity defined by a map $s : \mathbb{R} \to \mathbb{R}$ which satisfies* (2.4) *with $\mu = 0$ and $\lambda = 1$, and which satisfies $s(0) = 0$. Furthermore, suppose there is a real number $u^\star$ such that*

$$s(u^\star + M) - s(u^\star) = 0 \text{ for all } M \ge 0 \tag{2.10}$$

$$s(u^\star) > 0. \tag{2.11}$$

Then the SRG of S is the disc centred at $s(u^\star)/2u^\star$ with radius $s(u^\star)/2u^\star$.

Proof. We consider two input signals, supported on $[0,1]$:

$$u_1(t) = M, \quad u_2(t) = \begin{cases} M + u^\star & 0 \le t < \tau \\ 0 & \tau \le t \le 1, \end{cases}$$

where $\tau \in [0,1]$, and $M \ge u^\star$. The corresponding output signals are

$$\begin{aligned} y_1(t) &= s(M) = s(u^\star) \\ y_2(t) &= \begin{cases} s(M + u^\star) & 0 \le t < \tau \\ 0 & \tau \le t \le 1, \end{cases} \end{aligned}$$

giving the incremental signals

$$\Delta u(t) = \begin{cases} -u^\star & 0 \le t < \tau \\ M & \tau \le t \le 1, \end{cases} \quad \Delta y(t) = \begin{cases} 0 & 0 \le t < \tau \\ s(u^\star) & \tau \le t \le 1. \end{cases}$$

Define $\beta(M) \coloneqq s(u^\star)/M$. Then Δy can be written as $k(t)\Delta u(t)$, where

$$k(t) = \begin{cases} 0 & 0 \le t < \tau \\ \beta(M) & \tau \le t \le 1. \end{cases}$$

Calculating gain then gives

$$\begin{aligned}\|\Delta y\| &= \left(\int_0^1 k^2(t)\Delta u^2(t)\,\mathrm{d}t\right)^{\frac{1}{2}} \\ &= \beta(M)\left(\int_\tau^1 \Delta u^2(t)\,\mathrm{d}t\right)^{\frac{1}{2}} \\ &= \beta(M)\gamma\|\Delta u\|,\end{aligned}$$

for some γ which varies between 0 and 1 as τ varies between 1 and 0. It follows that

$$\frac{\|\Delta y\|}{\|\Delta u\|} = \beta(M)\gamma.$$

Calculating the phase gives

$$\begin{aligned}\frac{\langle \Delta u|\Delta y\rangle}{\|\Delta u\|\|\Delta y\|} &= \frac{\int_0^1 k(t)\Delta u^2(t)\,\mathrm{d}t}{\beta(M)\gamma\|\Delta u\|^2} \\ &= \frac{\beta(M)\int_\tau^1 \Delta u^2(t)\,\mathrm{d}t}{\beta(M)\gamma\|\Delta u\|^2} \\ &= \gamma.\end{aligned}$$

Since $\gamma \in [0,1]$, we can define ϑ by $\cos(\vartheta) = \gamma$. We then have the locus of points on the SRG given by

$$\beta(M)\cos(\vartheta)\exp(\pm j\vartheta), \quad 0 \le \vartheta \le \pi/2.$$

This is the circle with centre $\beta(M)/2$ and radius $\beta(M)/2$. Varying M between $u^\star$ and ∞ varies $\beta(M)$ between $s(u^\star)/u^\star$ and 0, so we fill the disc with centre $s(u^\star)/2u^\star$ and radius $s(u^\star)/2u^\star$. □

Proposition 2.12 allows us to gives an exact characterization of the SRGs of a range of static nonlinearities, including the unit saturation, the ReLU, and the limiting cases of the relay and ideal diode.

The proof of Proposition 2.11 uses probing signals which have an arbitrarily small magnitude variation about a "worst case" input value. This shows the local or worst case nature of the SRG - the boundary of the SRG is generated by these probing signals.

Remark 2.1. We conclude this section by remarking that the characterization of output-strict incrementally positive *static* nonlinearities allows the SRGs of a large class of *dynamic* output-strict incrementally positive nonlinear systems to be characterized. Output-strict incremental positivity is preserved under negative feedback with an incrementally positive system, as shown in Theorem 2.3. This means that any scalar system of the form

$$\dot{y} = a(y) + u,$$

where a obeys an incremental sector bound with positive constants, is output-strict incrementally positive. ⌟

2.6 EXAMPLE 1: FEEDBACK WITH SATURATION AND DELAY

In this section, we use SRGs to analyze feedback systems with delays, dynamic components and static nonlinearities. We will derive incremental stability bounds which depend both on the delay time and the dynamic time constant, similar to the state of the art non-incremental bounds obtained using the roll-off IQC [82]. These bounds are obtained by approximating the SRG of the delay and the dynamics, treated as a single component. In the simple example of this section, where the dynamic component is LTI, this approach reduces to the incremental circle criterion. However, the approach allows for arbitrary dynamic components, as shown in Section 2.8. One of the advantages of our approach is the derivation of stability margins and incremental L_2 gain bounds for the closed loop.

We begin with the system of Figure 2.5, showing a time delay and an LTI transfer function in feedback with a $1/\beta$-output-strict incrementally passive component Δ.

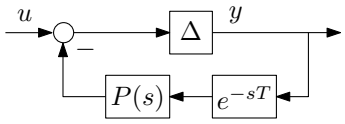

Figure 2.5: Simple system with delay in the feedback loop.

We take $P(s) = s^2/(s^3 + 2s^2 + 2s + 1)$, also considered in [68, §3]. The Nyquist diagram of $P(s)$ cascaded with the delay, and a bounding approximation of the SRG, are shown in the left hand side of Figure 2.6. As the delay is increased, the Nyquist diagram, and hence the SRG, extend further into the left half plane.

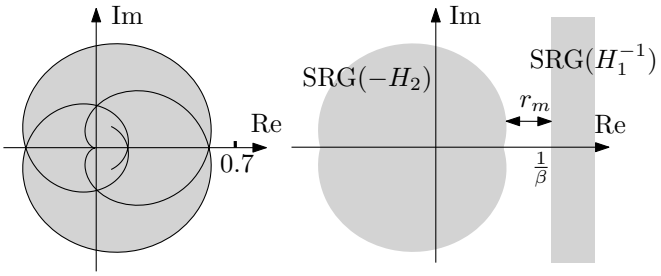

Figure 2.6: Left: Nyquist diagram of $e^{-sT}s^2/(s^3 + 2s^2 + 2s + 1)$ (black) and a bounding approximation of its SRG. Right: feedback with $1/\beta$-output-strict incrementally passive system.

Applying Theorem 2.2 with $H_2 = e^{-sT}P(s)$ and $H_1 = \Delta$, we obtain the right hand side of Figure 2.6. Stability is verified if the delay SRG always has real part greater than $1/\beta$, which ensures that $r_m > 0$. Solving numerically for $\min_\omega \mathrm{Re}(P(j\omega)e^{j\omega T})$ gives a stability bound on β, as a function of T, shown in Figure 2.7, which also shows the non-incremental stability bound obtained by Megretski and Rantzer [68] using IQC analysis, for the particular case where Δ is a saturation. For short delay times, the non-incremental bound is shown to tend to infinity, using the Zames-Falb-O'Shea multiplier.

The incremental bound obtained using SRG analysis has a non-smooth point where the leftmost segment of the Nyquist diagram switches, and is bounded for all delay times.

The SRG analysis gives a bound which guarantees incremental L_2 gain, a stronger property than the L_2 gain from IQC analysis. Finite incremental L_2 gain in particular implies input-output continuity. As noted by Kulkarni and Safonov [73], stability results using Zames-Falb-O'Shea and Popov multipliers do not guarantee continuity, as these multipliers do not preserve the incremental passivity of static nonlinear elements. This issue was also alluded to in the discussion of [83, Thm. 1], in the context of incremental IQC analysis. The situation for proving finite incremental L_2 gain with these multipliers is similar; the loss of incremental passivity of the static nonlinearity means the incremental passivity theorem cannot be applied, so another method of proving stability is needed. One such method would be to apply Theorem 2.2 to the transformed loop, and indeed there are multipliers which destroy incremental passivity but which still verify an incremental L_2 gain bound. For this particular example, the transfer function $(s+1)/(s-1)$ could be used as a multiplier, although it gives a more conservative bound than Figure 2.7. Global [84], universal [85] and equilibrium-independent [77] L_2 gain are weaker than incremental L_2 gain but stronger than L_2 gain, and afford differing levels of tractability.

In addition to proving incremental L_2 stability, we can give an incremental L_2 gain bound. For a fixed β, $1/r_m$ is an incremental L_2 gain bound from u to y, which depends on the time delay T. For $\beta = 1$, this bound is plotted in Figure 2.7.

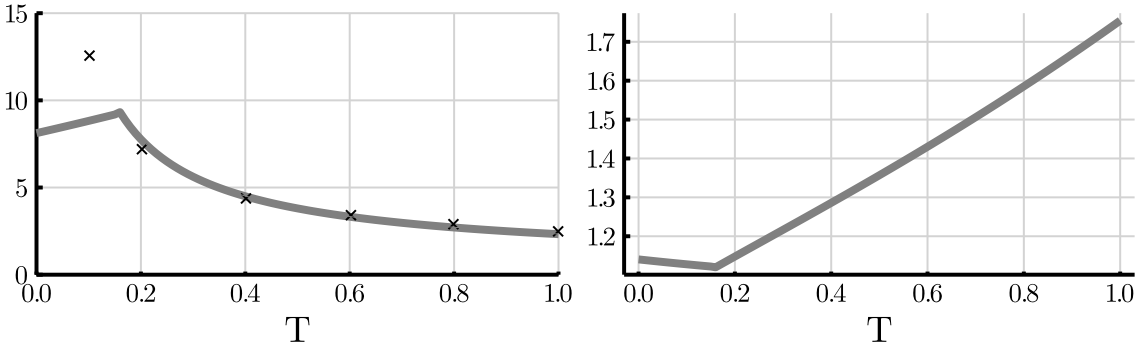

Figure 2.7: Left: The grey line is an upper bound on β which guarantees that the system of Figure 2.5 has bounded incremental L_2 gain with a delay of T. The crosses give a bound on β which guarantees (non-incremental) L_2 stability, obtained using IQC analysis [68, Fig. 6]. Right: the incremental L_2 gain bound from u to y for $\beta = 1$.

The motivation behind the traditional structure of the Lur'e system is to put all of the "troublesome" elements in the nonlinear component, and all of the dynamics in the LTI component. The availability of explicit SRGs for elements which are usually troublesome, such as saturations and delays, means that this structure is not necessarily ideal for SRG analysis, and the feedback system may be better modelled in a different way. This is illustrated in the following two examples.

2.7 EXAMPLE 2: CYCLIC FEEDBACK SYSTEMS

We now turn to the analysis of cyclic feedback systems. Such systems are often found in biological models [86], among many other application domains (see, for example, the discussion of Mallet-Paret and Sell [87]). We derive the SRG of a cascade of output-strict incrementally positive systems, and a gain margin condition for stability gives rise to the incremental secant condition [74], giving a geometric interpretation to the original result. The result we give here is tight in the sense that stronger conditions than output strict incremental positivity of the plants are required for any stronger bound.

We consider the cascade of n output-strict incrementally passive systems, with parameters $1/\gamma_i$, $i = 1, \dots, n$, in unity gain negative feedback, shown in Figure 2.8. By Theorem 2.1, the system is stable if the SRG of the cascade doesn't intersect the point $-1/\tau$ for $\tau \in (0, 1]$.

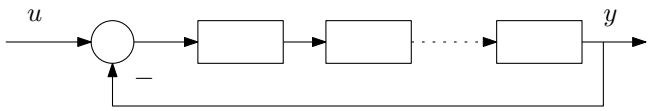

Figure 2.8: Cascade of subsystems in unity gain negative feedback.

The SRG of the i^{th} system is the disc with centre $\gamma_i/2$ and radius $\gamma_i/2$. The perimeter of this disc has the parameterization

$$z_i(\vartheta) = \gamma_i \cos(\vartheta) e^{-j\vartheta} \quad -\pi/2 \le \vartheta < \pi/2 \tag{2.12}$$

As this disc satisfies the right hand arc property, the SRG of the full cascade is the product of n discs. We claim that the perimeter of this SRG has the parameterization

$$z(\phi) = \gamma_1 \gamma_2 \dots \gamma_n \left(\cos \frac{\phi}{n}\right)^n e^{-j\phi}, \quad -\pi \le \phi < \pi. \tag{2.13}$$

For instance, take any $z_1, z_2, \dots, z_n$. Using (2.12) and Proposition 2.8 gives the point

$$w = \gamma_1 \dots \gamma_n \cos(\vartheta_1) \dots \cos(\vartheta_n) e^{-j(\vartheta_1 + \dots + \vartheta_n)}, \tag{2.14}$$

for $-\pi < \vartheta_1, \vartheta_2, \dots, \vartheta_n < \pi$. Letting $\vartheta_1 = \vartheta_2 = \dots = \vartheta$, and setting $\phi = n\vartheta$ gives the parameterization (2.13) (noting that $-\pi \le \phi < \pi$ as (2.13) is 2π-periodic). This shows that all the points $z(\phi)$ lie within the SRG. To show that they are indeed on the perimeter of the SRG, we take any point w and show that its magnitude is smaller than the point $z(\phi)$ with the same argument. This follows from (2.14) if we can show that

$$\cos(\vartheta_1) \cos(\vartheta_2) \dots \cos(\vartheta_n) \le \cos(\vartheta_1 + \vartheta_2 + \dots + \vartheta_n).$$

This is proved in [74]: $f(\phi) = -\ln \cos(\phi)$ is convex on $(-\pi/2, \pi/2)$. Applying Jensen's inequality gives $f(\sum_i \vartheta_i) \le \sum_i f(\vartheta_i)$, and the required inequality follows by taking the exponential. Note that the inequality still holds in the limit as one angle $\vartheta_i \to \pm\pi/2$. This

result is closely related to [63, Thm. 1], which characterizes the SRG of the composition of two averaged operators.

The SRG of an example cascade with every $\gamma_i = 1$ is shown in Figure 2.9. The intercept with the negative real axis is at the point $z(\pi) = -\gamma_1\gamma_2\dots\gamma_n\left(\cos\frac{\pi}{n}\right)^n$. A direct application of Theorem 2.1 thus gives the following incremental secant condition.

Theorem 2.5. *The system of Figure 2.8, where the n interconnected systems are each output-strict incrementally passive with parameters γ_i, $i = 1,\dots,n$, has a finite incremental L_2 gain if*

$$\gamma_1\gamma_2\dots\gamma_n < \left(\sec\frac{\pi}{n}\right)^n.$$

The SRG of a cascade allows several other useful values to be computed. An incremental L_2 gain bound can be found by minimizing the distance between -1 and $1/(\gamma_1\dots\gamma_n\cos(\vartheta_1)\dots\cos(\vartheta_n)e^{-j(\vartheta_1+\dots+\vartheta_n)})$. This distance is shown for $n = 4$ in Figure 2.10. Furthermore, we can calculate the shortage of input-strict incremental positivity of the cascade by finding the distance the SRG extends into the left half plane. For example, for a cascade of two systems each with $\gamma_i = 1$, the shortage of input-strict incremental positivity is 1/8. Stan, Hamadeh, Sepulchre, *et al.* [88] show that if the coupling strength in a network of oscillators modelled as cascade feedback systems is large enough compared to the shortage of each oscillator, the network will synchronize.

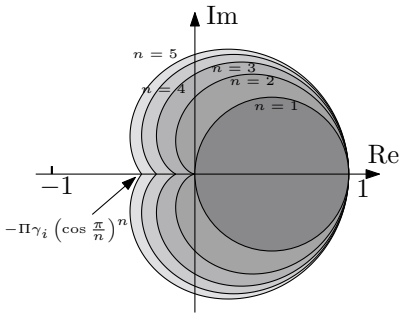

Figure 2.9: SRGs of the cascade of Figure 2.8, where each subsystem is 1-output-strict incrementally positive, for 1 to 5 subsystems.

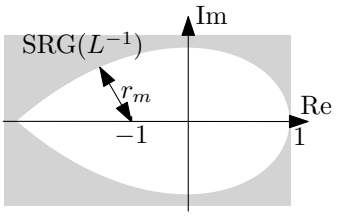

Figure 2.10: Inverse SRG of a cascade of four output-strict incrementally positive systems. The stability margin is r_m. The intercept with the negative real axis is at $-1/(\Pi_i\gamma_i(\cos(\pi/n))^n)$.

If an uncertain gain k_Δ is placed in feedback with the cascade, as shown in Figure 2.11, SRG analysis allows us to give a bound on k_Δ which guarantees incremental stability. The

inverse SRG of the cascade (Figure 2.10) is shifted to the right by k_Δ; if it does not intersect -1, the closed loop has finite incremental gain. This allows us to conclude stability if

$$k_\Delta < -1 + \left(\gamma_1\gamma_2\dots\gamma_n\left(\cos\frac{\pi}{n}\right)^n\right)^{-1}.$$

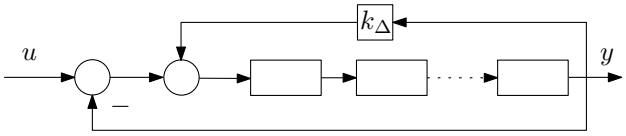

Figure 2.11: Cascade of subsystems with an uncertain feedback gain k_Δ, in unity gain negative feedback.

2.8 EXAMPLE 3: COMBINING CASCADES AND DELAYS

In this final example, we combine a delay with a cascade of two output-strict incrementally positive systems, and revisit the internet congestion control example of Summers, Arcak, and Packard [82]. In that paper, equilibrium-independent IQCs are verified numerically in order to compute a bound on the variables δ, β and N_u in the left of Figure 2.12, which guarantees (non-incremental) input/output stability of the system. Here, we derive a bound which guarantees finite incremental gain of the system.

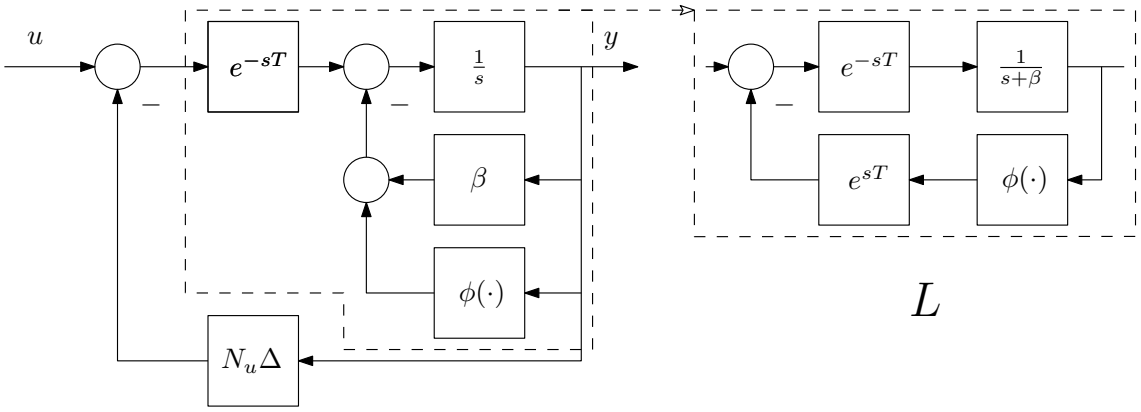

Figure 2.12: Left: internet congestion control example of [82]. $\beta > 0$, $\phi(w)$ is γ-output-strict incrementally positive, $N_u \in \mathbb{N}$, Δ is δ-output-strict incrementally positive. $0 < 1/\gamma < \beta$. Right: equivalent representation of the forward path, L.

In order to combine the delay and first order lag, we rearrange the forward path as shown in the right of Figure 2.12. This gives a delay-dependent bounding SRG, shown in Figure 2.13, for the forward path.

To apply Theorem 2.2, we solve for the largest radius r as shown in the right hand side of Figure 2.13, before the two SRGs overlap. This is equal to the reciprocal of the distance the SRG of L extends into the left half plane, which is solved numerically. This gives the bound on N_u/δ, plotted in Figure 2.14, that guarantees an incremental L_2 gain bound for the closed loop.

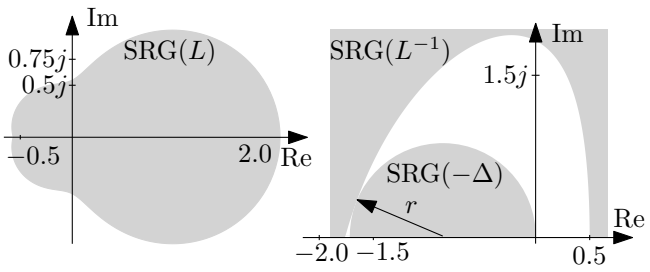

Figure 2.13: Left: bounding SRG of L, for $\beta = 1$, $T = 1$, $\gamma = 2$. Right: inverse of L and negative of an r-output-strict incrementally positive block Δ. Only the upper half is shown.

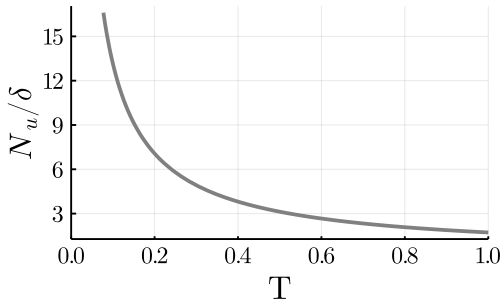

Figure 2.14: Upper bound on N_u/δ for the system of Figure 2.12 to have finite incremental L_2 gain, derived by applying Theorem 2.2. Plotted for $\beta = 1$, $\gamma = 0.5$.

2.9 A ROLLED-OFF PASSIVITY THEOREM

The conditions of the small gain and passivity theorems are restrictive, and, as illustrated in the previous three examples, there are many feedback systems which are stable, but do not meet the assumptions of either theorem. A common issue in practice is that a system would satisfy the conditions of the passivity theorem, were it not for high frequency dynamics destroying passivity. The input/output gain, however, is small at these high frequencies. This issue played an important part in the development of adaptive control - see [89] and references therein. The prevalence of such systems has motivated several specialized stability results. The LTI *mixed small gain/passivity* condition of Griggs et al.[90] divides the frequency spectrum into frequencies at which two systems are passive, frequencies at which they have small gain, and frequencies at which they satisfy both criteria. This is generalized directly to nonlinear systems by Forbes and Damaren [91], using the terminology *hybrid small gain/passivity*, and is connected to the Generalized KYP lemma of Iwasaki and Hara [92] in reference [93]. The nonlinear generalization of Griggs et al.[94] uses a pair of linear operators to define a "blended" supply rate which represents mixed small gain and passivity. The *roll-off IQC* was introduced by Summers, Arcak and Packard [82] to capture the roll-off of input/output gain at high frequency.

In this section, we introduce an incremental *rolled-off passivity* theorem, which applies

to incrementally stable systems which only violate incremental passivity when their incremental input/output gain is small. Rather than requiring gain to roll-off over any particular frequency range, we simply require the gain to roll off when the phase shift, measured as an angle in signal space, exceeds $\pi/2$. The idea takes inspiration from the blended supply rate of Griggs et al.[94], however, rather than using a smoothly blended supply, we simply split the space of input signals into those pairs of signals where the two systems have incremental small gain, are incrementally passive, or both. We call this property *incremental* (μ,γ)*-dissipativity*. Unlike the results of references [91], [94], [95], we do not require systems to be incrementally (μ,γ)-dissipative for *the same* partition of signals. This maintains the "worst case" nature of the small gain and passivity theorems, but simplifies the verification of the property. The resulting condition for finite incremental gain bears a strong resemblance to the classical incremental small gain condition.

Incremental (μ,γ)-dissipativity is defined as follows.

Definition 2.5. Let $H : L_2 \to L_2$ and $\mu,\gamma,\varepsilon \geq 0$. We say that H is *ε-strongly incrementally (μ,γ)-dissipative* if, for all $u_1, u_2 \in L_2$ and all $y_1 \in H(u_1)$, $y_2 \in H(u_2)$, either:

$$\|y_1 - y_2\| \leq \mu \|u_1 - u_2\|, \tag{2.15}$$

or both:

$$\langle u_1 - u_2 | y_1 - y_2 \rangle \geq \varepsilon \|u_1 - u_2\|^2 \tag{2.16a}$$

and

$$\|y_1 - y_2\| \leq \gamma \|u_1 - u_2\|, \tag{2.16b}$$

or all of (2.15), (2.16a) and (2.16b) hold. If $\varepsilon = 0$, we simply say that H is *incrementally (μ,γ)-dissipative*. ⌟

Incremental (μ,γ)-dissipativity is defined independently of the frequency spectra of signals, however it captures those systems which are incrementally passive except for high frequency dynamics, when the system has low gain. Incremental (μ,γ)-dissipativity is easily verified for systems with low-pass dynamics whose passivity is destroyed by effects such as input saturation and small delays, as explored further in Example 2.1.

If $\gamma < \mu$, incremental (μ,γ)-dissipativity reduces to an incremental gain bound of μ. If $\mu = 0$, the property reduces to finite incremental gain and input strict incremental passivity.

Incremental (μ,γ)-dissipativity has an appealing graphical interpretation, developed in the following lemma. This lemma is especially useful as it allows the property of incremental (μ,γ)-dissipativity to be easily determined from the SRG of a system.

Lemma 2.2. *Let $\mu,\gamma > 0$, $\varepsilon \geq 0$, and let $\mathcal{S}^{\varepsilon}_{\mu,\gamma}$ be the class of operators which are ε-strongly incrementally (μ,γ)-dissipative. Then*

$$\mathrm{SRG}\left(\mathcal{S}^{\varepsilon}_{\mu,\gamma}\right) = \mathcal{D}_1 \cup \mathcal{D}_2,$$

where

$$\mathcal{D}_1 \coloneqq \{z \,|\, z \in \mathbb{C}, |z| \leq \mu\},$$
$$\mathcal{D}_2 \coloneqq \{z \,|\, z \in \mathbb{C}, |z| \leq \gamma, \mathrm{Re}\{z\} \geq \varepsilon\},$$

as shown in Figure 2.15. Furthermore, $\mathcal{S}^{\varepsilon}_{\mu,\gamma}$ is SRG-full.

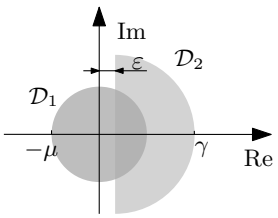

Figure 2.15: Graphical interpretation of ε-strong incremental (μ, γ)-dissipativity. Lemma 2.2 shows that the SRG of the class of ε-strongly incrementally (μ, γ)-dissipative systems is $\mathcal{D}_1 \cup \mathcal{D}_2$.

Proof. We begin by showing $\mathrm{SRG}\,(\mathcal{S}^{\varepsilon}_{\mu,\gamma}) \subseteq \mathcal{D}_1 \cup \mathcal{D}_2$. Let $H \in \mathcal{S}^{\varepsilon}_{\mu,\gamma}$ and $u_1, u_2 \in L_2$ be arbitrary inputs. Then, by assumption, for all $y_1 \in H(u_1)$, $y_2 \in H(u_2)$, either (2.15) is true, or (2.16a) and (2.16b) are true, or all three inequalities are true. Suppose first that (2.15) is true. Then $\|y_1 - y_2\|/\|u_1 - u_2\| \leq \mu$, so $z_H(u_1, u_2) \subseteq \{z \,|\, z \in \mathbb{C}, |z| \leq \mu\} = \mathcal{D}_1$.

We now treat the second case. Suppose that (2.16a) and (2.16b) are true. Note that, for $z \in z_H(u_1, u_2)$ corresponding to outputs y_1, y_2,

$$\mathrm{Re}(z) = \frac{\langle u_1 - u_2 | y_1 - y_2 \rangle}{\|u_1 - u_2\|^2}. \tag{2.17}$$

It then follows from Equation (2.16a) that $z_H(u_1, u_2) \subseteq \{z \,|\, z \in \mathbb{C}, \mathrm{Re}(z) \geq \varepsilon\}$. Equation (2.16b) gives $z_H(u_1, u_2) \subseteq \{z \,|\, z \in \mathbb{C}, |z| \leq \mu\}$, so $z_H(u_1, u_2) \subseteq \{z \,|\, z \in \mathbb{C}, \mathrm{Re}(z) \geq \varepsilon\} \cap \{z \,|\, z \in \mathbb{C}, |z| \leq \mu\} = \mathcal{D}_2$. Combining the two cases, we have $z_H(u_1, u_2) \subseteq \mathcal{D}_1 \cup \mathcal{D}_2$. Since u_1 and u_2 were arbitrary, it follows that $\mathrm{SRG}\,(\mathcal{S}^{\varepsilon}_{\mu,\gamma}) \subseteq \mathcal{D}_1 \cup \mathcal{D}_2$.

To show the opposite inclusion, let $z \in \mathcal{D}_1 \cup \mathcal{D}_2$ be arbitrary, and consider $A_z : L_2(\mathbb{C}) \to L_2(\mathbb{C})$ defined by $A_z(w) = |z| e^{j \arg(z)} w$. A straightforward calculation shows that $\mathrm{SRG}\,(A_z) = \{z, \bar{z}\}$. If we can show that $A_z \in \mathcal{S}^{\varepsilon}_{\mu,\gamma}$, it follows that $\mathrm{SRG}\,(\mathcal{S}^{\varepsilon}_{\mu,\gamma}) \supseteq \mathcal{D}_1 \cup \mathcal{D}_2$. The fact that $A_z \in \mathcal{S}^{\varepsilon}_{\mu,\gamma}$ is shown using the following argument, which also proves SRG-fullness of $\mathcal{S}^{\varepsilon}_{\mu,\gamma}$.

Take an arbitrary operator H which satisfies $\mathrm{SRG}\,(H) \subseteq \mathcal{D}_1 \cup \mathcal{D}_2$. Take $z \in \mathrm{SRG}\,(H)$, and let u_1, u_2, y_1, y_2 be any inputs and outputs that correspond to the point z. If $z \in \mathcal{D}_1$, then u_1, u_2, y_1, y_2 obey (2.15). If $z \in \mathcal{D}_2$, then u_1, u_2, y_1, y_2 obey (2.16a) and (2.16b). It follows that $H \in \mathcal{S}^{\varepsilon}_{\mu,\gamma}$. □

A direct application of Theorem 2.1 and Lemma 2.2 gives the following "rolled-off passivity theorem".

Theorem 2.6. *Let $H_1, H_2 : L_2 \to L_2$. Suppose there exist $\mu_1, \mu_2, \gamma_1, \gamma_2 \geq 0$ and $\varepsilon > 0$ such that $\mu_1 < \gamma_1$, $\mu_2 < \gamma_2$, H_1 is incrementally (μ_1, γ_1)-dissipative and H_2 is ε-strongly incrementally (μ_2, γ_2)-dissipative. Then the feedback interconnection of H_1 and H_2 shown in Figure 2.3 maps L_2 to L_2 and has finite incremental gain from u to y if*

$$\mu_1\gamma_2 < 1, \qquad \mu_2\gamma_1 < 1.$$

Note that setting $\mu_1 = \mu_2 = 0$ and letting $\gamma_1, \gamma_2 \to \infty$ recovers the incremental passivity theorem. If the conditions $\gamma_1 < \mu_1$, $\gamma_2 < \mu_2$ hold, the requirement for stability is the incremental small gain theorem: $\mu_1\mu_2 < 1$ [50].

We conclude this section with an example of the application of Theorem 2.6.

Example 2.1. Consider the feedback system shown in Figure 2.16. The forward path H_1 consists of a first order lag in feedback with a relay, with a unit saturation on the input. The feedback path H_2 consists of a delayed first order lag with a unit saturation on the input.

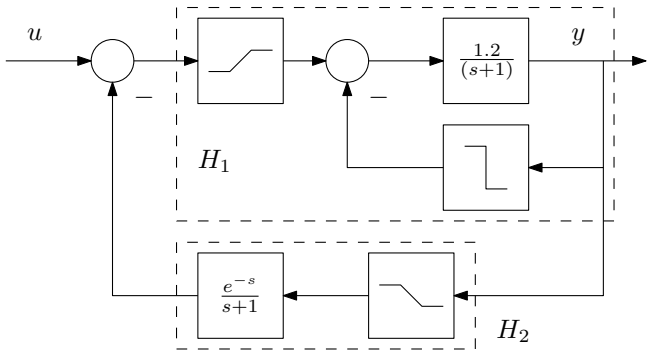

Figure 2.16: Example feedback system.

The unit saturation is defined as

$$y = \begin{cases} u & |u| < 1 \\ u/|u| & \text{otherwise.} \end{cases}$$

The relay is defined as

$$y = \begin{cases} u/|u| & u \neq 0 \\ 0 & u = 0. \end{cases}$$

We verify incremental (μ, γ)-dissipativity for H_1 and H_2 by plotting bounding approximations of their SRGs. The bounding SRG for H_1 is obtained by taking the SRGs of the saturation, relay and unit lag, given by Theorem 2.4 and Proposition 2.12, and composing them according to the interconnection rules of Propositions 2.5 to 2.8. The approximation for H_2 is similarly derived using Theorem 2.4 and Proposition 2.12 and applying Proposition 2.8. The SRGs for H_1 and H_2 are shown in Figure 2.17.

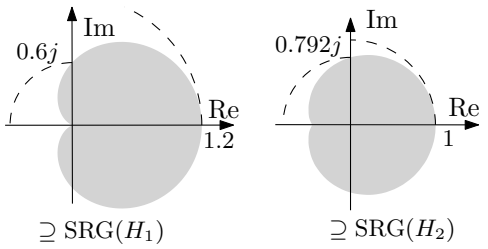

Figure 2.17: Over-approximations of the SRGs of H_1 and H_2 in Figure 2.16.

Note that neither H_1 nor H_2 is incrementally positive (their SRGs are not contained in the right half plane), nor do they obey the incremental small gain condition (the product of the maximum moduli of their SRGs exceeds 1).

It can be read from the SRGs that H_1 is incrementally (μ_1, γ_1)-dissipative, with $\mu_1 = 0.6$ and $\gamma_1 = 1.2$. The circles centred at the origin with radii 0.6 and 1.2 are shown in Figure 2.17; the SRG of H_1 lies within the union of these circles.

Similarly, it can be verified from the SRG and the circles plotted in Figure 2.17 that, for all $\mu_2 > 0.792$, there exists an $\varepsilon > 0$ such that H_2 is ε-strongly incrementally (μ_2, γ_2)-dissipative, with $\gamma_2 = 1$. Therefore, the conditions of Theorem 2.6 are met, and we conclude finite incremental L_2 gain of the feedback system.

⌟

2.10 CONCLUSIONS

We have introduced the tool of Scaled Relative Graphs to system analysis, and used it to analyze the incremental stability of operators in feedback. Characterizing stability by the separation of two SRGs unifies existing theorems such as the incremental small gain and passivity theorems, the incremental circle criterion and the incremental secant condition, using an intuitive graphical language. This graphical language is particularly suited to the calculation and visualization of stability margins, and furthermore allows the input-output gain of a feedback system to be estimated. It also allows for a formulation of H_∞ control design for nonlinear operators. There are many questions for future work; here we will list only two.

A first question is concerned with approximating the SRGs of nonlinear operators defined by state space models, or directly from input/output data.

A second question is concerned with the extension of the Nyquist theorem to the general case of unstable open loop plants.

2.11 PROOF OF THEOREM 2.4

The proof has three components. We begin by showing that, for an LTI transfer function $G(s)$, the Nyquist diagram at the frequencies $n2\pi/T$ is a subset of the SRG of $G(s)$. We

then show, for operators on the space $L_{2,T}$ of $T-$periodic, finite energy signals, the SRG is in the convex hull of the points generated by applying the operator to the basis of $L_{2,T}$ given by $\{e^{jtn2\pi/T}\}_{n\in\mathbb{Z}}$, which are exactly the points on the Nyquist diagram. The result then follows by taking the limit as $T \to \infty$, analogous to the classical derivation of the Fourier transform from the Fourier series.

We begin by observing that the point on the Nyquist diagram of G corresponding to frequency $\omega \in \mathbb{R}$ is precisely $z_G(e^{j\omega t})$. Set $u = ae^{j\omega t}$, then $y = G(u) = \alpha a e^{j\omega t + j\psi}$, where $\alpha = |G(j\omega)|$ and $\psi = \angle G(j\omega)$. A direct calculation gives

$$\begin{aligned}\langle u|y\rangle &= \int_0^T u(t)\bar{y}(t)\mathrm{d}t \\ &= T\alpha a^2 e^{j\phi}, \\ \|u\| &= \sqrt{T}a, \\ \|y\| &= \sqrt{T}\alpha a,\end{aligned}$$

where $\langle\cdot|\cdot\rangle$ is the inner product on $L_{2,T}$. It follows immediately that

$$z_G(u) = \alpha e^{j\psi},$$

that is, the point on the Nyquist diagram of G corresponding to frequency ω.

The next part of the proof closely follows Huang, Ryu, and Yin [63, Thm 3.1]. In the interests of brevity, we point out only the main arguments and modifications required to that proof.

Let G be an LTI operator on L_2. The restriction of G to $L_{2,T}$ is then an operator on $L_{2,T}$. Let $\mathcal{B}$ be the set of functions in t given by $\mathcal{B} = \{e^{jtn2\pi/T}, n \in \mathbb{Z}\}$. We show that

$$z_G(\mathrm{span}(\mathcal{B}) \setminus \{0\}) = \mathrm{Poly}\left(z_G(\mathcal{B})\right). \tag{2.18}$$

We begin by noting that $\mathcal{B}$ is an orthonormal basis for $L_{2,T}$, and in particular, for all $u, v \in \mathcal{B}$, $u \neq v$, $\langle v|u\rangle = \langle v|Gu\rangle = \langle Gv|u\rangle = \langle Gv|Gu\rangle = 0$. Therefore, the result of Part 2 of the proof of Huang, Ryu, and Yin [63, Thm. 3.1] holds: for all such u, v, we have

$$z_G(\mathrm{span}(u,v) \setminus \{0\}) = \mathrm{Arc}_{\min}\left(z_G(u), z_G(v)\right).$$

The only modification required to the proof is that the inner product here is complex valued, and the real part must be taken. Parts 3 and 4 of the proof of Huang, Ryu, and Yin [63, Thm. 3.1] show that $z_G(\mathrm{span}(\mathcal{B}) \setminus \{0\}) \subseteq \mathrm{Poly}\left(z_G(\mathcal{B})\right)$ and $z_G(\mathrm{span}(\mathcal{B}) \setminus \{0\}) \supseteq \mathrm{Poly}\left(z_G(\mathcal{B})\right)$ respectively, with the proof requiring only the additional fact that $\mathrm{Poly}\,(S)$ (in the proof of [63, Thm. 3.1]) is defined for a countably infinite set, as described in Section 2.4.1. This concludes the second part of the proof: $z_G(\mathrm{span}(\mathcal{B}) \setminus \{0\}) = \mathrm{Poly}\left(z_G(\mathcal{B})\right)$.

Finally, we extend to aperiodic signals by letting the period $T \to \infty$ and the fundamental frequency $2\pi/T \to 0$. We give the proof here assuming that the Fourier transform of the input $u(t)$ is Riemann integrable. The result can be extended to arbitrary functions on L_2 using the same machinery for defining the Fourier transform on L_2 - see, for

instance, Rudin [96, Chap. 9]. Alternatively, it follows from [80, Thm. 1]. We first note that $z_G(ae^{i\omega t})$ may be computed using the inner product and norm on L_2, rather than $L_{2,T}$, as a limit, and the result will be unchanged. Let $u(t)$ be an input signal on L_2, and $y(t)$ the corresponding output. The Fourier inversion theorem gives

$$y(t) = \frac{1}{\sqrt{2\pi}} \int_{-\infty}^{\infty} G(j\omega)\hat{u}(\omega)e^{j\omega t}\mathrm{d}\omega. \tag{2.19}$$

Let

$$\frac{\Delta\omega}{\sqrt{2\pi}} \sum_{n=-\infty}^{\infty} G(jn\Delta\omega)\hat{u}(n\Delta\omega)e^{jn\Delta\omega}$$

be a Riemann sum approximation of the right hand side of (2.19), with uniform spacing $\Delta\omega$. By (2.18), we know this sum belongs to

$$\mathrm{Poly}\left(\{G(j\Delta\omega)e^{jn\Delta\omega_0 t}\}_{n\in\mathbb{Z}}\right) \subseteq \mathrm{Poly}\left(\{G(j\omega)e^{j\omega t}\}_{\omega\in\mathbb{R}}\right).$$

Letting $\Delta\omega \to 0$, we have that the right hand side of (2.19) belongs to $\mathrm{Poly}\left(\{G(j\omega)e^{j\omega t}\}_{\omega\in\mathbb{R}}\right)$, noting that the restriction of the Nyquist diagram to $\mathbb{C}_{\mathrm{Im}\geq 0}$ is compact in $\mathbb{C}$. Note that this is precisely the h-convex hull of the Nyquist diagram of G. □

3 MONOTONE ONE-PORT CIRCUITS

ABSTRACT

Maximal monotonicity is explored as a generalization of the linear theory of passivity, aiming at an algorithmic input/output analysis of physical models. The theory is developed for maximal monotone one-port circuits, formed by the series and parallel interconnection of basic elements. An algorithmic method is presented for solving the periodic output of a periodically driven circuit using a maximal monotone splitting algorithm, which allows computation to be separated for each circuit component. A new splitting algorithm is presented, which applies to any monotone circuit defined as a port interconnection of monotone elements.

3.1 INTRODUCTION

Passivity is the backbone of linear circuit theory. As a system theoretic concept, it provides a fundamental bridge between physics and computation, well beyond electrical circuits. Passive linear systems are those that can be realized as port interconnections of passive elements [15], and the KYP lemma provides an algorithmic framework for the analysis of passive circuits by convex optimization [97]–[99]. The circuit concept of passivity has generated amongst the most important developments of control theory over the last several decades, including dissipativity theory [100], [101], nonlinear passivity theory [102]–[104], and passivity based control [105]–[108].

This chapter explores the concept of *maximal monotonicity* as a generalization of the LTI theory of passivity that retains the fundamental bridge between physics and computation beyond the world of linear, time-invariant systems.

The property of maximal monotonicity first arose in the study of nonlinear electrical circuits, in early efforts to extend the tractability of linear, time invariant, passive networks to networks containing nonlinear resistors. The prototype of a maximal monotone element was Duffin's *quasi-linear* resistor [109], a nonlinear resistor with a non-decreasing $i - v$ characteristic. Other early forms of monotonicity are found in the work of Golomb [34], Zarantonello [35] and the work of Dolph [36] on "dissipative" linear mappings. Quasi-linearity was refined by Minty [37]–[39] to produce the modern concept of maximal monotonicity, in the context of an algorithm for solving networks of nonlinear resistors. Desoer and Wu [40] studied existence and uniqueness of solutions to networks of nonlinear resistors, capacitors and inductors defined by maximal monotone relations.

Following the influential paper of Rockafellar in 1976 [41], maximal monotonicity has grown to become a fundamental property in convex optimization [42]–[47], forming the basis of a large body of work on tractable first order methods for large scale and

nonsmooth optimization problems, which have seen a surge of interest in the last decade. However, the physical significance of maximal monotonicity in nonlinear circuit theory has been somewhat forgotten.

The operator-theoretic property of maximal monotonicity can be interpreted, when defined on an appropriate space, as the incremental form of cyclo-passivity [110]. It coincides with passivity only for linear systems. Like passivity, maximal monotonicity is preserved under port interconnections [111]. However, unlike passivity, maximal monotonicity comes equipped with a convex algorithmic theory, for linear *and* nonlinear systems. Maximal monotonicity plays an important role in the simulation of nonsmooth dynamical systems [112], [113]. The first connection between maximal monotone operators and passive linear systems appears in this area, in the work of Brogliato [114]. This work inspired a line of research on Lur'e systems consisting of a passive LTI system in feedback with a nonsmooth maximal monotone operator [115]–[120].

In this chapter, we revisit the classical study of nonlinear electrical networks in light of recent developments in the theory of maximal monotone operators. We study the problem of computing the periodic output of a system described by a series/parallel interconnection of basic elements, which is forced by a periodic input. The solution is computed using a fixed point iteration in the space of periodic trajectories, revisiting Zames' geometric iteration of feedback systems [22] with splitting algorithms for large scale optimization. The splitting corresponds precisely to the interconnection structure - computational steps are performed individually for each element. The interconnection must be monotone, however the elements themselves need not be. The approach of this chapter is reminiscent of the frequency response analysis of LTI systems using the transfer functions of their components. Existing frequency response methods for nonlinear systems are either approximate and limited in their applicability, as in harmonic analysis [57]–[59], [121], or involve performing a transient simulation and waiting for convergence [113], [122], [123]. A similar problem has been studied by Heemels *et al.* [124], for the class of systems described by a Lur'e-type feedback interconnection of a passive LTI state space system and a maximal monotone nonlinearity. They use a fixed point algorithm to perform a time-stepping simulation of the state space model. In contrast, here we use fixed point algorithms in the space of periodic trajectories.

The first part of this chapter introduces a general framework for modelling monotone one-port circuits, and a general method for solving their periodic input/output behavior. In Section 3.2, we motivate our work with a simple example. In Section 3.3, we introduce the basic theory of maximal monotonicity. In section 3.4, we develop a modelling framework for monotone one-port circuits, built from the series/parallel interconnection of smaller one-ports. In section 3.5, we develop a computational technique to compute the periodic output of a periodically driven maximal monotone one-port using off-the-shelf optimization methods, and introduce a new splitting algorithm which applies to arbitrary series/parallel circuits. The second part of this chapter applies this computational technique to two classes of systems. Section 3.6 applies the theory to resistors, inductors and

capacitors, and gives two detailed examples, including a large-scale circuit consisting of 300,000 elements. Section 3.7 applies the theory to memristive systems, using the specific example of a neuronal potassium conductance. Finally, in Section 3.8, several connections to the literature are explored.

3.2 MOTIVATING EXAMPLE

We begin with a simple example, which motivates the developments of this chapter: the series interconnection of two resistors (Figure 3.1).

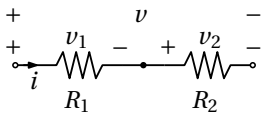

Figure 3.1: Series interconnection of two resistors.

Consider first the linear, time invariant case, $v_j = R_j i_j$. The series interconnection maps the applied current i to the port voltage v by the relation $v = R_1 i + R_2 i$. The inverse relation maps voltage v to current i by $i = v/(R_1 + R_2)$. A parallel connection is dual: voltage and current are exchanged, and resistance is replaced by its reciprocal, conductance.

The fundamentals of the circuit remain unchanged if the resistors are each replaced by a linear passive transfer function. Indeed, the series interconnection of two passive 1-ports remains passive, and the inverse of a passive transfer function is again passive.

If we replace the linear resistors by nonlinear, but passive resistors, however, several attractive properties of the resistors are lost. A passive resistor can have regions of negative slope in its $i - v$ curve (Chua, Yu, and Yu [125] give a catalogue of physical examples). The inverse of such a resistor may not be well defined. If, however, we consider monotone nonlinear resistors, the fundamentals of the LTI case remain unchanged. Monotonicity of a resistor means its $i - v$ curve is nondecreasing (see Figure 3.2); most importantly, invertibility of the interconnection is retained (in an algorithmic sense, which will be made clear in Section 3.5).

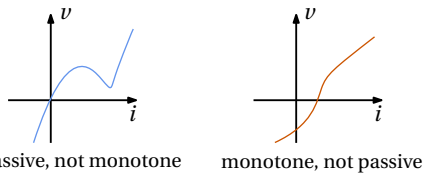

Figure 3.2: The *i-v* curves of a passive and a monotone resistor.

3.3 MAXIMAL MONOTONE RELATIONS

The property of *monotonicity* connects the physical property of energy dissipation in a device to algorithmic analysis methods. Given a Hilbert space $\mathcal{H}$, recall that a relation $S \subseteq \mathcal{H} \times \mathcal{H}$ is called *monotone* if

$$\langle u_1 - u_2 | y_1 - y_2 \rangle \geq 0$$

for any $(u_1, y_1), (u_2, y_2) \in S$. A monotone relation is called *maximal* if it is not properly contained in any other monotone relation.

Monotonicity is preserved under a number of operations. The proof of the following lemma may be found in [44].

Lemma 3.1. *Consider relations G and F which are monotone on $\mathcal{H}$. Then*

1. *G^{-1} is monotone;*
2. *$G + F$ is monotone;*
3. *αG is monotone for $\alpha > 0$.*

Maximality is preserved under inversion. However, in general, maximality is not preserved when two relations are added (indeed, their sum may be empty). We make the following assumption on summations throughout the rest of this chapter, which guarantees maximality of the sum, by [126, Thm. 1].

Assumption 3.1. Any summation of two relations G and F obeys

$$\operatorname{int} \operatorname{dom} F \cap \operatorname{dom} G \neq \varnothing$$
$$\text{or } \operatorname{int} \operatorname{dom} G \cap \operatorname{dom} F \neq \varnothing,$$

where $\operatorname{dom} S$ denotes the domain of the relation S. ⌟

This assumption is sufficient (but not necessary) for the existence of solutions to the summation (that is, the resulting relation is nonempty). We omit the proof of this fact.

Throughout this chapter, we will consider spaces of periodic signals. A trajectory $w(t)$ is said to be T-periodic if $w(t) = w(t + T)$ for all t. A T-periodic signal is described by a single period, and can be identified with a signal in a space such as $L_{2,[0,T]}$ or $l_{2,[0,T]}$, as defined in Section 1.1.

3.4 MONOTONE ONE-PORT CIRCUITS

The systems considered in this chapter are electrical one-port circuits. The study of circuits modelled as one-ports is classical, dating back to work by Foster [127], Brune [13], Bott and Duffin [15], and others. In the spirit of this classical work, and of the "tearing,

zooming and linking" modelling methodology advocated by Willems [28], we will model one-port circuits by building them as series and parallel interconnections of smaller one-port circuits.

One-port circuits have two external terminals. The port voltage v may be measured across these terminals, and the port current i may be measured through them. We assume that each of these variables takes values in $\mathbb{R}$. A one-port circuit E is defined by a relation on $L_{2,T}$ between current and voltage. We denote by $d(E) \in \{i \to v, v \to i\}$ the direction of the relation E, either current to voltage (current controlled) or voltage to current (voltage controlled). We will often denote current controlled circuits by R, and voltage controlled circuits by G. We say that E is a *μ-monotone one-port* if it is defined by a μ-monotone relation.

3.4.1 *Series and parallel interconnections*

Two one-ports may be combined to build a new one-port by series or parallel interconnection. These are illustrated in Figure 3.3.

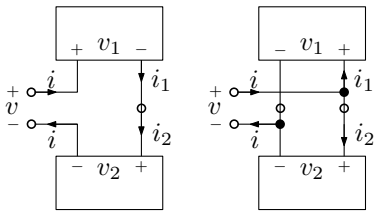

Figure 3.3: Series (left) and parallel (right) interconnections of two 1-ports.

When two one-ports are connected in parallel, their relations must be from voltage to current. If they are not, one or both relations must be inverted before interconnection. Let G_1 and G_2 be two one-port circuits such that $d(G_1) = d(G_2) = v \to i$. For a parallel interconnection, the composition of Kirchoff's laws and the relations G_1 and G_2 creates a natural forward relation from voltage to current, as follows.

1. KVL: $v = v_1 = v_2$
2. Device: $(v_1, i_1) \in G_1, \quad (v_2, i_2) \in G_2$
3. KCL: $i_1 + i_2 = i$.

We therefore have a new relation $G = G_1 + G_2$, $d(G) = v \to i$. This is illustrated in the left of Figure 3.4. Calculating the inverse relation, we have

$$\begin{aligned} i &\in (G_1 + G_2)(v) \\ G_1(v) &\in i - G_2(v) \\ v &\in G_1^{-1}(i - G_2(v)), \end{aligned}$$

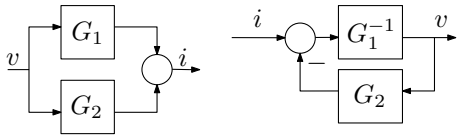

Figure 3.4: Block diagram of parallel interconnection, illustrating parallel forward relation from voltage to current, and negative feedback relation from current to voltage.

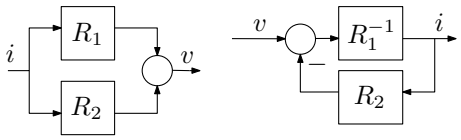

Figure 3.5: Block diagram of series interconnection, illustrating parallel forward relation from current to voltage, and negative feedback relation from voltage to current.

which is the negative feedback interconnection of G_1^{-1} and G_2, illustrated in the right of Figure 3.4.

For a series interconnection, the roles of current and voltage are reversed. Letting R_1 and R_2 be two one-port circuits such that $d(R_1) = d(R_2) = i \to v$, their series interconnection gives a relation from current to voltage, as follows.

1. KCL: $i = i_1 = i_2$
2. Device: $(i_1, v_1) \in R_1, \quad (i_2, v_2) \in R_2$
3. KVL: $v_1 + v_2 = v$.

The new relation is $R = R_1 + R_2$, with $d(R) = i \to v$. The inverse relation, from v to i, is the negative feedback interconnection of R_1^{-1} and R_2. This is illustrated in Figure 3.5.

Monotonicity of circuits is preserved under series and parallel interconnection. Precisely, we have the following.

Proposition 3.1. *1. Let E_1 and E_2 be monotone one-port circuits such that $d(E_1), d(E_2) \in \{i \to v, v \to i\}$. Then the series and parallel interconnections of E_1 and E_2 are both monotone one-ports.*

2. Let G_1 and G_2 be one-port circuits such that G_1 is α-monotone, G_2 is β-monotone, and $d(G_1) = d(G_2) = v \to i$. Then the parallel interconnection of G_1 and G_2 is $(\alpha + \beta)$-monotone.

3. Let R_1 and R_2 be one-port circuits such that R_1 is α-monotone, R_2 is β-monotone, and $d(R_1) = d(R_2) = i \to v$. Then the series interconnection of R_1 and R_2 is $(\alpha + \beta)$-monotone.

Proof. The proof of Part 1 follows directly from the preservation of monotonicity under inversion and addition (Lemma 3.1). Parts 2 and 3 follow from the fact that if E_1 is

α-monotone and E_2 is β-monotone, $E_1 + E_2$ is $(\alpha + \beta)$-monotone:

$$\begin{aligned}
&\langle u_1 - u_2 | (E_1 + E_2)u_1 - (E_1 + E_2)u_2 \rangle \\
=&\langle u_1 - u_2 | E_1 u_1 - E_1 u_2 \rangle + \langle u_1 - u_2 | E_2 u_1 - E_2 u_2 \rangle \\
\geq&(\alpha + \beta)\|u_1 - u_2\|^2.
\end{aligned}$$

□

Preservation of monotonicity under port interconnections is explored in more detail by Çamlibel and van der Schaft [111].

Repeatedly applying series and parallel interconnections allows a collection of one-port circuits to be assembled into a single, larger one-port circuit, using the relational operations of inversion and addition.

3.4.2 *Monotonicity and cyclo-passivity*

Monotone one-ports have close connections to the classical theory of feedback systems, and in particular, passivity and cyclo-passivity.

Cyclo-passivity is a generalisation of passivity to storages that are not necessarily lower bounded, first introduced by Willems [110] and later developed by Hill and Moylan [128]. For recent work on cyclo-passivity of multi-ports, see van der Schaft [129] and van der Schaft and Jeltsema [130], [131]. The incremental version of this property was first studied by Trip and De Persis [132]. We define incremental cyclo-passivity as follows:

Definition 3.1. A relation S on $L_{2,(-\infty,\infty)}$ is said to be *incrementally cyclo-passive* if, for all $(u_1, y_1), (u_2, y_2) \in S$ each supported on $[-T, T]$ and with the property that $u_1(-T) = u_1(T)$ and $u_2(-T) = u_2(T)$ for some fixed T (respectively for y_1 and y_2), then

$$\langle u_1 - u_2 | y_1 - y_2 \rangle \geq 0.$$

⌟

This corresponds to monotonicity on the space of all periodic trajectories *of any period*. The property required for the computational methods described in this paper, monotonicity on the space of periodic signals with a particular period, is a weaker notion.

We conclude this section by remarking that the preservation of monotonicity under port interconnection, proved in Proposition 3.1, can be reinterpreted in terms of negative feedback. As shown in Figures 3.4, the negative feedback interconnection of two operators F and G can be represented as a parallel interconnection of F^{-1} and G. Proposition 3.1 then allows us to recover the incremental form of the fundamental theorem of passivity.

Corollary 3.1. *Given two operators F and G, each monotone on a Hilbert space $\mathcal{H}$, their negative feedback interconnection $(F^{-1} + G)^{-1}$ is monotone on $\mathcal{H}$.*

3.5 ALGORITHMIC STEADY-STATE ANALYSIS OF SERIES/PARALLEL MONOTONE ONE-PORTS

In this section, we develop an algorithmic method for computing the periodic response of a monotone one-port which is forced by a periodic input. We consider a circuit made of series and parallel interconnections of one-port elements, each defining a (discrete time) monotone operator on $l_{2,[0,T]}$. The circuit defines a monotone operator M. Concrete examples of such circuits are given in Sections 3.6 and 3.7.

Without loss of generality, we consider the problem of computing the "output" current $i^\star$ of the monotone operator M corresponding to an "input" voltage $v^\star$.

We compute the solution as the fixed point of an iterative splitting algorithm determined from the series and parallel structure of the circuit. The algorithm is first presented for two elements, then generalized to an arbitrary composition of series and parallel interconnections.

3.5.1 *Splitting algorithms for two element circuits*

There is a large body of literature on splitting algorithms, which solve problems of the form $0 \in M_1(u) + M_2(u)$, where $M_1 + M_2$ is a maximal monotone relation. If M consists of two elements, connected in series or parallel, we can convert our problem to this form by writing $0 \in M_1(i) + M_2(i) - v^\star$ (assuming a series interconnection - the parallel interconnection is obtained by exchanging i and v). The offset $-v^\star$ does not affect the monotonicity properties of M. Splitting algorithms allow computation to be performed separately for the components M_1 and M_2, and are useful when computation for the individual components is easy, but computation for their sum is hard. Here, we describe two splitting algorithms - the forward/backward splitting, and the Douglas-Rachford splitting. Given an operator S and a scaling factor α, the α-resolvent of S is defined to be the operator

$$\operatorname{res}_{\alpha S} \coloneqq (I + \alpha S)^{-1}.$$

If S is maximal monotone, res_S is single-valued [38].

Forward/backward splitting

The simplest splitting algorithm is the forward/backward splitting [133]–[135]. Suppose M_1 and $\operatorname{res}_{\alpha M_2}$ are single-valued. Then:

$$\begin{aligned}
& 0 \in M_1(x) + M_2(x) \\
\iff \quad & 0 \in x - \alpha M_1(x) - (x + \alpha M_2(x)) \\
\iff \quad & (I + \alpha M_2)x \ni (I - \alpha M_1)x \\
\iff \quad & x = \operatorname{res}_{\alpha M_2}(I - \alpha M_1)x.
\end{aligned}$$

The fixed point iteration $x^{j+1} = \mathrm{res}_{\alpha M_2}(x^j - \alpha M_1(x^j))$ is the forward/backward splitting algorithm. The most general convergence conditions for this algorithm are given by Giselsson and Moursi [53, §6], which guarantee that this iteration is an averaged operator. These conditions may be summarised as follows.

Proposition 3.2. *Let $\mu \geq 0$, $\omega \geq 0$ and $\beta > 0$, and M_1 and M_2 be operators on a Hilbert space $\mathcal{H}$. The forward/backward algorithm, with scaling factor $\alpha \in (0, 2/(\beta + 2\mu))$, converges to a zero of $M_1 + M_2$, if one exists, in each of the following cases:*

- *M_1 is maximally μ-monotone, $M_1 - \mu I$ is $1/\beta$-cocoercive, M_2 is maximally $(-\omega)$-monotone and $\mu \geq \omega$.*
- *M_1 is maximally $(-\omega)$-monotone, $M_1 + \omega I$ is $1/\beta$-cocoercive, M_2 is maximally μ-monotone and $\mu \geq \omega$.*
- *M_1 is β-Lipschitz, M_2 is maximally μ-monotone and $\mu \geq \beta$.*

Douglas-Rachford splitting

One of the most successful splitting algorithms is the Douglas-Rachford algorithm [136], [137], which forms the basis of the Alternating Direction Method of Multipliers [138].

Given an operator S, its reflected resolvent, or Cayley operator, is the operator

$$R_{\alpha S} \coloneqq 2\mathrm{res}_{\alpha S} - I.$$

Given two operators M_1 and M_2, a scaling factor α and an initial value z^0, the Douglas-Rachford algorithm is the iteration in k given by

$$\begin{aligned} z^{k+1} &= T(z^k), \\ x^k &= \mathrm{res}_{\alpha M_2} z^k, \end{aligned}$$

where T is given by

$$T = \frac{1}{2}(I + R_{\alpha M_1} R_{\alpha M_2}), \tag{3.1}$$

and $x^k = \mathrm{res}_{\alpha M_1} z^k$ converges to a zero of $M_1 + M_2$.

Giselsson and Moursi [53, Thm 5.1] give the most general conditions for convergence of the Douglas-Rachford algorithm, which guarantee that T is averaged.

Proposition 3.3. *Let M_1 and M_2 be operators on a Hilbert space $\mathcal{H}$. Let $\mu > \omega \geq 0$ and $\alpha \in (0, (\mu - \omega)/(2\mu\omega))$. The Douglas-Rachford algorithm converges to a zero of $M_1 + M_2$, if one exits, in each of the following cases.*

- *M_1 is maximally $(-\omega)$-monotone and M_2 is maximally μ-monotone.*
- *M_2 is maximally $(-\omega)$-monotone and M_1 is maximally μ-monotone.*

3.5.2 *A nested splitting algorithm for three element circuits*

If M is composed of three elements, with one series interconnection and one parallel interconnection (see Figure 3.6), M has the form $M = M_1 + (M_2 + M_3)^{-1}$, and we can convert our problem to the form $0 \in (M_1 + (M_2 + M_3)^{-1})(u)$ again by offsetting by the input current or voltage. A naive approach to solving this problem is to using a splitting algorithm such as the forward/backward algorithm, with the resolvent step applied for M_1 and the forward step applied for $(M_2 + M_3)^{-1}$. Applying this forward step amounts to solving $y = (M_2 + M_3)^{-1}(u)$ for some u, which may be rewritten as $0 \in (M_2 + M_3)(y) - u$. This can be solved by again applying the forward/backward algorithm.

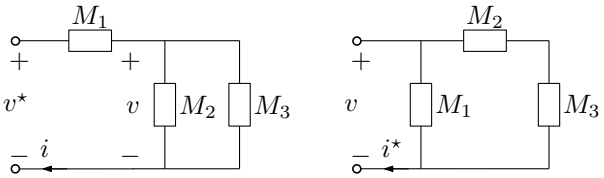

Figure 3.6: The two possible configurations of three elements with one series interconnection and one parallel interconnection.

This naive procedure has poor complexity: for every forward/backward step for $M_1 + (M_2 + M_3)^{-1}$, an *entire* fixed point iteration has to be computed for (an offset version of) $M_2 + M_3$. In this section, we propose an alternative procedure. Rather than apply a forward step for the relation $(M_2 + M_3)^{-1}$, we simply apply a *single step* of the fixed point iteration needed to compute this forward step, using the forward/backward algorithm. Assume, without loss of generality, that $d(M_1) = i \to v$ and $d(M_2) = d(M_3) = v \to i$ (the configuration shown on the left of Figure 3.6). Suppose that $v^\star \in (M_1 + (M_2 + M_3)^{-1})(i)$. Assume that M_3, $\operatorname{res}_{\alpha_1 M_2}$ and $\operatorname{res}_{\alpha_2 M_1}$ are single-valued. We then have:

$$v^\star \in v + M_1(i) \tag{3.2}$$

$$v \in (M_2 + M_3)^{-1}(i), \tag{3.3}$$

where v is the voltage over M_2, illustrated on the left of Figure 3.6. Equation (3.2) gives

$$\begin{aligned} i + \alpha_2 M_1(i) &\ni i - \alpha_2 v + \alpha_2 v^\star \\ i &= (I + \alpha_2 M_1)^{-1}(i - \alpha_2 v + \alpha_2 v^\star) \\ i &= \operatorname{res}_{\alpha_2 M_1}(i - \alpha_2 v + \alpha_2 v^\star). \end{aligned}$$

Equation (3.3) gives

$$\begin{aligned} i &\in (M_2 + M_3)(v) \\ v + \alpha_1 M_2(v) &\ni v - \alpha_1 M_3(v) + \alpha_1 i \\ v &= (I + \alpha_1 M_2)^{-1}(v - \alpha_1 M_3(v) + \alpha_1 i) \\ v &= \operatorname{res}_{\alpha_1 M_2}(v - \alpha_1 M_3(v) + \alpha_1 i). \end{aligned}$$

This shows that a fixed point of the iteration

$$v^{k+1} = \mathrm{res}_{\alpha_1 M_2}(v^k - \alpha_1 M_3(v^k) + \alpha_1 i^k)$$
$$i^{k+1} = \mathrm{res}_{\alpha_2 M_1}(i^k - \alpha_2 v^{k+1} + \alpha_2 v^\star)$$

is a solution to our original problem. In the next section, we generalize this algorithm to an arbitrary series/parallel monotone one-port, and in Theorem 3.1, we give a general condition under which the algorithm is guaranteed to converge to such a fixed point.

3.5.3 *A nested splitting algorithm for arbitrary series/parallel circuits*

In this section, we introduce a new splitting algorithm, the *nested forward/backward algorithm*, which generalizes the algorithm described in the previous section to monotone one-ports with arbitrary series and parallel interconnections, which have the general form shown in Figure 3.7 (allowing elements to be open circuits, short circuits, or whole subcircuits). We assume for simplicity that the relations G_j and R_j are single-valued, although the extension to multi-valued relations is straightforward.

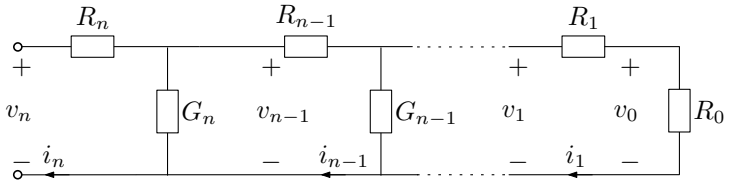

Figure 3.7: Circuit structure with nested series and parallel interconnections. R_n represents a one-port whose $i - v$ relation is known, G_n represents a one-port whose $v - i$ relation is known.

The $v - i$ relation of the circuit in Figure 3.7 is given by

$$i_n = (R_n + (G_n + (\ldots + (R_1 + R_0)^{-1} \ldots)^{-1})^{-1})^{-1}(v_n). \tag{3.4}$$

If each inversion is solved using a fixed point iteration, the number of fixed points that must be computed scales with order $\mathcal{O}(m^n)$, where n is the number of inverses in Equation (3.4), and m is the number of steps needed to compute each inverse. Following the argument of the previous section, the nested forward/backward algorithm, given in Algorithm 1, solves equations of the form (3.4) by replacing inverse operators with a single step of the forward/backward iteration needed to compute them. In this way, every inversion is computed simultaneously, using a single fixed point algorithm.

Theorem 3.1. *Algorithm 1 converges to a solution of Equation 3.4 as $k \to \infty$ if R_0 is coercive and Lipschitz, all the R_j, G_j are monotone for $j = 1, \ldots, n$, and the eigenvalues of $\mathcal{A}$ all lie within*

Algorithm 1 Nested Forward/Backward Algorithm

1: **Data:** Step sizes α_j, $j = 1, \dots, 2n-1$, external signal v_n, convergence tolerance ε.
2: **for** $j = 1, \dots, n$ **do**
3: Initialize v_{j-1}^1, i_j^1.
4: **end for**
5: $k = 1$
6: **do**
7: $i_1^{k+1} = \operatorname{res}_{\alpha_1 R_1}(i_1^k - \alpha_1 R_0(i_1^k) + \alpha_1 v_1^k)$
8: **for** $j = 2, \dots, n$ **do**
9: $v_{j-1}^{k+1} = \operatorname{res}_{\alpha_{2j-2} G_j}(v_{j-1}^k - \alpha_{2j-2} i_{j-1}^{k+1} + \alpha_{2j-2} i_j^k)$
10: $i_j^{k+1} = \operatorname{res}_{\alpha_{2j-1} R_j}(i_j^k - \alpha_{2j-1} v_{j-1}^{k+1} + \alpha_{2j-1} v_j^k)$
11: **end for**
12: $k = k + 1$.
13: **while** $\max_j(|v_j^{k+1} - v_j^k|, |i_j^{k+1} - i_j^k|) > \varepsilon$

the unit circle, where $\mathcal{A}$ is defined as the matrix

$$\begin{pmatrix} \beta_1\gamma_1 & \gamma_1\alpha_1 & 0 & 0 & \dots \\ \alpha_2\beta_1\gamma_2\gamma_1 & \gamma_2(1+\gamma_1\alpha_1\alpha_2) & \gamma_2\alpha_2 & 0 & \dots \\ \alpha_3\alpha_2\beta_1\gamma_3\gamma_2\gamma_1 & \alpha_3\gamma_2\gamma_3(1+\gamma_1\alpha_1\alpha_2) & \gamma_3(1+\gamma_2\alpha_2\alpha_3) & \gamma_3\alpha_3 & \dots \\ \alpha_4\alpha_3\alpha_2\beta_1\gamma_4\gamma_3\gamma_2\gamma_1 & \alpha_4\alpha_3\gamma_4\gamma_3\gamma_2(1+\gamma_1\alpha_1\alpha_2) & \alpha_4\gamma_4\gamma_3(1+\gamma_2\alpha_2\alpha_3) & \gamma_4(1+\gamma_3\alpha_3\alpha_4) & \dots \\ \vdots & \vdots & \vdots & \vdots & \ddots \end{pmatrix},$$

where, for $j = 1, \dots, n$, γ_{2j-2} is a Lipschitz constant of $\operatorname{res}_{\alpha_{2j-2}R_j}$, γ_{2j-1} is a Lipschitz constant of $\operatorname{res}_{\alpha_{2j-1}G_j}$ and β_1 is a Lipschitz constant of the operator $(I - \alpha_1 R_0)$.

To clarify, the constants α_j may be chosen to tune the convergence rate of the algorithm. The constants β_1 and γ_j must be Lipschitz constants for the relevant operators. Coercivity and Lipschitz continuity of R_0 means that α_1 can be chosen so that $0 < \beta_1 < 1$ [44, p. 39]. Monotonicity of R_j and G_j for all j implies that all resolvents used in the algorithm are nonexpansive, so the γ_j can always be set to 1, and this gives the simplest test for convergence. A less conservative test is given by setting the γ_j to their minimum possible values.

Proof of Theorem 3.1. We begin by showing that a fixed point of the iteration in Algorithm 1 is a solution to Equation 3.4. Indeed, substituting $v_j^{k+1} = v_j^k$ and $i_j^{k+1} = i_j^k$ into lines 7, 9 and 10 of Algorithm 1 gives

$$\begin{aligned} v_1 &= R_1(i_1) + R_0(i_1) \\ i_j &= G_j(v_{j-1}) + i_{j-1} \\ v_j &= R_j(i_j) + i_{j-1}, \end{aligned}$$

from which we obtain

$$\begin{aligned} i_1 &= (R_1 + R_0)^{-1}(v_1) \\ i_2 &= (R_2 + (G_2 + (R_1 + R_0)^{-1})^{-1})^{-1}(v_2), \end{aligned}$$

and so on, to arrive at Equation 3.4, as required.

We now show that Algorithm 1 converges to a fixed point under the stated conditions. We simplify notation by defining $u_j = i_j$, j odd, and $u_j = v_j$, j even.

Let u^k and w^k be two sequences of iterates generated by Algorithm 1, with the same input $u_n^k = w_n^k = v^\star$, and denote $u_j^k - w_j^k$ by Δu_j^k. It then follows from lines 7, 9 and 10 of Algorithm 1 that, for $j = 1, \ldots, 2n-1$,

$$\begin{aligned} \left\|\Delta u_1^{k+1}\right\| &\leq \gamma_1 \left\|\Delta u_1^k - \alpha_1 \Delta R_0(u_1^k) + \alpha_1 \Delta u_2^k\right\| \\ \left\|\Delta u_j^{k+1}\right\| &\leq \gamma_j \left\|\Delta u_j^k - \alpha_j \Delta u_{j-1}^{k+1} + \alpha_j \Delta u_{j+1}^k\right\|, \end{aligned}$$

from which it follows, via the triangle inequality, that

$$\begin{aligned} \left\|\Delta u_1^{k+1}\right\| &\leq \gamma_1 \beta_1 \left\|\Delta u_1^k\right\| + \gamma_1 \alpha_1 \left\|\Delta u_2^k\right\| \\ \left\|\Delta u_j^{k+1}\right\| &\leq \gamma_j \left\|\Delta u_j^k\right\| + \gamma_j \alpha_j \left\|\Delta u_{j-1}^{k+1}\right\| + \gamma_j \alpha_j \left\|\Delta u_{j+1}^k\right\|, \end{aligned}$$

where $\Delta u_n^k = 0$ for all k. Let $n(\Delta u^k)$ denote the vector $(\|\Delta u_1^k\|, \|\Delta u_2^k\|, \|\Delta u_3^k\|, \|\Delta u_4^k\|, \ldots)^\top$. It follows that

$$\begin{aligned} n(\Delta u^{k+1}) &\leq \mathcal{A} n(\Delta u^k) \\ &\leq \mathcal{A}^k n(\Delta u^1), \end{aligned}$$

where $\mathcal{A}$ is the matrix given in the statement of the theorem. It follows from the nonnegativity of $n(\Delta u^{k+1})$ (or from the elementwise nonnegativity of $\mathcal{A}$) that $\mathcal{A}^k n(\Delta u^1)$ is elementwise nonnegative for all k. We then have $0 \leq n(\Delta u^{k+1}) \leq z^{k+1}$, where z^{k+1} is the solution to the difference equation $z^{k+1} = \mathcal{A} z^k$ with initial condition $n(\Delta u^1)$. Since the eigenvalues of $\mathcal{A}$ are within the unit circle, it is a standard result of linear systems theory that there exist a norm $\|\cdot\|_P$ and rate $0 < \lambda < 1$ such that $\left\|z^{k+1}\right\|_P \leq \lambda \left\|z^k\right\|_P$. It follows that the sequence $n(\Delta u^k)$ converges to the zero vector in the norm $\|\cdot\|_P$ at least as fast as the sequence z^k. It then follows from the Banach fixed point theorem that each u_j^k converges to a limit $u_j^\star$ as $k \to \infty$, which completes the proof. □

3.6 RLC CIRCUITS

Here, we consider one-port circuits formed by the series and parallel interconnection of resistors, capacitors and inductors.

A resistor is a relation R on $\mathbb{R}$, the *device law*, between current and voltage:

$$\begin{aligned} R &= \{(i, v) \in \mathbb{R} \times \mathbb{R} \mid v \in R(i)\} \\ \text{or } R &= \{(v, i) \in \mathbb{R} \times \mathbb{R} \mid i \in G(v)\}. \end{aligned}$$

A resistor defines a 1-port relation on $L_{2,[0,T]}$ by applying the relation R at each time:

$$S = \left\{(v,i) \in L_{2,[0,T]} \times L_{2,[0,T]} \mid (v(t),i(t)) \in R \text{ for all } t\right\}.$$

A capacitor is a relation C on $L_{2,[0,T]}$ between current and voltage, defined by a device law $C(\cdot) : \mathbb{R} \to \mathbb{R}$, which is assumed to be a differentiable function:

$$C = \left\{(i,v) \in L_{2,[0,T]} \times L_{2,[0,T]} \mid i \in \frac{\mathrm{d}}{\mathrm{d}t} C(v)\right\}$$

An inductor is given by a relation L on $L_{2,[0,T]}$ between voltage and current, defined by a device law $L(\cdot) : \mathbb{R} \to \mathbb{R}$, which again is assumed to be a differentiable function:

$$L = \left\{(v,i) \in L_{2,[0,T]} \times L_{2,[0,T]} \mid v \in \frac{\mathrm{d}}{\mathrm{d}t} L(i)\right\}$$

The following proposition shows that resistors map T-periodic inputs to T-periodic outputs, capacitors map T-periodic voltages to T-periodic currents, and inductors map T-periodic currents to T-periodic voltages.

Proposition 3.4. *Memoryless, single-valued relations and the derivative map T-periodic inputs to T-periodic outputs.*

Proof. Let f be a memoryless, single-valued relation, that is, a relation between u and y such that $y(t) = f(u(t))$. Then $y(t+T) = f(u(t+T)) = f(u(t)) = y(t)$.

The property also holds for the derivative:

$$\begin{aligned}\frac{\mathrm{d}u(t)}{\mathrm{d}t} &= \lim_{h\to 0} \frac{u(t) + u(t+h)}{h} \\ &= \lim_{h\to 0} \frac{u(t+T) + u(t+T+h)}{h} \\ &= \frac{\mathrm{d}u(t+T)}{\mathrm{d}t}.\end{aligned}$$

□

The following proposition gives a characterization of the monotonicity of resistors on $L_{2,[0,T]}$ in terms of their devices laws.

Proposition 3.5. *A resistor is monotone on $L_{2,[0,T]}$ if and only if its device law defines a monotone relation on $\mathbb{R}$ between $i(t)$ and $v(t)$ for all t.*

Proof. If: By monotonicity of the device law on $\mathbb{R}$, we have

$$(i_1(t) - i_2(t))(v_1(t) - v_2(t)) \geq 0 \text{ for all } t,$$

from which it follows that

$$\begin{aligned}\langle i_1 - i_2 | v_1 - v_2 \rangle &= \int_0^T (i_1(t) - i_2(t))(v_1(t) - v_2(t))\,\mathrm{d}t \\ &\geq 0.\end{aligned}$$

Only if: Assume by contradiction that the device law is not monotone on $\mathbb{R}$, that is, there exist $\iota_1, \iota_2 \in \mathbb{R}$ such that

$$(\iota_1 - \iota_2)(R(\iota_1) - R(\iota_2)) < 0.$$

Taking the constant signals $i_1(t) = \iota_1$, $i_2(t) = \iota_2$ on $L_{2,[0,T]}$ shows that the resistor is not monotone on $L_{2,[0,T]}$. □

A natural question is whether the same can be said for inductors and capacitors - are these devices monotone if their device laws C and L are monotone? A striking result of Kulkarni and Safonov [73] is that this is true if and only if the device laws are *linear*.

Proposition 3.6. *Capacitors and inductors with monotone device laws on* $\mathbb{R}$ *are monotone on* $L_{2,[0,T]}$ *for all* $T \geq 0$ *if and only if their device laws are linear.*

Proof. The result is given by [73, Lemma A.2], noting that the signals used in their proof (Equation A.4) are truncated square waves, which are signals on $L_{2,[0,T]}$ for T equal to the length of the truncation. □

We now collect some results which show that, under mild conditions, series/parallel RLC circuits define operators on $L_{2,[0,T]}$.

Proposition 3.7. *A series (resp. parallel) interconnection of n one-ports which map T-periodic currents (voltages) to T-periodic voltages (currents) also maps T-periodic currents (voltages) to T-periodic voltages (currents).*

Proof. Periodicity is preserved under summation of signals, and therefore preserved by Kirchoff's laws. Indeed, if $y(t) = u_1(t) + u_2(t)$, and u_1 and u_2 are both T-periodic, then $y(t+T) = u_1(t+T) + u_2(t+T) = u_1(t) + u_2(t) = y(t)$. □

Next, we show that one-port circuits which obey simple conditions on their interconnections map periodic inputs to periodic outputs. Other classes of systems with this property include contractive state space systems [139] and approximately finite memory input/output maps [140].

Theorem 3.2. *Let* M *be the relation on* $L_{2,[0,T]}$*, from either* v *to* i *or* i *to* v*, of a 1-port constructed from the series and parallel interconnection of n constituent one-ports* M_i*, such that the construction obeys the following conditions*

1. $M_i : L_{2,[0,T]} \to L_{2,[0,T]}$ *for all* i*;*

2. *any one-port which must be inverted during the construction is coercive and Lipschitz.*

Then M *maps any input in* $L_{2,[0,T]}$ *to a unique output in* $L_{2,[0,T]}$*.*

Proof. By assumption, each of the relations M_i maps T-periodic inputs to T-periodic outputs (we denote this property by PIPO for the remainder of this proof). We show that constructing a circuit under the given conditions preserves this property. This amounts to showing that the PIPO property is preserved under summation and inversion. We have already observed that it is preserved under summation in Proposition 3.7. It remains to show that inversion preserves the PIPO property if the one-port to be inverted is coercive and Lipschitz. We do this by showing invertibility on the space of periodic trajectories. Let F be μ-coercive and λ-Lipschitz. Define the incremental relation $\Delta F(u) = F(u) - y^\star$ on $L_{2,[0,T]}$. ΔF has the same coercivity and Lipschitz properties as F. We show that the operator $I - \gamma\Delta F$ is a contraction mapping on $L_{2,[0,T]}$ for small enough $\gamma > 0$. Indeed,

$$\begin{aligned}
&\|(I-\gamma\Delta F)(x) - (I-\gamma\Delta F)y\|^2 \\
&= \|x-y\|^2 - 2\gamma\langle x-y|\Delta Fx - \Delta Fy\rangle + \gamma^2\|\Delta Fx - \Delta Fy\|^2 \\
&\leq \left(1 - 2\gamma\mu + \gamma^2\lambda^2\right)\|x-y\|^2,
\end{aligned}$$

where the inequality follows from the definitions of coercive and Lipschitz operators. Solving $0 < \left(1 - 2\gamma\mu + \gamma^2\lambda^2\right) < 1$ gives an allowable range of $\gamma \in (0, 2\mu/\lambda^2)$ for $I - \gamma\Delta F$ to be a contraction mapping on $L_{2,[0,T]}$. It then follows from the Banach fixed point theorem that $I - \gamma\Delta F$ has a unique fixed point $u^\star \in L_{2,[0,T]}$ [44, §2.4.2], [141]:

$$\begin{aligned}
& u^\star = u^\star - \gamma\Delta F(u^\star) \\
\iff\ & \Delta F(u^\star) = 0 \\
\iff\ & F(u^\star) = y^\star.
\end{aligned}$$

This shows that F is invertible on $L_{2,[0,T]}$. □

When applied to RLC circuits, condition 1 of Theorem 3.2 requires capacitors to be connected in parallel and inductors to be connected in series.

The definitions of inductors and capacitors above are time-invariant. Georgiou, Jabbari, and Smith [142] define time-varying, or adjustable, capacitors and inductors, termed the *varcapacitor* and *varinductor*:

$$\begin{aligned}
i(t) &= c(t)\frac{\mathrm{d}}{\mathrm{d}t}(c(t)v(t)) && \text{varcapacitor} \\
v(t) &= l(t)\frac{\mathrm{d}}{\mathrm{d}t}(l(t)i(t)) && \text{varinductor.}
\end{aligned}$$

If $i(t)$, $v(t)$, $l(t)$ and $c(t)$ are T-periodic, these devices are monotone on $L_{2,[0,T]}$.

Proposition 3.8. *Varcapacitors with T-periodic $c(t)$ and varinductors with T-periodic $l(t)$ are monotone on $L_{2,[0,T]}$.*

Proof. For a varcapacitor, we have

$$\begin{aligned}
&\int_0^T (v_1(t) - v_2(t))(i_1(t) - i_2(t))\,\mathrm{d}t \\
=&\int_0^T c(t)(v_1(t) - v_2(t))\frac{\mathrm{d}}{\mathrm{d}t}(c(t)(v_1(t) - v_2(t)))\,\mathrm{d}t \\
=&\int_0^T \frac{\mathrm{d}}{\mathrm{d}t}\frac{1}{2}c^2(t)(v_1(t) - v_2(t))^2\,\mathrm{d}t \\
=&\frac{1}{2}c^2(T)v^2(T) - \frac{1}{2}c^2(0)v^2(0) \\
=&0.
\end{aligned}$$

Likewise, for a varinductor, we have

$$\begin{aligned}
&\int_0^T (v_1(t) - v_2(t))(i_1(t) - i_2(t))\,\mathrm{d}t \\
=&\int_0^T l(t)(i_1(t) - i_2(t))\frac{\mathrm{d}}{\mathrm{d}t}(l(t)(i_1(t) - i_2(t)))\,\mathrm{d}t \\
=&\int_0^T \frac{\mathrm{d}}{\mathrm{d}t}\frac{1}{2}l^2(t)(i_1(t) - i_2(t))^2\,\mathrm{d}t \\
=&\frac{1}{2}l^2(T)i^2(T) - \frac{1}{2}l^2(0)i^2(0) \\
=&0.
\end{aligned}$$

□

We now give two detailed examples of the steady-state analysis of an RLC circuit. In order to obtain relations on $l_{2,[0,\tau]}$, the derivative is discretized to give an operator D. Any discretization may be used. For the examples in this chapter, we use the backwards finite difference, given by the relation

$$D = \left\{(u, y) \;\middle|\; y = \tau D_\tau u\right\},$$

where D_τ is the $\tau \times \tau$ matrix

$$D_\tau = \begin{bmatrix} 1 & 0 & \dots & 0 & -1 \\ -1 & 1 & \dots & 0 & 0 \\ 0 & -1 & \dots & 0 & 0 \\ \vdots & \vdots & \ddots & \vdots & \vdots \\ 0 & 0 & \dots & -1 & 1 \end{bmatrix}.$$

Note that D is a maximal monotone relation, as $D_\tau + D_\tau^\top \succeq 0$ [44, §2.2.3]. To obtain an accurate discrete model, a sufficient number of time steps must be used.

Example 3.1. An envelope detector is a simple nonlinear circuit consisting of a diode in series with an LTI RC filter (Figure 3.8). It is used to demodulate AM radio signals.

We model the diode using the Shockley equation:

$$v = R_{\text{diode}}(i) \coloneqq nV_T \ln\left(\frac{i}{I_s} + 1\right),$$

where I_s is the reverse bias saturation current, V_T is the thermal voltage and n is the ideality factor. The $i - v$ graph of the diode relation is strictly increasing with no endpoints; the diode relation is therefore maximal monotone.

The RC filter is itself a parallel interconnection of a resistor and capacitor, which maps voltage to current:

$$G_{RC} = CD + \frac{1}{R}I.$$

As G_{RC} is linear, it has a Lipschitz constant L equal to its largest singular value and is coercive with constant $m = \lambda_{\min}((G_{RC} + G_{RC}^{\mathsf{T}})/2)$ [44].

The incremental voltage $\Delta v = v - v^\star$ is given as a relation of i by

$$\Delta v = R_{\text{diode}}(i) + R_{RC}(i) - v^\star.$$

Given an input voltage $v^\star$, we solve for the corresponding current $i^\star$ using the Douglas-Rachford splitting. This involves applying both the resolvents res_{RC} and $\text{res}_{\text{diode}}$. The resolvent res_{RC} is given by $(I + \lambda G_{RC}^{-1})^{-1}$. This matrix is pre-computed and stored in memory. The resolvent of the diode, $\text{res}_{\text{diode}}$, is given by $\text{res}_{\text{diode}}^{-1}(x) = (I + \lambda R_{\text{diode}}(x) - \lambda v^\star)$. There is no analytic expression for this operator. Rather, the resolvent is computed numerically using the guarded Newton algorithm [45].

Figure 3.9 shows the results of performing this scheme with an input of $v^\star = \sin(2\pi t)$ A, with $R = 1\,\Omega$, $C = 1$ F, $I_s = 1 \times 10^{-14}$ A, $n = 1$ and $V_T = 0.02585$ V. The number of time steps used is 500.

⌟

Example 3.2. In this example, we analyze the large-scale circuit shown in Figure 3.10, which consists of n identical units, each consisting of a diode and LTI RC filter. The diode and RC filter are modelled as in Example 3.1.

When viewed as an interconnection of one-ports, the circuit has a recursive structure. Following the notation of Figure 3.10, for $1 \le m \le n$, we have:

$$\begin{aligned} v_m &= R_m(i_m) \\ &= R_{\text{diode}}(i_m) + G_n^{-1}(i_m), \\ i_m &= G_{m-1}(v_{m-1}) \\ &= G_{RC}(v_{m-1}) + R_{m-1}^{-1}(v_{m-1}). \end{aligned}$$

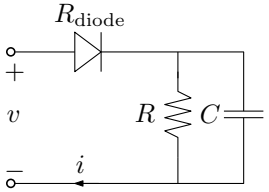

Figure 3.8: An envelope detector, configured as a 1-port.

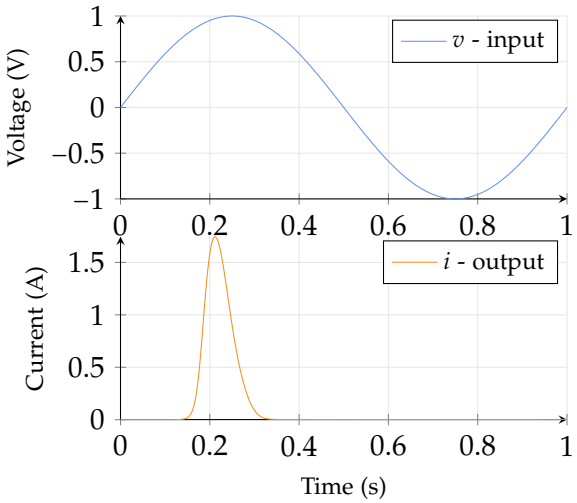

Figure 3.9: Input voltage $v^\star$ and the resulting current i for an envelope detector. One period of a periodic input and output is shown. Circuit parameters are $R = 1\,\Omega$, $C = 1$ F, $I_s = 1 \times 10^{-14}$ A, $n = 1$ and $V_T = 0.02585$ V. Algorithmic parameters are $\alpha = 0.01$, $\varepsilon = 1 \times 10^{-5}$ and 500 time steps.

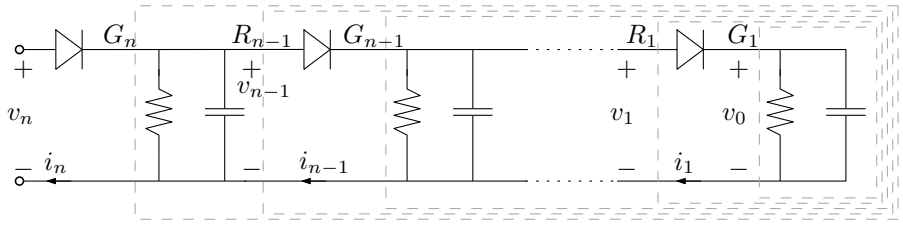

Figure 3.10: Circuit for Example 3.2. The circuit consists of n repeated units, each consisting of a diode and LTI RC filter.

The base case is $G_1 = G_{RC}$. This circuit has the form of Figure 3.7, with $R_0 = G_{RC}^{-1}$, $R_j = R_{\text{diode}}$ and $G_j = G_{RC}$ for all $j > 1$. The circuit is solved using the nested forward/backward algorithm introduced in Section 3.5.3.

Figure 3.11 shows the results of performing this scheme with $n = 100,000$ repeated units (a total of 300,000 components). The input is $v^\star = 1 + \sin(2\pi t)$ A, with circuit parameters $R = 1\,\Omega$, $C = 1$ F, $I_s = 1 \times 10^{-14}$ A, $n = 1$ and $V_T = 0.02585$ V. The number of time steps used is 256. With $n = 100,000$ units, computation took 1937 s on a standard desktop computer. With $n = 10$ units, computation took an average of 243 ms, over 21 runs.

⌟

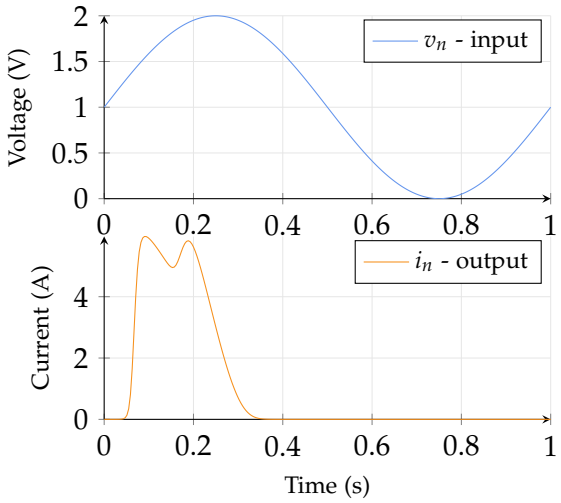

Figure 3.11: Input voltage v_n and the resulting current i_n for the circuit of Figure 3.10, with $n = 100,000$. Circuit parameters are $R = 1\,\Omega$, $C = 1$ F, $I_s = 1 \times 10^{-14}$ A, $n = 1$ and $V_T = 0.02585$ V. Algorithm parameters are $\alpha_j = 1.5$ for all j and $\varepsilon = 1 \times 10^{-4}$. One period of a periodic input and output is shown.

3.7 MEMRISTIVE SYSTEMS

In 1976, Chua and Kang [143] introduced the class of *memristive systems*, described by state space models of the form

$$\dot{x} = f(x, u, t) \tag{3.5a}$$

$$y = g(x, u, t)u. \tag{3.5b}$$

This model class describes systems which behave like resistors, in that they cannot store energy and do not produce a phase shift, but, unlike resistors, do have a memory. This work was motivated by systems such as the Hodgkin-Huxley neural membrane model [144], thermistors and discharge tubes. In this section, we show that our methods may be applied to particular members of this class.

If $\dot{x} = f(x, u)$ is a contractive, time-invariant state space system and $u(t)$ is a T-periodic input, there is a unique, globally asymptotically stable T-periodic output $y(t)$ to the memristive system (3.5) [145]. The memristive system then defines an operator on $L_{2,T}$, mapping the T-periodic input $u(t)$ to the T-periodic output $y(t)$.

To determine the monotonicity properties of memristive systems, we use the Scaled Relative Graph (SRG), introduced in Chapter 2. Recall that an operator is μ-monotone if and only if its SRG lies in the region $\{z \in \mathbb{C} \mid \mathrm{Re}(z) \geq \mu\}$.

Example 3.3. The Hodgkin-Huxley model represents a nerve axon membrane as a parallel interconnection of active *ion channels* with a capacitor [144]. Each ion channel is a time-varying conductance, which may be modelled as a memristive system. In this example,

we consider the potassium conductance $i = G_K(v)$, which is given by the equations

$$\begin{aligned} i &= \bar{g}_K n^4 (v - v_K) \\ \frac{dn}{dt} &= \alpha_n(v)(1-n) - \beta_n(v) n \\ \alpha_n(v) &= \frac{0.01(10+v)}{\exp(1+v/10)-1} \\ \beta_n(v) &= 0.125 \exp(v/80). \end{aligned}$$

Following Hodgkin and Huxley [146], the constants $\bar{g}_K$ and v_K are set to 19 m mho/cm^2 and 12 mV, respectively. The dynamics in n are contractive [147, Prop. 1], therefore the potassium conductance defines an operator on $L_{2,[0,T]}$.

The analytical SRG of the potassium conductance is difficult to determine, but we can test its monotonicity by sampling its SRG. Figure 3.12 shows points in the SRG of the potassium conductance, computed over signals of the form $u = \alpha \sin(\gamma t) + \delta$, for real parameters α, γ, δ. This plot suggests that the potassium conductance is (-0.002)-monotone on $L_{2,[0,T]}$. While we do not have a theoretical guarantee that this is the case, we can test whether the potassium conductance behaves as if it is (-0.002)-monotone when connected in a circuit.

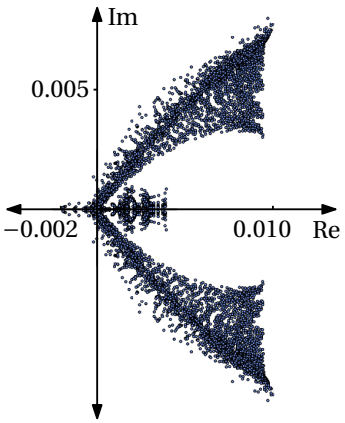

Figure 3.12: Sampling of the SRG of a potassium conductance.

We consider the parallel interconnection of the potassium current with an LTI resistor, shown in Figure 3.13. The port relation of this circuit is given by

$$i = R^{-1} v + G_K(v).$$

Given a periodic input current $i^\star$, the corresponding voltage is solved using the forward/backward algorithm. The algorithm converges when $R \geq 500\,\Omega$, supporting the hypothesis that the potassium conductance is (-0.002)-monotone. The Lissajous figure, or $i - v$ plot, is shown in Figure 3.14 for an input current of $i(t) = \sin(2\pi t)$. The potassium conductance exhibits the characteristic zero-crossing Lissajous figure of a memristive system [143].

⌟

3.8 CONNECTIONS WITH THE LITERATURE

The class of systems which can be represented by a series and parallel interconnection of maximal monotone resistors and LTI capacitors and inductors encompasses Lur'e systems with a passive LTI system in the forward path and a maximal monotone relation in the return path. Indeed, if the forward path has a transfer function $G(s)$ and the feedback path is a relation R, the Lur'e system can be synthesized as the series interconnection of a resistor with resistance relation R and an LTI network with impedance $G(s)^{-1}$ (which can be synthesized using the Bott-Duffin construction [15]). The $i-v$ relation on $L_{2,[0,T]}$ of this 1-port is $i = (R + \bar{G}^{-1})^{-1}(v)$, where $\bar{G}$ is the relation on $L_{2,[0,T]}$ corresponding to G.

Lur'e systems with passive linear part and a maximal monotone nonlinearity in the feedback path have been a focus of research on nonsmooth dynamical systems – see, for example, the survey by Brogliato and Tanwani [120]. These systems may be modelled by differential inclusions, linear complementarity systems or evolution variational inequalities. A number of specialized time-stepping methods have been developed for these classes of systems [112]. The periodic response of such Lur'e systems was first studied by [148]. Heemels *et al.* [124], give two algorithms specialized for computing the periodic output of such systems. Given a state space realization, they show that the system can be represented as a maximal monotone differential inclusion, and that backwards Euler discretization corresponds to computing the resolvent of this differential inclusion at each time step. Their first algorithm involves iteratively computing

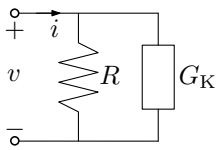

Figure 3.13: Parallel interconnection of an LTI resistor and a potassium conductance.

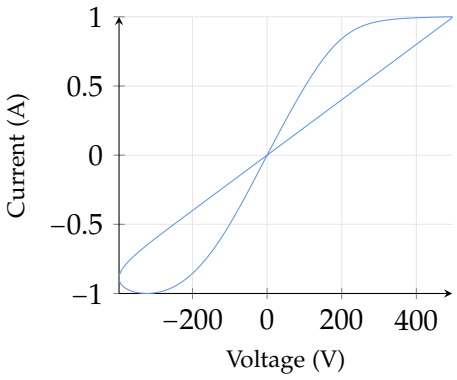

Figure 3.14: Lissajous figure of a potassium conductance in parallel with a 500 Ω resistor. The large signal magnitudes are not physically realistic, but are chosen for illustrative purposes. The Lissajous figure always passes through the origin, a fundamental characteristic of a memristive system.

this resolvent forward in time. Their second algorithm combines the computation of this resolvent over a period with a periodic boundary condition. In comparison, the algorithm we present here iterates through signal space, rather than forwards in time, and has several advantages. It is independent of a state space realization or differential inclusion representation - the relations used in computation represent the components of the system and retain their physical meaning. This structure allows splitting algorithms to be applied to separate computation for each system component. Other methods for computing the periodic output of non-smooth and multi-valued systems include the work of Iannelli, Vasca, and Angelone [149] and Meingast, Legrand, and Pierre [150].

Our method may be regarded as a signal space analog of the shooting method for solving boundary value problems in the time domain (see, for example, [151]). Given a transition mapping $\phi(t, y_0) : [0, T] \times \mathbb{R}^n \to \mathbb{R}^n$, which takes an initial condition y_0 to the output value of a dynamical system at time t, and a boundary condition $\phi(T, \cdot) = y_T$, the shooting method solves for a compatible initial condition by finding a zero of $F(a) \coloneqq y(T, a) - y_T$. It is interesting to note that if the dynamical system is order-preserving, or monotone in the sense of Smith [152] (that is, $a \leq b \implies \phi(t, a) \leq \phi(t, b)$ for all $t \geq 0$), then F is a monotone operator on $\mathbb{R}^n$.

In the linear, time invariant case, the physical property of passivity allows questions to be answered in a computationally tractable way, for example, a passive storage function can be found by solving an LMI [100]. For nonlinear passive systems, these computationally tractable methods no longer apply, in general. For nonlinear systems with incremental properties, however, tractable methods do exist. This is the fundamental result of contraction theory [145] and has been noted more recently in dissipativity analysis by Verhoek, Koelewijn and Tóth [153] and Forni, Sepulchre and van der Schaft [154]. The approaches in these works differ from that of this paper, however, in their reliance on differentiable state space models and state-dependent linear matrix inequalities, rather than monotone operator methods.

3.9 CONCLUSIONS

We have applied monotone operator optimization methods to the problem of computing the periodic output of a periodically forced, maximal monotone one-port circuit. Splitting algorithms allow the computation to be separated in a way which mirrors the structure of the system, and a new splitting algorithm has been introduced which is suited to circuits with nested series/parallel interconnections. This method has been demonstrated on the classes of circuits built from maximal monotone resistors and LTI capacitors and inductors, and memristive dynamic conductances such as the neuronal conductances of the Hodgkin-Huxley model.

The mathematical property of monotonicity connects the physical property of energy dissipation with a well-established algorithmic theory for computation, for systems

modelled as nonlinear operators. This mirrors the connection between energy dissipation in LTI state space systems and computational methods for LMIs, established by the theory of dissipativity [100]. In the next chapter, we will show that the algorithmic methods proposed here may be extended beyond the class of systems formed by the interconnection of monotone elements, to those systems formed by the *difference* of monotone elements. This includes systems with self-sustaining oscillations.

4 OSCILLATIONS IN NEGATIVE CONDUCTANCE CIRCUITS

The engineer who embarks upon the design of a feedback amplifier must be a creature of mixed emotions.

— HENDRIK BODE [155]

ABSTRACT

Circuits which contain monotone and anti-monotone components may exhibit rich steady state behaviors, including the excitable rest/spike transitions of conductance-based neuronal models. The algorithmic methods of the previous chapter are extended in order to solve such steady-state behaviors, using an adaptation of DC (difference of convex) programming.

4.1 INTRODUCTION

Mixed positive and negative feedback is a ubiquitous mechanism for the generation of switches and oscillations, in both the natural and artificial worlds [76], [88], [156]–[158]. Negative feedback regulates a passive system to equilibrium. Introducing a local positive feedback to destabilize the equilibrium allows robust oscillations to be generated. This mechanism has long been used in electrical circuits to design oscillators, such as the relaxation oscillator illustrated on the cover of Chua and Desoer's classic circuit theory text [158]. The mechanism also underpins biological systems such as the Hodgkin-Huxley model of a neuron [144], [159].

Beyond phase-plane analysis of two-dimensional mixed feedback systems, such as the van der Pol and FitzHugh-Nagumo models [160]–[162], there is a dearth of general methods for the analysis of such systems. The approximate methods of describing function analysis can be used to analyse systems where the oscillation is known to be approximately sinusoidal; this method is known, however, to work poorly for relaxation oscillations [59].

Mixed feedback systems can often be realized as passive electrical circuits containing a single *negative resistance device* [158] - this method of creating an oscillator dates back at least as far as the work of van der Pol [160]. In this chapter, we formalize this approach using the language of monotone one-ports introduced in Chapter 3. A negative resistance device is formalized as an *anti-monotone one-port*; interconnected with a monotone one-port it forms a *Difference-of-Monotone (DM) one-port*. The oscillatory steady-state solution of a mixed feedback system can be expressed as a zero of a mixed-monotone operator. In the same way as the difference of two convex functions can be minimized using an adaptation of convex optimization known as Difference of Convex (DC) Programming [163]–[169], the algorithmic methods of Chapter 3 can be adapted to the DM case to

solve the steady-state behavior of mixed-monotone one-ports. Unlike existing algorithms for DC programming, this allows splitting algorithms to be used to exploit the natural structure of mixed feedback systems.

DM operators and one-ports are formally introduced in Section 4.2. An algorithmic approach to their analysis is introduced in Section 4.3, and a generalization of the Douglas-Rachford algorithm is developed for the mixed feedback structure. This is demonstrated on the van der Pol and FitzHugh-Nagumo systems in Section 4.4.

4.2 DIFFERENCE-OF-MONOTONE ONE-PORTS

This chapter studies circuits which are defined by the *difference* of monotone elements. Before formalising this notion, we recall some definitions from the theory of convex optimization. Let $\mathcal{H}$ be a Hilbert space.

Definition 4.1. A set $C \subseteq \mathcal{H}$ is *convex* if, for all $x, y \in C$, the line $\{\alpha x + (1-\alpha)y \mid \alpha \in (0,1)\} \subseteq C$. ⌟

Definition 4.2. A function $f : \mathcal{H} \to [-\infty, \infty]$ is *convex* if its domain is a convex set and

$$f(\vartheta x + (1-\vartheta)y) \leq \vartheta f(x) + (1-\vartheta) f(y)$$

for all $x, y \in \operatorname{dom} f$ and $\vartheta \in (0,1)$. f is *concave* if $-f$ is convex. A function is said to be *proper* if its value is never $-\infty$ and is finite somewhere. A function is said to be *closed* if its epigraph is a closed set. ⌟

Definition 4.3. Given a convex function $f : \mathcal{H} \to [-\infty, \infty]$, the subgradient of f, denoted ∂f, is the set

$$\partial f \coloneqq \{g \in \mathcal{H} \mid f(y) \geq f(x) + \langle g | y - x \rangle \text{ for all } y \in \mathcal{H}\}.$$

⌟

The following standard result is due to Rockafellar [170, Lemma 1], and largely captures the reason for the success of monotone operator theory.

Proposition 4.1. *Given a convex and proper function f, its subgradient ∂f is monotone. If f is, in addition, closed, ∂f is maximal monotone.*

We define an anti-monotone operator as follows.

Definition 4.4. An operator $A : \mathcal{H} \to \mathcal{H}$ is *anti-monotone* if $-A$ is monotone. ⌟

It follows immediately that if f is concave and closed, ∂f is anti-monotone. Finally, we define a difference-of-monotone operator.

Definition 4.5. An operator $A : \mathcal{H} \to \mathcal{H}$ is *Difference-of-Monotone (DM)* if there exist monotone operators $A_1, A_2 : \mathcal{H} \to \mathcal{H}$ such that $A = A_1 - A_2$. ⌟

We adopt the one-port formalism introduced in Chapter 3, Section 3.4. A *Difference-of-Monotone (DM) one-port* is a circuit built from the series and parallel interconnection of monotone and anti-monotone one-ports. A particularly useful structure is the parallel interconnection of two monotone one-ports and one anti-monotone one-port. As illustrated in Figure 4.1, this structure can be interpreted as a monotone operator in feedback with a monotone channel and an anti-monotone channel. The steady state behavior of such a circuit can be found by solving a zero-finding problem: $0 \in A_1(v) + A_2(v) - B(v) - i$.

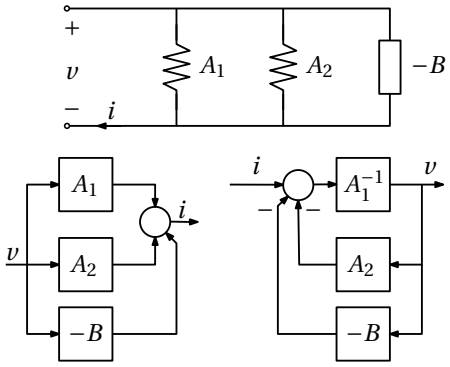

Figure 4.1: Circuit diagram and block diagrams for a mixed feedback interconnection. A_1 is a monotone operator mapping current to voltage, A_2 and B are monotone operators mapping voltage to current.

This parallel structure is general, and does not restrict the behavior of the circuit. However, by restricting ourselves to circuits in which the anti-monotone element only disrupts the monotonicity of the circuit in a local region, we can study circuits which exhibit non-equilibrium behavior but are sufficiently well-behaved to be algorithmically tractable. A basic but informative example is given by the polynomial $\frac{x^3}{3} - x$.

Example 4.1. Let $A(x) = \frac{x^3}{3}$ and $B(x) = -x$. A is maximal monotone and B is maximal anti-monotone. Graphs of A, B and $A + B$ are shown in Figure 4.2. $A + B$ is anti-monotone on $(-1, 1)$, but monotone everywhere else. ⌟

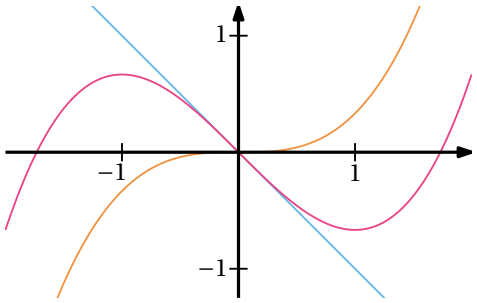

Figure 4.2: Graphs of $A(x) = \frac{x^3}{3}$ (orange), $B(x) = -x$ (blue) and $A(x) + B(x)$ (red).

4.3 DIFFERENCE-OF-MONOTONE PROGRAMS

The difference of two convex functions can be minimized using the heuristic *Convex-Concave Procedure (CCP)*, introduced by Yuille and Rangarajan [168]. This procedure is a descent algorithm, in the sense that the objective value decreases monotonically [163], [171], although the final value depends on the initial condition. The procedure is described by Algorithm 2.

Algorithm 2 Convex-Concave Procedure

1: **Data:** Closed, convex and proper f, concave and proper g, convergence tolerance ε.
2: $j = 1$
3: **do**
4: Solve $0 \in \partial f(x_{j+1}) + \partial g(x_j)$.
5: $j = j + 1$.
6: **while** $\max_j(|x_{j+1} - x_j|) > \varepsilon$

Example 4.2. Let $f(x) = \frac{x^4}{12}$ and $g(x) = -\frac{x^2}{2}$, and consider the problem $\operatorname{argmin}_{x\in\mathbb{R}} f(x) + g(x)$. As shown by Lipp and Boyd [163], Algorithm 2 converges to a local extremum of $f(x) + g(x)$, that is, to a zero of $\partial f(x) + \partial g(x)$.

Step 4 of Algorithm 2 can be rewritten using an intermediate variable z_j:

$$z_j \in -\partial g(x_j)$$
$$x_{j+1} = (\partial f)^{-1}(z_j).$$

The procedure thus involves iteratively applying $-\partial g$ and $(\partial f)^{-1}$. The iterates for a particular choice of initial condition are shown in Figure 4.3.

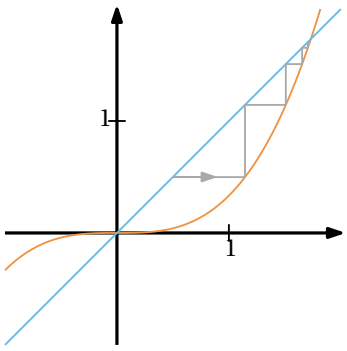

Figure 4.3: Iterates of Algorithm 2 for $f(x) = \frac{x^4}{12}$ and $g(x) = -\frac{x^2}{2}$. ∂f is plotted in orange, $-\partial g$ is plotted in blue, and the iterates are plotted in grey.

⌟

Example 4.2 demonstrates that the Convex-Concave Procedure of Algorithm 2 involves iteratively inverting one gradient then applying another. Both of these gradients are maximal monotone operators, which suggests the following extension of the CCP to arbitrary monotone operators A and B, which solves the problem $0 \in A(x) - B(x)$.

Algorithm 3 Difference-of-Monotone Procedure

1: **Data:** Maximal monotone A, monotone B, initial value x_1, convergence tolerance ε.
2: $j = 1$
3: **do**
4: Solve $x_{j+1} \in A^{-1}B(x_j)$.
5: $j = j + 1$.
6: **while** $|x_{j+1} - x_j| > \varepsilon$

A convergence result for Algorithm 3 has been submitted for publication by the author and his colleagues in reference [172].

If A^{-1} is unknown, it can be computed using a fixed point algorithm, provided A is maximal. This, however, involves an inner iteration, raising the question of whether the inner loop can be replaced by a single step, along the lines of Algorithm 1, presented in Chapter 3. A first step in this direction is to replace the update rule $x_{j+1} \in A^{-1}B(x_j)$ (line 4 of Algorithm 3) with the following:

$$\begin{aligned} z_{k+1} &= B(x_k) \\ x_{k+1} &= \operatorname{res}_{\alpha A} x_k + \alpha z_{k+1}. \end{aligned}$$

The second line applies the resolvent of the offset operator $x \mapsto A(x) - z_{k+1}$. The intuition behind this step is that the inverse A^{-1} doesn't need to be applied *exactly* – it is sufficient to simply make a step in the right direction (see Figure 4.2), for instance, the first step of the proximal iteration to invert A at z_{k+1}. It turns out that this scheme is exactly the *DC proximal algorithm* of Sun, Sampaio, and Candido [164].

To solve the mixed feedback structure of Figure 4.1, it is desirable to exploit the split structure $A = A_1 + A_2$. Following the same intuition, we propose Algorithm 4, which replaces A^{-1} with a single step of the Douglas-Rachford iteration needed to invert it. In Algorithm 4, we denote the Douglas-Rachford operator, for operators A_1 and A_2 and step size α, by $T_\alpha(A_1, A_2)$:

$$T_\alpha(A_1, A_2) \coloneqq \frac{1}{2}(I + R_{\alpha A_1} R_{\alpha A_2}). \tag{4.1}$$

Recall that $R_{\alpha S}$ denotes the Cayley operator $2\operatorname{res}_{\alpha S} - I$.

Note that a fixed point of this algorithm is a solution to $0 \in A_1(x) + A_2(x) - B(x)$: we know, by convergence of the Douglas-Rachford algorithm, that x is a solution to $0 \in A_1^j(x) + A_2(x)$, which is equal to $A_1(x) + A_2(x) - B(x)$ at a fixed point. We now make some remarks on the convergence of the algorithm. The update step of Algorithm 4 can be rewritten as

$$z_{j+1} = (\alpha B \operatorname{res}_{\alpha A_1} + T_\alpha(A_1, A_2))z_j. \tag{4.2}$$

This suggests the following result.

Theorem 4.1. *Let $A_1, A_2, B : \mathcal{H} \to \mathcal{H}$ satisfy the assumptions of Algorithm 4, and suppose there exists $\mathcal{D} \subseteq \mathcal{H}$ such that*

Algorithm 4 Difference-of-Monotone Douglas-Rachford

1: **Data:** Maximal monotone A_1, A_2, monotone, single-valued B, initial value x_1, convergence tolerance ε.
2: Define A_1^j by $x \mapsto A_1(x) - y_j$ for all j.
3: $j = 1$
4: **do**
5: Solve

$$\begin{aligned} x_{j+1} &= \operatorname{res}_{\alpha A_2}(z_j) \\ y_{j+1} &= B(x_{j+1}) \\ z_{j+1} &= T_\alpha(A_1^{j+1}, A_2)(z_j). \end{aligned}$$

6: $j = j + 1$.
7: **while** $|x_{j+1} - x_j| > \varepsilon$

1. *$\mathcal{D}$ is closed,*
2. *$T_\alpha(A_1, A_2)(\mathcal{D}) \subseteq \mathcal{D}$,*
3. *$B \operatorname{res}_{\alpha A_1}(\mathcal{D}) \subseteq \mathcal{D}$,*
4. *either A_1 or A_2 is η-coercive and λ-Lipschitz on $\mathcal{D}$,*
5. *B is μ-Lipschitz on $\mathcal{D}$.*

Then the operator of Equation 4.2 has a Lipschitz constant of

$$l = \left(1 - \frac{4\alpha\eta}{(1-\alpha\lambda)^2}\right)^{\frac{1}{2}} + \alpha\mu$$

on $\mathcal{D}$, and if $l < 1$ and $x_1 \in \mathcal{D}$, Algorithm 4 converges to a unique fixed point in $\mathcal{D}$.

The proof uses the following local version of the Banach fixed point theorem.

Lemma 4.1. *Let $T : \mathcal{D} \to \mathcal{D}$, where $\mathcal{D}$ is a closed subset of a Hilbert space $\mathcal{H}$. Suppose that T is a contraction mapping, that is,*

$$\|T(x) - T(y)\| < \|x - y\|$$

for all $x, y \in \mathcal{D}$. Then the iteration $x^{k+1} = T(x^k)$ converges to a unique fixed point of T.

Proof. The proof follows the same lines as the standard proof of the Banach fixed point theorem, using the invariance of $\mathcal{D}$ under T to ensure that the sequence of iterates remains in $\mathcal{D}$, and the closedness of T to ensure that it contains the limit of the sequence of iterates (which is shown to be Cauchy). Completeness of $\mathcal{H}$ ensures that the limit of this sequence exists in $\mathcal{H}$. □

Proof of Theorem 4.1. If either A_1 or A_2 is η-coercive and λ-Lipschitz on $\mathcal{D}$, then $R_\alpha(A_1)$ (respectively $R_\alpha(A_2)$) is a contraction with Lipschitz constant [43, p. 20]

$$\left(1 - \frac{4\alpha\eta}{(1-\alpha\lambda)^2}\right)^{\frac{1}{2}}.$$

The result then follows from the observation that $B\,\mathrm{res}_{\alpha A_2}$ has a Lipschitz constant no larger than μ, as $\mathrm{res}_{\alpha A_2}$ is nonexpansive. The convergence of Algorithm follows from Lemma 4.1 in the case that $l < 1$. □

4.4 EXAMPLES

Example 4.3. The classical van der Pol oscillator [160] is described by the differential equation

$$\ddot{v} - \mu(1 - v^2)\dot{v} + v = 0.$$

Making the substitution $i_1 = \mu v - \mu\frac{v^3}{3}$ gives

$$\begin{aligned} \ddot{v} + v &= \dot{i_1} \\ i_1 &= \mu v - \mu\frac{v^3}{3}, \end{aligned}$$

which has the one-port structure shown in Figure 4.4, where $i = 0$ and the operators A_1, A_2 and B on $L_{2,T}$ (T arbitrary) are described by

$$\begin{aligned} A_1 &: \quad \hat{v} = \frac{s^2+1}{s}\hat{i}_1 \\ A_2 &: \quad i_2 = \mu\frac{v^3}{3} \\ B &: \quad i_3 = \mu v, \end{aligned}$$

where $\hat{u}$ denotes the Laplace transform of the signal u and s denotes the Laplace transform of the derivative operator. The currents i_2 and i_3 are the currents through A_2 and B, respectively, and are related to i_1 by Kirchoff's current law: $i_1 + i_2 + i_3 = 0$.

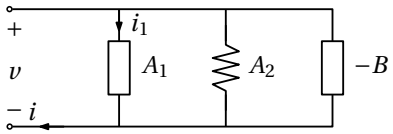

Figure 4.4: One-port model of the van der Pol ocillator and FitzHugh Nagumo neuron.

To solve for a periodic steady-state solution to the van der Pol oscillator, we apply Algorithm 4. The period T is set to the approximate period of the steady-state oscillation as predicted by Cartwright's formula [173]. The derivative operator is discretized using the central difference, with periodic boundary conditions, to give the operator

$$D = \left\{(u, y) \;\middle|\; y = TD_T u\right\},$$

where D_T is the $T \times T$ matrix

$$D_T = \begin{bmatrix} 0 & 1/2 & 0 & \dots & -1/2 \\ -1/2 & 0 & 1/2 & \dots & 0 \\ 0 & -1/2 & 0 & \dots & 0 \\ \vdots & \vdots & \vdots & \ddots & \vdots \\ 0 & 0 & 0 & \dots & 0 \end{bmatrix}.$$

Solutions for $\mu = 0.0002, 1.5$ and 10 are shown in Figure 4.5 below. ⌟

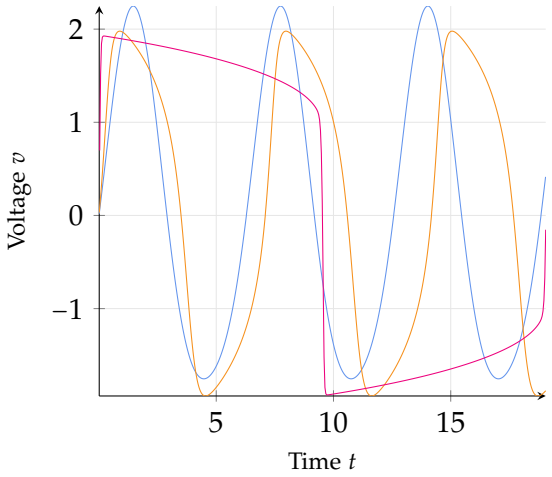

Figure 4.5: Steady-state solutions to the van der Pol oscillator for $\mu = 0.0002$ (blue), 1.5 (orange) and 10 (red). Algorithmic parameters are a step size of $\alpha = 0.05$, convergence tolerance of $\varepsilon = 0.01$ and 5000 time steps.

Example 4.4. The Hodgkin-Huxley model is a fourth order differential equation which described the electrical behavior of a nerve axon membrane [144]. The FitzHugh-Nagumo model [161], [162] is a generalization of the van der Pol oscillator which captures the main features of the Hodgkin-Huxley model but is two-dimensional, allowing phase-plane analysis. The FitzHugh-Nagumo model in particular captures *excitable behavior* – the neuron model responds passively to sub-threshold inputs, and *spikes* given super-threshold inputs. In this example, we exhibit this rest/spike transition, using a DM program to solve the neuron behavior.

The FitzHugh-Nagumo model is described by the equations

$$\begin{aligned} \dot{v} &= v - \frac{v^3}{3} - w + i \\ \tau \dot{w} &= v - bw. \end{aligned}$$

Making the substitution $i_1 = v - \frac{v^3}{3}$ gives

$$\begin{aligned} \dot{v} &= i_1 - w + i \\ \tau \dot{w} &= v - bw \\ i_1 &= v - \frac{v^3}{3}, \end{aligned}$$

which has the one-port structure shown in Figure 4.4, where the port current i is an input, and the operators A_1, A_2 and B on $L_{2,T}$ (T arbitrary) are described by

$$\begin{aligned} A_1 : &\qquad \hat{v} = \frac{\tau s^2 + bs + 1}{\tau s + b} \hat{i}_1 \\ A_2 : &\qquad i_2 = \frac{v^3}{3} \\ B : &\qquad i_3 = v, \end{aligned}$$

where $\hat{u}$ denotes the Laplace transform of the signal u and s denotes the Laplace transform of the derivative operator. i is the port current, and the currents i_2 and i_3 are the currents through A_2 and B, respectively, and are related to i_1 by Kirchoff's current law: $i_1 + i_2 + i_3 = i$.

Figure 4.6 shows the steady-state behavior of the FitzHugh-Nagumo model, with a periodic voltage signal, and demonstrates the excitable behavior of the neuron. The solution method is identical to Example 4.3.

⌟

4.5 CONCLUSIONS

Many circuits which spike or oscillate can be represented in a mixed feedback form – a passive forward path in feedback with the difference of two monotone operators. This chapter has developed monotone operator methods for solving the steady state behaviors of such circuits, via an adaptation of Difference of Convex Programming. A new splitting algorithm, the Difference-of-Monotone Douglas-Rachford algorithm, has been introduced, the structure of which matches the circuit structure of mixed feedback oscillators.

The representation of spiking circuits such as the FitzHugh-Nagumo model as the difference of monotone one-ports gives rise not only to algorithmic methods for solving their behaviors, but suggests a new paradigm for the design of such neuromorphic circuits. This is an exciting avenue for future research.

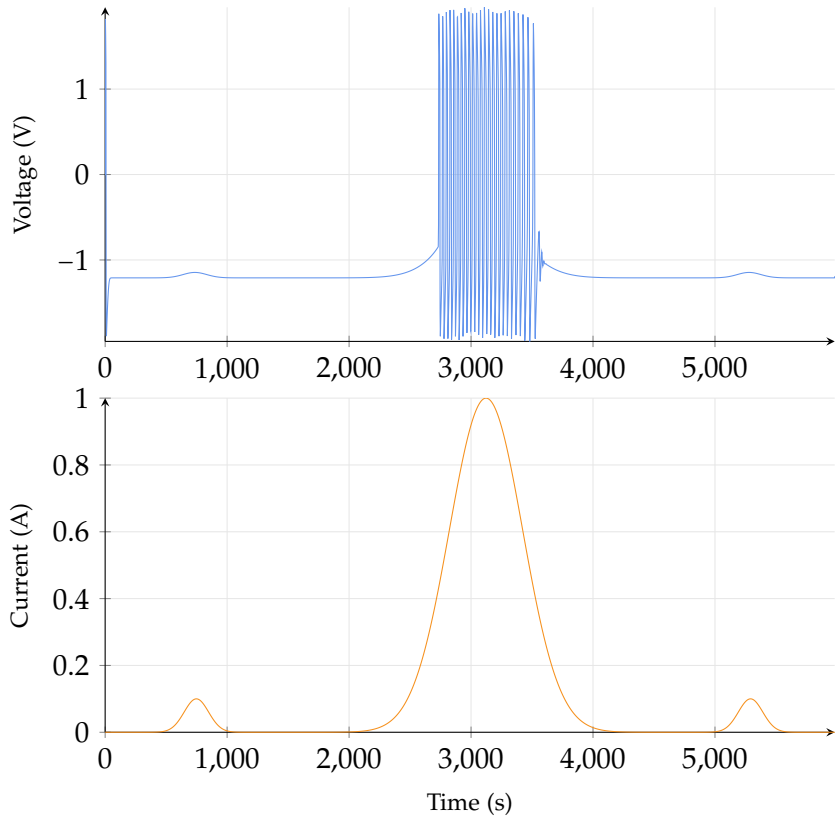

Figure 4.6: Input current i and the resulting membrane voltage v for the FitzHugh Nagumo neuron, demonstrating an excitable threshold above which behavior switches from passive to spiking. Algorithmic parameters are a step size of $\alpha = 0.05$, convergence tolerance of $\varepsilon = 0.01$ and 5000 time steps.

5 CONCLUSIONS

5.1 SUMMARY

This thesis has introduced new methods in input/output systems theory. These methods rely primarily on two novel connections: the connection between the Scaled Relative Graph and the Nyquist diagram; and the connection between the splitting algorithms of monotone operator theory and series/parallel electrical circuits.

Chapter 2 develops the Scaled Relative Graph (SRG) of Ryu, Hannah, and Yin [48] as a tool for systems theory. The SRG is shown to generalize the Nyquist diagram [9] and the incremental disc [30] to arbitrary nonlinear operators. Using a homotopy argument, we are able to infer the stability of a negative feedback interconnection from the separation of two SRGs. This amounts to verifying non-zero incremental gain of the inverse of the feedback interconnection. Special cases of this theorem include the Nyquist criterion for stable transfer functions, the incremental circle criterion, the incremental small gain and passivity theorems, the incremental secant condition and a novel "rolled-off passivity" theorem. The graphical theorem furthermore gives a natural definition of an incremental robustness margin (the distance between two SRGs, or the minimum incremental gain of the inverse of the feedback interconnection), and allows an incremental gain bound to be computed for the closed loop. To the best of the author's knowledge, this theorem represents the state of the art in incremental stability analysis; furthermore, it lends graphical intuition to a wide range of existing incremental stability results.

Chapter 3 develops new methods for solving the steady state behavior of circuits composed of monotone elements. Monotonicity is a generalization of the linear property of passivity, and is the foundation of the theory of large-scale, first order convex optimization. Given a circuit whose interconnections are either all series or all parallel, its steady state behavior can be written as the zero of a sum of monotone operators. Such a zero can be found with a direct application of a splitting algorithm. Given a circuit which contains both series and parallel interconnections, its steady state behavior is the zero of an operator formed by sums *and inverses* of the circuit components. We propose a new algorithm, the *nested forward-backward algorithm*, which solves problems with this structure.

Chapter 4 extends the methods of Chapter 3 to circuits composed of the *difference* of monotone elements. The steady state behavior of such a circuit can be solved using an adaptation of *Difference of Convex (DC) Programming*, by iteratively solving a sequence of monotone zero-finding problems. These circuits exhibit a much wider range of steady-state behaviors, including the oscillatory behavior of the van der Pol oscillator and the excitable rest/spike threshold of the FitzHugh-Nagumo model. These two circuits have a

mixed feedback structure – they consist of a passive, LTI dynamic component in feedback with the difference of two static, monotone components. We propose a new splitting algorithm, *Difference-of-Monotone Douglas-Rachford*, which matches this circuits structure, and replaces a sequence of zero-finding problems with a single zero-finding problem.

5.2 OUTLOOK

We conclude this thesis with some ideas for future research.

There are several avenues for developing the tools presented in this thesis. In many cases, SRGs remain difficult to compute, and efficient algorithms for both the estimation and analytical computation of SRGs would be a useful addition to the theory. Promising avenues include estimation techniques from nonlinear spectral theory, and automated graphical operations using methods from computational geometry.

There are also some immediate developments that can be made to the monotone operator methods presented in this thesis. The two splitting algorithms proposed in this thesis rely on replacing an inverse with a single-step approximate inverse. We have only presented the most elementary applications of this idea, but we anticipate an entire class of "nested" splitting algorithms. It will be particularly interesting to see whether the favourable convergence properties of the Douglas-Rachford algorithm can be carried over to the nested setting. A more speculative question is whether there exist splitting algorithms which correspond to circuit structures more general than series/parallel.

A natural question is how broad the class of monotone one-port circuits is. Can any monotone operator be approximated by such a circuit? An algorithm for constructing such an approximate circuit on the basis of data would find applications in analog machine learning, giving a direct, passive hardware implementation of a model. The physical intuition given by the realization is also practical. It suggests, for example, a natural model reduction strategy – simply removing the circuit elements furthest from the port terminals (algebraically, this corresponds to truncating a continued fraction expansion).

LTI systems map sinusoids into sinusoids – this makes the sinusoid the natural test signal for characterizing an LTI system. Similarly, static nonlinearities map square waves into square waves. This fact leads to the characterization of the SRG of a saturation given in Chapter 2. The idea can be formalized in the language of wavelets: a static nonlinearity is a transfer function on the space of Haar wavelets (and, in fact, is completely characterized by its action on the first two wavelets of the Haar system, making it "low-pass" in an amplitude sense). This raises two questions: can other types of systems be neatly described by choosing an appropriate wavelet; and is there a basis which allows both LTIs and static nonlinearities to be conveniently analyzed simultaneously?

Perhaps the most promising avenue for future research is the development of the theory of difference-of-monotone oscillators. Such systems are unstable, and thus do

not define operators. Their inverses, however, are the difference of monotone operators, and the methods of Chapter 4 have shown that this fact can be exploited for efficient simulation. The natural question is whether the monotone/anti-monotone structure of the inverse can be also be exploited for analysis and design.

BIBLIOGRAPHY

[1] M. A. Zidan, J. P. Strachan, and W. D. Lu, "The future of electronics based on memristive systems," *Nature Electronics*, vol. 1, no. 1, pp. 22–29, 1 Jan. 2018. DOI: 10.1038/s41928-017-0006-8.

[2] J. J. Yang, D. B. Strukov, and D. R. Stewart, "Memristive devices for computing," *Nature Nanotechnology*, vol. 8, no. 1, pp. 13–24, 1 Jan. 2013. DOI: 10.1038/nnano.2012.240.

[3] Q. Xia and J. J. Yang, "Memristive crossbar arrays for brain-inspired computing," *Nature Materials*, vol. 18, no. 4, pp. 309–323, 4 Apr. 2019. DOI: 10.1038/s41563-019-0291-x.

[4] K. Boahen, "A neuromorph's prospectus," *Computing in Science & Engineering*, vol. 19, no. 2, pp. 14–28, Mar. 2017, ISSN: 1521-9615. DOI: 10.1109/MCSE.2017.33.

[5] C. Frenkel, D. Bol, and G. Indiveri, "Bottom-Up and Top-Down Neural Processing Systems Design: Neuromorphic Intelligence as the Convergence of Natural and Artificial Intelligence," Jun. 2, 2021. arXiv: 2106.01288 [cs].

[6] D. V. Christensen, R. Dittmann, B. Linares-Barranco, A. Sebastian, M. L. Gallo, A. Redaelli, S. Slesazeck, T. Mikolajick, S. Spiga, S. Menzel, I. Valov, G. Milano, C. Ricciardi, S.-J. Liang, F. Miao, M. Lanza, T. J. Quill, S. T. Keene, A. Salleo, J. Grollier, D. Marković, A. Mizrahi, P. Yao, J. J. Yang, G. Indiveri, J. P. Strachan, S. Datta, E. Vianello, A. Valentian, J. Feldmann, X. Li, W. H. P. Pernice, H. Bhaskaran, S. Furber, E. Neftci, F. Scherr, W. Maass, S. Ramaswamy, J. Tapson, P. Panda, Y. Kim, G. Tanaka, S. Thorpe, C. Bartolozzi, T. A. Cleland, C. Posch, S.-C. Liu, G. Panuccio, M. Mahmud, A. N. Mazumder, M. Hosseini, T. Mohsenin, E. Donati, S. Tolu, R. Galeazzi, M. E. Christensen, S. Holm, D. Ielmini, and N. Pryds, "2022 Roadmap on Neuromorphic Computing and Engineering," Jan. 13, 2022. arXiv: 2105.05956 [cond-mat].

[7] G. Gallego, T. Delbruck, G. Orchard, C. Bartolozzi, B. Taba, A. Censi, S. Leutenegger, A. Davison, J. Conradt, K. Daniilidis, and D. Scaramuzza, "Event-based Vision: A Survey," *IEEE Transactions on Pattern Analysis and Machine Intelligence*, vol. 44, no. 1, pp. 154–180, Jan. 1, 2022, ISSN: 0162-8828, 2160-9292, 1939-3539. DOI: 10.1109/TPAMI.2020.3008413. arXiv: 1904.08405.

[8] M. Davies, N. Srinivasa, T.-H. Lin, G. Chinya, Y. Cao, S. H. Choday, G. Dimou, P. Joshi, N. Imam, S. Jain, Y. Liao, C.-K. Lin, A. Lines, R. Liu, D. Mathaikutty, S. McCoy, A. Paul, J. Tse, G. Venkataramanan, Y.-H. Weng, A. Wild, Y. Yang, and H. Wang, "Loihi: A Neuromorphic Manycore Processor with On-Chip Learning,"

IEEE Micro, vol. 38, no. 1, pp. 82–99, Jan. 2018, ISSN: 1937-4143. DOI: 10.1109/MM.2018.112130359.

[9] H. Nyquist, "Regeneration theory," *The Bell System Technical Journal*, vol. 11, no. 1, pp. 126–147, 1932. DOI: 10.1002/j.1538-7305.1932.tb02344.x.

[10] H. W. Bode, *Network Analysis and Feedback Amplifier Design*. D. Van Nostrand Company, Incorporated, 1945, 592 pp. Google Books: kSYhAAAAMAAJ.

[11] W. R. Evans, "Control System Synthesis by Root Locus Method," *Transactions of the American Institute of Electrical Engineers*, vol. 69, no. 1, pp. 66–69, Jan. 1950, ISSN: 2330-9431. DOI: 10.1109/T-AIEE.1950.5060121.

[12] H. W. Bode, "Feedback – the history of an idea," in *Proceedings of the Symposium on Active Networks and Feedback Systems*, ser. Microwave Research Institute Symposia Series, Brooklyn: Polytechnic Press, 1960.

[13] O. Brune, "Synthesis of a finite two-terminal network whose driving-point impedance is a prescribed function of frequency," Thesis, Massachusetts Institute of Technology, 1931.

[14] W. Cauer, "Die Verwirklichung von Wechselstromwiderständen vorgeschriebener Frequenzabhängigkeit," *Archiv für Elektrotechnik*, vol. 17, no. 4, pp. 355–388, 1926. DOI: 10.1007/BF01662000.

[15] R. Bott and R. J. Duffin, "Impedance Synthesis without Use of Transformers," *Journal of Applied Physics*, vol. 20, no. 8, pp. 816–816, 1949. DOI: 10.1063/1.1698532.

[16] N. Wiener, *Nonlinear Problems In Random Theory*. Cambridge, MA, USA: MIT Press, Dec. 15, 1958, 142 pp., ISBN: 978-0-262-23004-9.

[17] H. E. Singleton, "Theory of nonlinear transducers," Research Laboratory of Electronics, Massachusetts Institute of Technology, 160, 1950.

[18] A. G. Bose, "A theory of nonlinear systems," Thesis, Massachusetts Institute of Technology, 1956. [Online]. Available: https://dspace.mit.edu/handle/1721.1/38918 (visited on 02/08/2022).

[19] M. B. (B. Brilliant, "Theory of the analysis of nonlinear systems," 1958. [Online]. Available: https://dspace.mit.edu/handle/1721.1/4476 (visited on 02/08/2022).

[20] D. A. George, "Continuous Nonlinear Systems," MIT Technical Report 355, 1959, p. 108.

[21] J. F. Barrett, "The Use of Functionals in the Analysis of Non-linear Physical Systems," *Journal of Electronics and Control*, vol. 15, no. 6, pp. 567–615, Dec. 1, 1963, ISSN: 0368-1947. DOI: 10.1080/00207216308937611.

[22] G. Zames, "Nonlinear operators of system analysis," Massachusetts Institute of Technology, 1960.

[23] I. W. Sandberg, "B.S.T.J. briefs: An observation concerning the application of the contraction-mapping fixed-point theorem, and a result concerning the norm-boundedness of solutions of nonlinear functional equations," *The Bell System Technical Journal*, vol. 44, no. 8, pp. 1809–1812, 1965, ISSN: 0005-8580. DOI: 10.1002/j.1538-7305.1965.tb04204.x.

[24] J. C. Willems, "Stability, Instability, Invertibility and Causality," *SIAM Journal on Control*, vol. 7, no. 4, pp. 645–671, 1969, ISSN: 0036-1402. DOI: 10.1137/0307047.

[25] R. E. Kalman, "On the general theory of control systems," *IFAC Proceedings Volumes*, 1st International IFAC Congress on Automatic and Remote Control, Moscow, USSR, 1960, vol. 1, no. 1, pp. 491–502, Aug. 1, 1960, ISSN: 1474-6670. DOI: 10.1016/S1474-6670(17)70094-8.

[26] S. Boyd, L. E. Ghaoui, E. Feron, and V. Balakrishnan, *Linear Matrix Inequalities in System & Control Theory*, ser. Studies in Applied Mathematics. Society for Industrial & Applied Mathematics, 1994, vol. 15, ISBN: 0-89871-334-X.

[27] "In memoriam: Jan C. Willems," In memoriam: Jan C. Willems. (), [Online]. Available: https://jcwmemoriam.wordpress.com/ (visited on 01/25/2022).

[28] J. C. Willems, "The Behavioral Approach to Open and Interconnected Systems," *IEEE Control Systems*, vol. 27, no. 6, pp. 46–99, Dec. 2007. DOI: 10.1109/MCS.2007.906923.

[29] S. Mitter and A. R. Tannenbaum, "The legacy of George Zames (January 7, 1934 - August 10, 1997)," *IEEE Transactions on Automatic Control*, vol. 43, no. 5, pp. 590–595, May 1998, ISSN: 0018-9286, 1558-2523. DOI: 10.1109/TAC.1998.668826.

[30] G. Zames, "On the input-output stability of time-varying nonlinear feedback systems, part one: Conditions derived using concepts of loop gain, conicity, and positivity," *IEEE Transactions on Automatic Control*, vol. 11, no. 2, pp. 228–238, 1966. DOI: 10.1109/tac.1966.1098316.

[31] C. Szegedy, W. Zaremba, I. Sutskever, J. Bruna, D. Erhan, I. Goodfellow, and R. Fergus, "Intriguing properties of neural networks," Dec. 21, 2013.

[32] H. Gouk, E. Frank, B. Pfahringer, and M. J. Cree, "Regularisation of neural networks by enforcing Lipschitz continuity," *Machine Learning*, vol. 110, no. 2, pp. 393–416, Feb. 1, 2021, ISSN: 1573-0565. DOI: 10.1007/s10994-020-05929-w.

[33] M. Fazlyab, A. Robey, H. Hassani, M. Morari, and G. J. Pappas, "Efficient and Accurate Estimation of Lipschitz Constants for Deep Neural Networks," Jun. 12, 2019.

[34] M. Golomb, "Zur Theorie der nichtlinearen Integralgleichungen, Integralgleichungssysteme und allgemeinen Funktionalgleichungen," *Mathematische Zeitschrift*, vol. 39, no. 1, pp. 45–75, Dec. 1935, ISSN: 0025-5874, 1432-1823. DOI: 10.1007/BF01201344.

[35] E. H. Zarantonello, "Solving Functional Equations by Contractive Averaging.," Mathematics Research Center, Univ. of Wisconsin, Madison., PB166988, 1960, 19 pp.

[36] C. L. Dolph, "Recent developments in some non-self-adjoint problems of mathematical physics," *Bulletin of the American Mathematical Society*, vol. 67, no. 1, pp. 1–70, Jan. 1, 1961, ISSN: 0002-9904. DOI: 10.1090/S0002-9904-1961-10493-X.

[37] G. J. Minty, "Monotone networks," *Proceedings of the Royal Society of London. Series A. Mathematical and Physical Sciences*, vol. 257, no. 1289, pp. 194–212, 1960. DOI: 10.1098/rspa.1960.0144.

[38] ——, "Solving Steady-State Nonlinear Networks of 'Monotone' Elements," *IRE Transactions on Circuit Theory*, vol. 8, no. 2, pp. 99–104, Jun. 1961. DOI: 10.1109/TCT.1961.1086765.

[39] ——, "On the maximal domain of a "monotone" function.," *The Michigan Mathematical Journal*, vol. 8, no. 2, pp. 135–137, 1961. DOI: 10.1307/mmj/1028998564.

[40] C. A. Desoer and F. F. Wu, "Nonlinear Monotone Networks," *SIAM Journal on Applied Mathematics; Philadelphia*, vol. 26, no. 2, p. 19, 1974. DOI: 10.1137/0126030.

[41] R. T. Rockafellar, "Monotone operators and the proximal point algorithm," *SIAM Journal on Control and Optimization*, vol. 14, no. 5, pp. 877–898, 1976. DOI: 10.1137/0314056.

[42] R. T. Rockafellar and R. J.-B. Wets, *Variational Analysis*. 1997.

[43] E. K. Ryu and S. Boyd, "A primer on monotone operator methods," *Appl. Comput. Math.*, vol. 15, no. 1, pp. 3–43, 2016.

[44] E. K. Ryu and W. Yin, *Large-Scale Convex Optimization via Monotone Operators*, Draft. 2022.

[45] N. Parikh and S. Boyd, "Proximal Algorithms," *Foundations and Trends in Optimization*, vol. 1, no. 3, pp. 123–231, 2013.

[46] D. P. Bertsekas, "Incremental proximal methods for large scale convex optimization," *Mathematical Programming*, vol. 129, no. 2, pp. 163–195, 2011. DOI: 10.1007/s10107-011-0472-0.

[47] P. L. Combettes and J.-C. Pesquet, "Proximal Splitting Methods in Signal Processing," in *Fixed-Point Algorithms for Inverse Problems in Science and Engineering*, ser. Springer Optimization and Its Applications, H. H. Bauschke, R. S. Burachik, P. L. Combettes, V. Elser, D. R. Luke, and H. Wolkowicz, Eds., New York, NY: Springer, 2011, pp. 185–212. DOI: 10.1007/978-1-4419-9569-8_10.

[48] E. K. Ryu, R. Hannah, and W. Yin, "Scaled relative graphs: Nonexpansive operators via 2D Euclidean geometry," *Mathematical Programming*, 2021. DOI: 10.1007/s10107-021-01639-w.

[49] J. C. Willems, *The Analysis of Feedback Systems*, ser. The MIT Press Research Monograph Series, No. 62. Cambridge, Mass: The MIT Press, 1971, 188 pp., ISBN: 978-0-262-23046-9.

[50] C. A. Desoer and M. Vidyasagar, *Feedback Systems: Input–Output Properties*. Elsevier, 1975. DOI: 10.1016/b978-0-12-212050-3.x5001-4.

[51] J. W. Polderman and J. C. Willems, *Introduction to Mathematical Systems Theory: A Behavioral Approach*. Springer Science & Business Media, 1997, vol. 26, ISBN: 0-387-98266-3.

[52] D. Angeli and E. D. Sontag, "Monotone control systems," *IEEE Transactions on Automatic Control*, vol. 48, no. 10, pp. 1684–1698, Oct. 2003, ISSN: 1558-2523. DOI: 10.1109/TAC.2003.817920.

[53] P. Giselsson and W. M. Moursi, "On compositions of special cases of Lipschitz continuous operators," 2019. arXiv: 1912.13165 [math]. [Online]. Available: http://arxiv.org/abs/1912.13165 (visited on 07/26/2021).

[54] A. El-Sakkary, "The gap metric: Robustness of stabilization of feedback systems," *IEEE Transactions on Automatic Control*, vol. 30, no. 3, pp. 240–247, 1985. DOI: 10.1109/TAC.1985.1103926.

[55] G. Vinnicombe, *Uncertainty and Feedback: H_∞ Loop-Shaping and the ν-Gap Metric*. Imperial College Press, 2000, ISBN: 978-1-86094-163-4.

[56] G. Zames, "Feedback and optimal sensitivity: Model reference transformations, multiplicative seminorms, and approximate inverses," *IEEE Transactions on Automatic Control*, vol. 26, no. 2, pp. 301–320, 1981. DOI: 10.1109/TAC.1981.1102603.

[57] N. S. Krylov and N. N. Bogoliubov, *Introduction to Non-Linear Mechanics*. Princeton: Princeton University Press, 1947, ISBN: 978-0-691-07985-1.

[58] A. Blagquière, *Nonlinear System Analysis*. Academic Press, 1966.

[59] J.-J. E. Slotine and W. Li, *Applied Nonlinear Control*. Englewood Cliffs, N.J: Prentice Hall, 1991, 459 pp., ISBN: 978-0-13-040890-7.

[60] A. Pavlov, N. van de Wouw, and H. Nijmeijer, "Frequency response functions and Bode plots for nonlinear convergent systems," in *Proceedings of the 45th IEEE Conference on Decision and Control*, San Diego, CA, USA: IEEE, 2006, pp. 3765–3770. DOI: 10.1109/CDC.2006.377669.

[61] C. Chen, D. Zhao, W. Chen, S. Z. Khong, and L. Qiu, "Phase of Nonlinear Systems," 2020. arXiv: 2012.00692 [cs, eess, math].

[62] C. Chen, W. Chen, D. Zhao, S. Z. Khong, and L. Qiu, "The Singular Angle of Nonlinear Systems," Sep. 3, 2021. arXiv: 2109.01629 [cs, eess, math].

[63] X. Huang, E. K. Ryu, and W. Yin, "Tight Coefficients of Averaged Operators via Scaled Relative Graph," 2020. arXiv: 1912.01593 [math].

[64] G. Zames, "On the input-output stability of time-varying nonlinear feedback systems–Part II: Conditions involving circles in the frequency plane and sector nonlinearities," *IEEE Transactions on Automatic Control*, vol. 11, no. 3, pp. 465–476, Jul. 1966, ISSN: 1558-2523. DOI: 10.1109/TAC.1966.1098356.

[65] T. Georgiou and M. Smith, "Optimal robustness in the gap metric," *IEEE Transactions on Automatic Control*, vol. 35, no. 6, pp. 673–686, 1990. DOI: 10.1109/9.53546.

[66] C. Foias, T. Georgiou, and M. Smith, "Robust stability of feedback systems: A geometric approach using the gap metric," *SIAM Journal on Control and Optimization*, vol. 31, no. 6, p. 20, 1993, ISSN: 03630129. DOI: 10.1137/0331071.

[67] T. Georgiou and M. Smith, "Robustness analysis of nonlinear feedback systems: An input-output approach," *IEEE Transactions on Automatic Control*, vol. 42, no. 9, pp. 1200–1221, 1997. DOI: 10.1109/9.623082.

[68] A. Megretski and A. Rantzer, "System analysis via integral quadratic constraints," *IEEE Transactions on Automatic Control*, vol. 42, no. 6, pp. 819–830, 1997. DOI: 10.1109/9.587335.

[69] J. Carrasco and P. Seiler, "Conditions for the equivalence between IQC and graph separation stability results," *International Journal of Control*, vol. 92, no. 12, pp. 2899–2906, 2019. DOI: 10.1080/00207179.2018.1465205.

[70] G. Zames and P. L. Falb, "Stability conditions for systems with monotone and slope-restricted nonlinearities," *SIAM Journal on Control*, vol. 6, no. 1, pp. 89–108, 1968. DOI: 10.1137/0306007.

[71] R. O'Shea, "A combined frequency-time domain stability criterion for autonomous continuous systems," *IEEE Transactions on Automatic Control*, vol. 11, no. 3, pp. 477–484, 1966. DOI: 10.1109/TAC.1966.1098402.

[72] ——, "An improved frequency time domain stability criterion for autonomous continuous systems," *IEEE Transactions on Automatic Control*, vol. 12, no. 6, pp. 725–731, 1967. DOI: 10.1109/TAC.1967.1098725.

[73] V. V. Kulkarni and M. G. Safonov, "Incremental positivity non-preservation by stability multipliers," in *Proceedings of the 40th IEEE Conference on Decision and Control*, vol. 1, 2001, 33–38 vol.1. DOI: 10.1109/CDC.2001.980064.

[74] E. D. Sontag, "Passivity gains and the "secant condition" for stability," *Systems & Control Letters*, vol. 55, no. 3, pp. 177–183, 2006. DOI: 10.1016/j.sysconle.2005.06.010.

[75] M. Arcak and E. D. Sontag, "Diagonal stability of a class of cyclic systems and its connection with the secant criterion," *Automatica*, vol. 42, no. 9, pp. 1531–1537, 2006, ISSN: 0005-1098. DOI: 10.1016/j.automatica.2006.04.009.

[76] G.-B. Stan and R. Sepulchre, "Analysis of Interconnected Oscillators by Dissipativity Theory," *IEEE Transactions on Automatic Control*, vol. 52, no. 2, pp. 256–270, Feb. 2007. DOI: 10.1109/tac.2006.890471.

[77] G. H. Hines, M. Arcak, and A. K. Packard, "Equilibrium-independent passivity: A new definition and numerical certification," *Automatica*, vol. 47, no. 9, pp. 1949–1956, 2011. DOI: 10.1016/j.automatica.2011.05.011.

[78] J. C. Doyle, B. A. Francis, and A. R. Tannenbaum, *Feedback Control Theory*. Courier Corporation, 1992.

[79] T. Chaffey and R. Sepulchre, "Monotone Circuits," in *Proceedings of the European Control Conference*, 2021. arXiv: 2012.11533.

[80] R. Pates, "The scaled relative graph of a linear operator," 2021. arXiv: 2106.05650 [math].

[81] R. T. Rockafellar and R. J. B. Wets, *Variational Analysis*, red. by M. Berger, P. de la Harpe, F. Hirzebruch, N. J. Hitchin, L. Hörmander, A. Kupiainen, G. Lebeau, M. Ratner, D. Serre, Y. G. Sinai, N. J. A. Sloane, A. M. Vershik, and M. Waldschmidt, ser. Grundlehren Der Mathematischen Wissenschaften. Berlin, Heidelberg: Springer Berlin Heidelberg, 1998, vol. 317, ISBN: 978-3-540-62772-2 978-3-642-02431-3. DOI: 10.1007/978-3-642-02431-3.

[82] E. Summers, M. Arcak, and A. Packard, "Delay robustness of interconnected passive systems: An integral quadratic constraint approach," *IEEE Transactions on Automatic Control*, vol. 58, no. 3, pp. 712–724, 2013. DOI: 10.1109/TAC.2012.2219972.

[83] U. T. Jonsson, Chung-Yao Kao, and A. Megretski, "A semi-infinite optimization problem in harmonic analysis of uncertain systems," in *Proceedings of the 2001 American Control Conference*, vol. 4, 2001, 3029–3034 vol.4. DOI: 10.1109/ACC.2001.946379.

[84] R. Wang and I. R. Manchester, "Robust contraction analysis of nonlinear systems via differential IQC," in *2019 IEEE 58th Conference on Decision and Control (CDC)*, Nice, France: IEEE, Dec. 2019, pp. 6766–6771, ISBN: 978-1-72811-398-2. DOI: 10.1109/CDC40024.2019.9029867.

[85] I. R. Manchester and J.-J. E. Slotine, "Robust control contraction metrics: A convex approach to nonlinear state-feedback H^∞ control," *IEEE Control Systems Letters*, vol. 2, no. 3, pp. 333–338, 2018, ISSN: 2475-1456. DOI: 10.1109/LCSYS.2018.2836355.

[86] J. J. Tyson and H. G. Othmer, "The Dynamics of Feedback Control Circuits in Biochemical Pathways," in *Progress in Theoretical Biology*, Elsevier, 1978, pp. 1–62, ISBN: 978-0-12-543105-7. [Online]. Available: https://linkinghub.elsevier.com/retrieve/pii/B9780125431057500087 (visited on 06/22/2021).

[87] J. Mallet-Paret and G. R. Sell, "The Poincaré–Bendixson Theorem for Monotone Cyclic Feedback Systems with Delay," *Journal of Differential Equations*, vol. 125, no. 2, pp. 441–489, 1996, ISSN: 0022-0396. DOI: 10.1006/jdeq.1996.0037.

[88] G.-B. Stan, A. Hamadeh, R. Sepulchre, and J. Goncalves, "Output synchronization in networks of cyclic biochemical oscillators," in *IEEE American Control Conference*, 2007, pp. 3973–3978. DOI: 10.1109/ACC.2007.4282673.

[89] B. D. O. Anderson, "Failures of adaptive control theory and their resolution," *Communications in Information and Systems*, vol. 5, no. 1, pp. 1–20, 2005, ISSN: 15267555, 21634548. DOI: 10.4310/CIS.2005.v5.n1.a1.

[90] W. M. Griggs, B. D. O. Anderson, and A. Lanzon, "A "mixed" small gain and passivity theorem in the frequency domain," *Systems & Control Letters*, vol. 56, no. 9, pp. 596–602, Sep. 1, 2007, ISSN: 0167-6911. DOI: 10.1016/j.sysconle.2007.04.005.

[91] J. R. Forbes and C. J. Damaren, "Hybrid passivity and finite gain stability theorem: Stability and control of systems possessing passivity violations," *IET Control Theory & Applications*, vol. 4, no. 9, pp. 1795–1806, Sep. 1, 2010, ISSN: 1751-8652. DOI: 10.1049/iet-cta.2009.0137.

[92] T. Iwasaki and S. Hara, "Generalized KYP lemma: Unified frequency domain inequalities with design applications," *IEEE Transactions on Automatic Control*, vol. 50, no. 1, pp. 41–59, Jan. 2005, ISSN: 1558-2523. DOI: 10.1109/TAC.2004.840475.

[93] J. R. Forbes and C. J. Damaren, "Synthesis of optimal finite-frequency controllers able to accommodate passivity violations," *IEEE Transactions on Control Systems Technology*, vol. 21, no. 5, pp. 1808–1819, Sep. 2013, ISSN: 1558-0865. DOI: 10.1109/TCST.2012.2216268.

[94] W. M. Griggs, B. D. Anderson, A. Lanzon, and M. C. Rotkowitz, "Interconnections of nonlinear systems with "mixed" small gain and passivity properties and associated input–output stability results," *Systems & Control Letters*, vol. 58, no. 4, pp. 289–295, 2009, ISSN: 01676911. DOI: 10.1016/j.sysconle.2008.11.006.

[95] W. M. Griggs, B. D. O. Anderson, and A. Lanzon, "A "mixed" small gain and passivity theorem for an interconnection of linear time-invariant systems," in *IEEE European Control Conference*, 2007, pp. 2410–2416, ISBN: 978-3-9524173-8-6. DOI: 10.23919/ECC.2007.7068244.

[96] W. Rudin, *Real and Complex Analysis*, 3rd ed. New York: McGraw-Hill, 1987, 416 pp., ISBN: 978-0-07-054234-1.

[97] V. A. Yakubovich, "The solution of some matrix inequalities encountered in automatic control theory," *Dokl. Akad. Nauk SSSR.*, vol. 143, no. 6, pp. 1304–1307, 1962.

[98] R. E. Kalman, "Lyapunov Functions for the Problem of Lur'e in Automatic Control," *Proceedings of the National Academy of Sciences*, vol. 49, no. 2, pp. 201–205, 1963. DOI: 10.1073/pnas.49.2.201. pmid: 16591048.

[99] V. M. Popov, "Hyperstability and optimality of automatic systems with several control functions," *Rev. Roumaine Sci. Tech.*, vol. 9, no. 4, pp. 629–890, 1964.

[100] J. C. Willems, "Dissipative Dynamical Systems Part II: Linear systems with quadratic supply rates," *Archive for Rational Mechanics and Analysis*, vol. 45, no. 5, pp. 352–393, 1972. DOI: 10.1007/BF00276494.

[101] ——, "Dissipative dynamical systems part I: General theory," *Archive for Rational Mechanics and Analysis*, vol. 45, pp. 321–351, 1972.

[102] D. J. Hill and P. J. Moylan, "The stability of nonlinear dissipative systems," *IEEE Transactions on Automatic Control*, vol. 21, no. 5, pp. 708–711, 1976. DOI: 10.1109/TAC.1976.1101352.

[103] ——, "Dissipative dynamical systems: Basic input-output and state properties," *Journal of the Franklin Institute*, vol. 309, no. 5, pp. 327–357, May 1, 1980. DOI: 10.1016/0016-0032(80)90026-5.

[104] P. J. Moylan, *Dissipative Systems and Stability*. 2014. DOI: 10.13140/2.1.1110.8169.

[105] A. van der Schaft, *L2-Gain and Passivity Techniques in Nonlinear Control*, 3rd ed., ser. Communications and Control Engineering. Springer International Publishing, 2017, ISBN: 978-3-319-49991-8. DOI: 10.1007/978-3-319-49992-5.

[106] B. Jayawardhana, R. Ortega, E. Garcia-Canseco, and F. Castanos, "Passivity of nonlinear incremental systems: Application to PI stabilization of nonlinear RLC circuits," in *Proceedings of the 45th IEEE Conference on Decision and Control*, San Diego, CA: IEEE, 2006, pp. 3808–3812. DOI: 10.1109/CDC.2006.377132.

[107] R. Ortega, A. Loría, P. J. Nicklasson, and H. Sira-Ramírez, *Passivity-Based Control of Euler-Lagrange Systems: Mechanical, Electrical and Electromechanical Applications*, red. by B. W. Dickinson, A. Fettweis, J. L. Massey, J. W. Modestino, E. D. Sontag, and M. Thoma, ser. Communications and Control Engineering. London: Springer London, 1998, ISBN: 978-1-84996-852-2 978-1-4471-3603-3. DOI: 10.1007/978-1-4471-3603-3.

[108] R. Sepulchre, M. Janković, and P. V. Kokotović, *Constructive Nonlinear Control*. Springer London, 1997. DOI: 10.1007/978-1-4471-0967-9.

[109] R. J. Duffin, "Nonlinear networks. I," *Bulletin of the American Mathematical Society*, vol. 52, no. 10, pp. 833–839, 1946. DOI: 10.1090/S0002-9904-1946-08650-4.

[110] J. C. Willems, "Qualitative Behavior of Interconnected Systems," in *Annals of Systems Research: Publikatie van de Systeemgroep Nederland Publication of the Netherlands Society for Systems Research*, ser. Annals of Systems Research, B. van Rootselaar, Ed., Boston, MA: Springer US, 1974, pp. 61–80, ISBN: 978-1-4613-4555-8. DOI: 10.1007/978-1-4613-4555-8_4.

[111] M. K. Çamlibel and A. van der Schaft, "Incrementally port-hamiltonian systems," in *52nd IEEE Conference on Decision and Control*, Dec. 2013, pp. 2538–2543. DOI: 10.1109/CDC.2013.6760262.

[112] V. Acary and B. Brogliato, *Numerical Methods for Nonsmooth Dynamical Systems: Applications in Mechanics and Electronics*, ser. Lecture Notes in Applied and Computational Mechanics. 2008, vol. 35, ISBN: 978-3-540-75391-9.

[113] B. Brogliato, *Nonsmooth Mechanics: Models, Dynamics and Control*, ser. Communications and Control Engineering. Springer International Publishing, 2016. DOI: 10.1007/978-3-319-28664-8.

[114] ——, "Absolute stability and the Lagrange–Dirichlet theorem with monotone multivalued mappings," *Systems & Control Letters*, vol. 51, no. 5, pp. 343–353, 2004. DOI: 10.1016/j.sysconle.2003.09.007.

[115] B. Brogliato and W. P. M. H. Heemels, "Observer Design for Lur'e Systems With Multivalued Mappings: A Passivity Approach," *IEEE Transactions on Automatic Control*, vol. 54, no. 8, pp. 1996–2001, Aug. 2009, ISSN: 1558-2523. DOI: 10.1109/TAC.2009.2023968.

[116] B. Brogliato and D. Goeleven, "Well-posedness, stability and invariance results for a class of multivalued Lur'e dynamical systems," *Nonlinear Analysis: Theory, Methods & Applications*, vol. 74, no. 1, pp. 195–212, Jan. 2011, ISSN: 0362546X. DOI: 10.1016/j.na.2010.08.034.

[117] ——, "Existence, uniqueness of solutions and stability of nonsmooth multivalued Lur'e dynamical systems," *Journal of Convex Analysis*, vol. 20, Jan. 1, 2013.

[118] M. K. Çamlibel and J. M. Schumacher, "Linear passive systems and maximal monotone mappings," *Mathematical Programming*, vol. 157, no. 2, pp. 397–420, 2016. DOI: 10.1007/s10107-015-0945-7.

[119] S. Adly, A. Hantoute, and B. K. Le, "Maximal monotonicity and cyclic monotonicity arising in nonsmooth Lur'e dynamical systems," *Journal of Mathematical Analysis and Applications*, vol. 448, no. 1, pp. 691–706, 2017. DOI: 10.1016/j.jmaa.2016.11.025.

[120] B. Brogliato and A. Tanwani, "Dynamical Systems Coupled with Monotone Set-Valued Operators: Formalisms, Applications, Well-Posedness, and Stability," *SIAM Review*, vol. 62, no. 1, pp. 3–129, 2020. DOI: 10.1137/18M1234795.

[121] P. Feldmann, B. Melville, and D. Long, "Efficient frequency domain analysis of large nonlinear analog circuits," in *Proceedings of Custom Integrated Circuits Conference*, 1996, pp. 461–464. DOI: 10.1109/CICC.1996.510597.

[122] T. Aprille and T. Trick, "Steady-state analysis of nonlinear circuits with periodic inputs," *Proceedings of the IEEE*, vol. 60, no. 1, pp. 108–114, 1972. DOI: 10.1109/PROC.1972.8563.

[123] F. E. Cellier and E. Kofman, *Continuous System Simulation*. New York: Springer, 2006, 643 pp., ISBN: 978-0-387-26102-7 978-0-387-30260-7.

[124] W. Heemels, V. Sessa, F. Vasca, and M. Çamlibel, "Computation of periodic solutions in maximal monotone dynamical systems with guaranteed consistency," *Nonlinear Analysis: Hybrid Systems*, vol. 24, pp. 100–114, 2017. DOI: 10.1016/j.nahs.2016.10.006.

[125] L. O. Chua, J. Yu, and Y. Yu, "Negative resistance devices," *International Journal of Circuit Theory and Applications*, vol. 11, no. 2, pp. 161–186, 1983. DOI: 10.1002/cta.4490110205.

[126] R. T. Rockafellar, "On the Maximality of Sums of Nonlinear Monotone Operators," *Transactions of the American Mathematical Society*, vol. 149, no. 1, pp. 75–88, 1970. DOI: 10.2307/1995660.

[127] R. M. Foster, "A Reactance Theorem," *Bell System Technical Journal*, vol. 3, no. 2, pp. 259–267, 1924, ISSN: 1538-7305. DOI: 10.1002/j.1538-7305.1924.tb01358.x.

[128] D. J. Hill and P. J. Moylan, *Cyclo-Dissipativeness, Dissipativeness and Losslessness for Nonlinear Dynamical Systems*. Newcastle, N.S.W.: University of Newcastle, Dept. of Electrical Engineering, 1975, ISBN: 978-0-7259-0213-1.

[129] A. van der Schaft, "Cyclo-dissipativity revisited," Mar. 23, 2020. arXiv: 2003.10143 [math].

[130] A. van der Schaft and D. Jeltsema, "Limits to Energy Conversion," Jun. 29, 2020. arXiv: 2006.15953 [math].

[131] ——, "On Energy Conversion in Port-Hamiltonian Systems," 2021. arXiv: 2103.09116 [math].

[132] S. Trip and C. De Persis, "Distributed Optimal Load Frequency Control with Non-Passive Dynamics," *IEEE Transactions on Control of Network Systems*, vol. 5, no. 3, pp. 1232–1244, Sep. 2018, ISSN: 2325-5870. DOI: 10.1109/TCNS.2017.2698259.

[133] G. B. Passty, "Ergodic convergence to a zero of the sum of monotone operators in Hilbert space," *Journal of Mathematical Analysis and Applications*, vol. 72, no. 2, pp. 383–390, 1979. DOI: 10.1016/0022-247X(79)90234-8.

[134] D. Gabay, "Chapter IX Applications of the Method of Multipliers to Variational Inequalities," in *Studies in Mathematics and Its Applications*, ser. Augmented Lagrangian Methods: Applications to the Numerical Solution of Boundary-Value Problems, M. Fortin and R. Glowinski, Eds., vol. 15, Elsevier, 1983. DOI: 10.1016/S0168-2024(08)70034-1.

[135] P. Tseng, "Applications of a Splitting Algorithm to Decomposition in Convex Programming and Variational Inequalities," *SIAM Journal on Control and Optimization*, vol. 29, no. 1, pp. 119–138, 1988. DOI: 10.1137/0329006.

[136] J. Douglas and H. H. Rachford, "On the Numerical Solution of Heat Conduction Problems in Two and Three Space Variables," *Transactions of the American Mathematical Society*, vol. 82, no. 2, pp. 421–439, 1956, ISSN: 0002-9947. DOI: 10.2307/1993056.

[137] P. L. Lions and B. Mercier, "Splitting Algorithms for the Sum of Two Nonlinear Operators," *SIAM Journal on Numerical Analysis*, vol. 16, no. 6, pp. 964–979, 1979. DOI: 10.1137/0716071.

[138] S. Boyd, N. Parikh, E. Chu, B. Peleato, and J. Eckstein, "Distributed Optimization and Statistical Learning via the Alternating Direction Method of Multipliers," *Foundations and Trends® in Machine Learning*, vol. 3, no. 1, pp. 1–122, 2010. DOI: 10.1561/2200000016.

[139] E. D. Sontag, "Contractive Systems with Inputs," in *Perspectives in Mathematical System Theory, Control, and Signal Processing*, ser. Lecture Notes in Control and Information Sciences, J. C. Willems, S. Hara, Y. Ohta, and H. Fujioka, Eds., red. by M. Morari and M. Thoma, vol. 398, Berlin, Heidelberg: Springer Berlin Heidelberg, 2010, pp. 217–228, ISBN: 978-3-540-93917-7 978-3-540-93918-4. DOI: 10.1007/978-3-540-93918-4_20.

[140] I. W. Sandberg, "Approximately-finite memory and input-output maps," *IEEE Transactions on Circuits and Systems I: Fundamental Theory and Applications*, vol. 39, no. 7, pp. 549–556, Jul. 1992. DOI: 10.1109/81.257287.

[141] S. Banach, "Sur les opérations dans les ensembles abstraits et leur application aux équations intégrales," *Fundamenta Mathematicae*, vol. 3, pp. 133–181, 1922. DOI: 10.4064/fm-3-1-133-181.

[142] T. T. Georgiou, F. Jabbari, and M. C. Smith, "Principles of Lossless Adjustable One-Ports," *IEEE Transactions on Automatic Control*, vol. 65, no. 1, pp. 252–262, Jan. 2020, ISSN: 1558-2523. DOI: 10.1109/TAC.2019.2917853.

[143] L. O. Chua and S. M. Kang, "Memristive devices and systems," *Proceedings of the IEEE*, vol. 64, no. 2, pp. 209–223, 1976. DOI: 10.1109/PROC.1976.10092.

[144] A. L. Hodgkin and A. F. Huxley, "A quantitative description of membrane current and its application to conduction and excitation in nerve," *The Journal of Physiology*, vol. 117, no. 4, pp. 500–544, Aug. 1952. DOI: 10.1113/jphysiol.1952.sp004764.

[145] W. Lohmiller and J.-J. E. Slotine, "On Contraction Analysis for Non-linear Systems," *Automatica*, vol. 34, no. 6, pp. 683–696, 1998. DOI: 10.1016/S0005-1098(98)00019-3.

[146] A. L. Hodgkin and A. F. Huxley, "The components of membrane conductance in the giant axon of Loligo," *The Journal of Physiology*, vol. 116, no. 4, pp. 473–496, 1952, ISSN: 1469-7793. DOI: 10.1113/jphysiol.1952.sp004718.

[147] T. B. Burghi, M. Schoukens, and R. Sepulchre, "Feedback identification of conductance-based models," *Automatica*, vol. 123, p. 109 297, Jan. 1, 2021. DOI: 10.1016/j.automatica.2020.109297.

[148] H. Brézis, *Opérateurs maximaux monotones et semi-groupes de contractions dans les espaces de Hilbert*. North-Holland, 1973, 193 pp., ISBN: 978-0-08-087116-5. Google Books: cwCA6AYpBtcC.

[149] L. Iannelli, F. Vasca, and G. Angelone, "Computation of Steady-State Oscillations in Power Converters Through Complementarity," *IEEE Transactions on Circuits and Systems I: Regular Papers*, vol. 58, no. 6, pp. 1421–1432, Jun. 2011, ISSN: 1558-0806. DOI: 10.1109/TCSI.2010.2094390.

[150] M. B. Meingast, M. Legrand, and C. Pierre, "A linear complementarity problem formulation for periodic solutions to unilateral contact problems," *International Journal of Non-Linear Mechanics*, 4th Canadian Conference on Non-linear Solid Mechanics, vol. 66, pp. 18–27, Nov. 1, 2014, ISSN: 0020-7462. DOI: 10.1016/j.ijnonlinmec.2014.01.007.

[151] H. B. Keller, *Numerical Methods for Two-Point Boundary-Value Problems*, Dover edition [2018 edition]. Mineola, New York: Dover Publications, Inc, 2018, 397 pp., ISBN: 978-0-486-82834-3.

[152] H. L. Smith, *Monotone Dynamical Systems: An Introduction to the Theory of Competitive and Cooperative Systems*, ser. Mathematical Surveys and Monographs. American Mathematical Society, 1995, ISBN: 978-0-8218-4487-8.

[153] C. Verhoek, P. J. W. Koelewijn, and R. Tóth, "Convex Incremental Dissipativity Analysis of Nonlinear Systems," 2020. arXiv: 2006.14201 [cs, eess].

[154] F. Forni, R. Sepulchre, and A. J. van der Schaft, "On differential passivity of physical systems," in *52nd IEEE Conference on Decision and Control*, IEEE, Dec. 2013. DOI: 10.1109/cdc.2013.6760930.

[155] H. W. Bode, "Relations Between Attenuation and Phase in Feedback Amplifier Design," *Bell System Technical Journal*, vol. 19, no. 3, pp. 421–454, 1940.

[156] R. Sepulchre, G. Drion, and A. Franci, "Control Across Scales by Positive and Negative Feedback," *Annual Review of Control, Robotics, and Autonomous Systems*, vol. 2, no. 1, pp. 89–113, May 2019. DOI: 10.1146/annurev-control-053018-023708.

[157] R. Sepulchre and G.-B. Stan, "Feedback mechanisms for global oscillations in Lure systems," *Systems & Control Letters*, vol. 54, no. 8, pp. 809–818, Aug. 2005. DOI: 10.1016/j.sysconle.2004.12.004.

[158] L. O. Chua, C. A. Desoer, and E. S. Kuh, *Linear and Nonlinear Circuits*, ser. McGraw-Hill Series in Electrical Engineering. New York: McGraw-Hill, 1987, 839 pp., ISBN: 978-0-07-010898-1.

[159] R. Sepulchre, G. Drion, and A. Franci, "Excitable Behaviors," in *Emerging Applications of Control and Systems Theory: A Festschrift in Honor of Mathukumalli Vidyasagar*, ser. Lecture Notes in Control and Information Sciences - Proceedings, P. Misra, R. Tempo, and S. Yurkovich, Eds., 1st ed. 2018, Cham: Springer International Publishing : Imprint: Springer, 2018, ISBN: 978-3-319-67068-3. DOI: 10.1007/978-3-319-67068-3.

[160] B. van der Pol, "On "relaxation-oscillations"," *The London, Edinburgh, and Dublin Philosophical Magazine and Journal of Science*, vol. 2, no. 11, pp. 978–992, Nov. 1, 1926, ISSN: 1941-5982. DOI: 10.1080/14786442608564127.

[161] R. FitzHugh, "Impulses and Physiological States in Theoretical Models of Nerve Membrane," *Biophysical Journal*, vol. 1, no. 6, pp. 445–466, Jul. 1961. DOI: 10.1016/s0006-3495(61)86902-6.

[162] J. Nagumo, S. Arimoto, and S. Yoshizawa, "An Active Pulse Transmission Line Simulating Nerve Axon," *Proceedings of the IRE*, vol. 50, no. 10, pp. 2061–2070, Oct. 1962. DOI: 10.1109/jrproc.1962.288235.

[163] T. Lipp and S. Boyd, "Variations and extension of the convex–concave procedure," *Optimization and Engineering*, vol. 17, no. 2, pp. 263–287, Jun. 2016, ISSN: 1389-4420, 1573-2924. DOI: 10.1007/s11081-015-9294-x.

[164] W.-y. Sun, R. J. Sampaio, and M. Candido, "Proximal Point Algorithm for Minimization of DC Function," *Journal of Computational Mathematics*, vol. 21, no. 4, pp. 451–462, 2003, ISSN: 0254-9409. JSTOR: 43693086.

[165] S. Banert and R. I. Boţ, "A general double-proximal gradient algorithm for d.c. programming," *Mathematical Programming*, vol. 178, no. 1, pp. 301–326, Nov. 1, 2019, ISSN: 1436-4646. DOI: 10.1007/s10107-018-1292-2.

[166] H. A. Le Thi and T. Pham Dinh, "DC programming and DCA: Thirty years of developments," *Mathematical Programming*, vol. 169, no. 1, pp. 5–68, May 2018, ISSN: 0025-5610, 1436-4646. DOI: 10.1007/s10107-018-1235-y.

[167] P.-E. Maingé and A. Moudafi, "Convergence of New Inertial Proximal Methods for DC Programming," *SIAM Journal on Optimization*, vol. 19, no. 1, pp. 397–413, Jan. 1, 2008, ISSN: 1052-6234. DOI: 10.1137/060655183.

[168] A. L. Yuille and A. Rangarajan, "The Concave-Convex Procedure," *Neural Computation*, vol. 15, no. 4, pp. 915–936, Apr. 1, 2003, ISSN: 0899-7667, 1530-888X. DOI: 10.1162/08997660360581958.

[169] M. Ramazannejad, M. Alimohammady, and C. Cattani, "On Algorithms for Difference of Monotone Operators," in *Mathematical Analysis and Applications*, ser. Springer Optimization and Its Applications, T. M. Rassias and P. M. Pardalos, Eds., Cham: Springer International Publishing, 2019, pp. 459–479, ISBN: 978-3-030-31339-5. DOI: 10.1007/978-3-030-31339-5_17.

[170] R. T. Rockafellar, "Convex programming and systems of elementary monotonic relations," *Journal of Mathematical Analysis and Applications*, vol. 19, no. 3, pp. 543–564, Sep. 1, 1967. DOI: 10.1016/0022-247X(67)90011-X.

[171] G. Lanckriet and B. K. Sriperumbudur, "On the Convergence of the Concave-Convex Procedure," in *Advances in Neural Information Processing Systems*, vol. 22, Curran Associates, Inc., 2009.

[172] A. Das, T. Chaffey, and R. Sepulchre, "Oscillations in Mixed-Feedback Systems," 2021. arXiv: 2103.16379 [cs, eess].

[173] M. L. Cartwright, "I. Van der Pol's Equation for Relaxation Oscillations," in *Contributions to the Theory of Nonlinear Oscillations (AM-29), Volume II*. Princeton University Press, 1953, pp. 1–18, ISBN: 978-1-4008-8270-0. DOI: 10.1515/9781400882700-002.